Physics Department annual progress report 1 January - 31 December 1981

Risø National Laboratory, Roskilde

Publication date:
1981

Document Version
Publisher's PDF, also known as Version of record

RISØ

Risø-R-461

Physics Department Annual Progress Report

1 January — 31 December 1981

Risø National Laboratory, DK-4000 Roskilde Denmark
December 1981

RISØ-R-461

PHYSICS DEPARTMENTS ANNUAL PROGRESS REPORT

1 January - 31 December 1981

edited by H. Bjerrum Møller and B. Lebech

UDC 53

December 1981

Risø National Laboratory, DK 4000 Roskilde, Denmark

This report contains unpublished results and should not be quoted without permission from the authors.

ISBN 87-550-0858-5
ISSN 0106-2840

Risø Repro 1982

PREFACE

Research in the Physics Department at Risø covers three main fields:

Solid-State Physics
Plasma Physics
Meteorology

The principal activities in these fields are presented in this report, which covers the period from 1 January to 31 December 1981. Introductions to the work in each of the main fields are given in the respective sections of the report.

CONTENTS

Page

Page

Page

1. SOLID-STATE PHYSICS

The purpose of the work in solid-state physics is to contribute to the fundamental understanding of the physical properties of condensed matter. Neutron beams have properties that make them a unique tool for studies of solids and liquids on the microscopic level and the largest experimental facility at Risø - the DR 3 reactor - is excellently suited for this type of research. Although DR 3 is a medium flux reactor, the installation of a liquid hydrogen cold source in conjunction with a neutron conducting tube has made the experimental conditions at DR 3 competitive with high flux reactors elsewhere in terms of low background and a high flux of low energy neutrons. Hence the experimental work in the solid state physics section is primarily concerned with the use of the DR 3 reactor for a wide variety of neutron scattering experiments, and most of the sections theoretical efforts are also related to neutron scattering experiments.

In the last few years, however, a new intense radiation source - synchrotron x-ray radiation - has become available for diffraction studies of condensed matter, and an increasing portion of the section's efforts has been directed towards the use of this new technique which opens promising new areas of research. Allthough the section have a conventional x-ray source at Risø, the new activity is mainly taking place at HASYLAB, F.R.G. and the section's technical expertice in construction of neutron-diffraction instruments has been of essential value for the building of the x-ray diffractometers at HASYLAB.

The section's work covers many different research projects which it is difficult to summarize in short. However, despite the seemingly differences between the different projects it is quite often the same physical laws that are beeing studied. As an example, the studies of phase transitions, which has been one of the section's main interests throughout the years - have shown

that the same universal laws govern phase transitions in magnetic systems, molecules adsorbed on crystalline surfaces and structural transitions in crystalline matter or liquid crystals. In the following (1.1-1.38) a number of contributions elucidate the experimental and theoretical work of the section. The work falls into the following main categories: studies of magnetic materials (1.1-1.11) non-magnetic materials (1.12-1.13), crystal structures and structural phase transitions (1.19-1.23), liquid crystals and surface studies (1.24-1.30), biology (1.33-1.36) and studies of textures and catalysts (1.31-1.32). In the later years an increasing portion of the sections work is carried of in collaboration with Danish universities and research centres and universities in other countries.

The neutron scattering experiments are carried out using the following instruments placed at the horizontal neutron beams of the DR 3 reactor: four triple-axis spectrometers, a double-axis spectrometer, a four-circle diffractometer and a small angle scattering facility (SANS). In three of the four tangential through-tubes of the reactor, water scatterers placed close to the reactor core scatter beams of thermal neutrons out through the tubes to the spectrometers. The thermal flux in the centre of the beam tube is about $2 \cdot 10^{14}$ neutrons/cm^2/s. The liquid hydrogen cold source provides two of the spectrometers in the reactor hall with beams of cold neutrons. At these spectrometers the cold neutron flux peaks at 15 meV and the cross-over between the cold neutron flux and thermal flux is at about 20 meV. A curved neutron-conducting tube leading from the cold neutron beam in the reactor hall to an experimental hall supplies cold neutrons to SANS and an additional triple-axis spectrometer placed in the experimental hall at the end of the neutron conducting tube. Here the flux peaks at about 10 meV and the useful range is 2.5-15 meV. The low extrinsic background of less than one count per ten minutes makes this instrument an excellent tool for studies requiring high energy resolution. All the neutron spectrometers are fully automatized and may be operated from remote terminals via a modem and telephone line.

At present, three of the neutron spectrometers are controlled by PDP-8 computers and four by PDP-11 computers. Apart from controlling all the necessary spectrometer angles, the PDP programs allow setting and changing of sample temperature and/or ambient magnetic field. The data from the PDP-8 controlled spectrometers are stored in an 18-K memory buffer or on a DEC-cassette. From the buffers or the cassettes the data may either be transferred via (i) a direct line to an HP-9830 desk calculator and plotter system placed in the reactor hall, or (ii) via a modem and telephone line to the main computer at Risø, a Burroughs 7800. The data from the PDP-11 controlled spectrometers are stored on floppy discs and can be processed directly by a PDP-11 computer or after data transfer by the Burroughs 7800. With the exception of the double-axis spectrometer and the four-circle instrument, all the spectrometers move on air-cushions. The double-axis spectrometer is equipped with a tilting detector arm, which allows studies of reflection out of the horizontal scattering plane.

The four-circle neutron-diffractometer (1.40) has been in operation since August 1981. The new instrument was financed partly though a grant, to the Danish National Committee for Crystallography, from the Danish Natural Science Research Council and serves all Danish crystallographers. The instrument consists of a HUBER four-circle goniometer controlled by a PDP-11 computer. Minor parts of the software used to control the diffractometer were developed at Risø while the major parts of the control and data reduction software were a gift from the Institute Laue-Langevin, France.

The small-angle neutron scattering facility, SANS (1.39) will be used, for instance, for problems of metallurgical nature or for structure studies of biological molecules. This project is supported by grants from both the Danish and the Swedish Natural Sciences Research Councils. The facility will become operational during 1982 and is intended to serve Swedish and Danish biologists as well as Risø staff. An advisory committee consisting of a member from each of the two research councils and two members from Risø has been formed. The purpose of the committee

is to set general guide lines for the research carried out at SANS.

The x-ray scattering experiments are carried out either at Risø or at HASYLAB, F.R.G. The x-ray facility at Risø is a joint project between Risø National Laboratory and the University of Copenhagen, supported by the Danish Natural Sciences Research Council. The x-ray source is a 12 kW x-ray generator with a rotating anode of Cu or Mo. The source has two exit ports. Installed at one of the ports is a general-purpose triple-axis spectrometer controlled by a PDP-11 computer. Placed at the other port is a mechanically simple diffractometer consisting of a position-sensitive x-ray detector in conjunction with a multichannel analyzer. This diffractometer has proved to be an efficient instrument for studying the two-dimensional structures of adsorbed monolayers. It is planned to install both instruments permanently at the electron storage ring DORIS at HASYLAB, and build another x-ray diffractometer to be used for trial experiments at Risø. The construction of a computer controlled spectrometer for x-ray energy dispersive diffraction was carried out as a joint project between Risø, the University of Copenhagen, the Thechnical University of Denmark, and HASYLAB. The spectrometer is installed permanently at HASYLAB and used mainly for structural phase transformation studies at high pressures and high temperatures.

1.1. Theory of the excitations in a singlet-doublet system

(P.-A. Lindgård and A. Lehmann-Szweykowska (University of Poznan, Poznan, Poland))

A S = 1 spin system described by the following Hamiltonian

$$H = - \sum_{ij} J_{ij} \vec{S}_i \cdot \vec{S}_j + D \sum_i S_i^{z\,2}$$

is called a singlet-doublet system because the crystal field levels consist of a singlet $|0\rangle$ and a doublet $|\pm 1\rangle$. When the anisotropy constant $D > 4\sum_i J_{oi}$, the ground state is non magnetic (singlet $|0\rangle$). This is found in Pr, for example. There are in

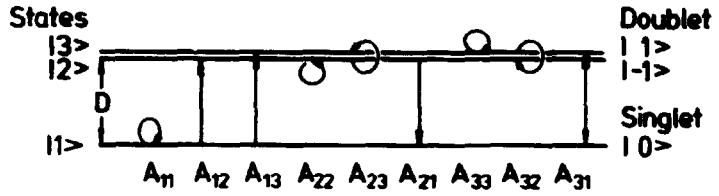

Fig. 1. Transition operators $A_{np} = |n\rangle\langle p|$ between the singlet and doublets $|\pm1|$ separated by the energy D.

principle nine transition-operators $A_{np} = |n\rangle\langle p|$ (see Fig. 1) between the singlet $|0\rangle$ and the doublets $|+1\rangle$ and $|-1\rangle$. A theory in terms of frequency moments and susceptibilities has previously been developed for a general crystal field system (Lindgård, 1980). Using this method we find that the 9×9 generalized dydynamic susceptibility matrix $(A^q_{np}(\omega)|A^{-q}_{rs})$ reduces exactly into three (2×2) and one (3×3) matrix which do not interact. The transverse susceptibility $\chi^{\perp}_q(\omega)$ is the 11 element of the (2×2) submatrix for the operators S^x and $S^yS^z + S^zS^y$. Similarily, the longitudinal $\chi^{zz}_q(\omega)$ is that for S^z and $S^xS^y + S^yS^x$. The static susceptibility $\chi^{\alpha\beta}_q$ was calculated by a perturbation theory in J_q/D to second order and the first and second moments were calculated exactly. The random-phase results were obtained as a first approximation to the dynamic properties.

1.2. Hyperfine interactions, magnetic impurities and magnetic ordering in Pr metal

(M. Wulff*, A.R. Mackintosh* (*University of Copenhagen), H. Bjerrum Møller, J.Z. Jensen, O.D. McMasters+ and K.A. Gschneidner, Jr.+ (+Ames Laboratory - DOE, Iowa State University, Iowa, USA))

The dhcp phase of Pr is a singlet ground-state system in which the exchange is slightly below the critical value necessary to induce magnetic ordering among the 4f electrons. An ordered magnetic structure may therefore be induced by, for example, uniaxial stress or large magnetic fields. By means of neutron scattering, we have studied the antiferromagnetism which develops in a pure monocrystal at very low temperatures due to the hyper-

fine coupling between the electrons and the nuclei, and the magnetic ordering and excitations in a crystal containing 2.5% of magnetic Nd impurities.

In the pure crystal (with a Nd-content of less than 1 ppm), the magnetic ordering is heralded by a ridge of quasi-elastic scattering or "central peak", which is observable at temperatures as high as 10 K. Below about 0.2 K a narrow component within the central peak grows dramatically, corresponding to fluctuations of very long-range, but not true long-range order. Below about 60 mK a static incommensurable antiferromagnetic moment develops, which increases rapidly as the temperature is reduced (see Fig. 2), and reaches 0.4 μ_B/atom at about 40 mK, a value much greater than has been observed previously. We ascribe the ordering to

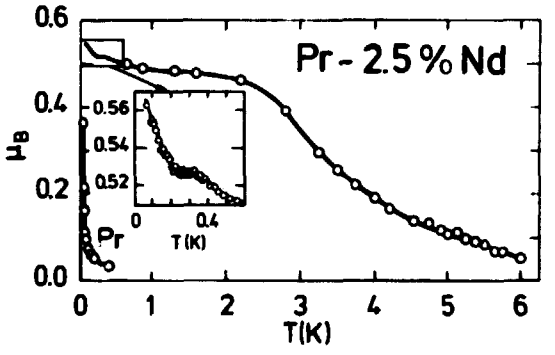

Fig. 2. Effective moments in Pr and Pr-2.5% Nd. Below the ordering temperatures of about 60 mK and 3.5 K, respectively, the displayed moments correspond to incommensurable antiferromagnetic structures, while at higher temperatures they indicate the temperature-dependence of very long-range magnetic fluctuations.

the hyperfinel coupling between the electrons and nuclei. The same pattern of ordering is observed when 2.5% Nd is added, but the transition is shifted to much higher temperatures. The long-range fluctuations now grow markedly below about 6 K, as shown in Fig. 2, and true magnetic ordering develops below about 3.5 K. After approaching saturation, the moment begins to increase again at around 1 K, reaches another plateau, and then rises again more rapidly below about 0.2 K. The first rise is attributed to the splitting and repopulation of the ground state of the Nd ions in the molecular field, which is also manifested in the inelastic scattering, and the second to the hyperfine interaction. Measurements of inelastic scattering above T_N reveal a crystal-field level of the Nd ions at about 1.2 meV, which inter-

acts strongly with the excitations of the host. In the magnetically ordered phase the level shifts and splits due to the molecular field, and evidence is observed for another split level about 0.5 meV above the ground state. The dependence of these levels on magnetic field has also been studied.

1.3. Magnetic anisotropy in Pr metal

(B. Lebech and K.A. McEwen (University of Salford, Salford, U.K.))

Praseodymium metal is a well-known singlet ground-state magnet in which the crystal field interactions and exchange forces are comparable in magnitude. Pr crystallises in the dhcp-structure which has the stacking sequence ABA'C along the hexagonal axis. Atoms in the A(A') layers have a local surrounding of approximately cubic symmetry (cubic sites), while the atoms in the B and C layers have a hexagonal close packed arrangement of nearest neighbours (hexagonal sites). Measurements of the magnetic anisotropy in Pr (Lebech and Rainford, 1971 and Johansson et al., 1971) revealed that the susceptibility was highly anisotropic and that the anisotropy at the hexagonal sites was about ten times higher than at the cubic sites.

Neutron diffraction allows an unambiguous separation of the contributions to the magnetic anisotropy from the cubic and hexagonal sites by measurements of the effects of an applied magnetic field on the Bragg intensities at the different reciprocal lattice positions of the dhcp lattice. The previous study by neutron diffraction (Lebech and Rainford, 1971) of the magnetic anisotropy in Pr was limited to applied magnetic fields along the hexagonal ($\hat{c}$) axis and the basal plane $\hat{a}$-axis. We have now extended these measurements and studied the effect of a magnetic field applied along the basal plane $\hat{b}$-axis.

The results are summarised in Fig. 3 which shows the sum and difference moments (Fig. 3a) and the moments (μ_c and μ_h) on the two sites (Fig. 3b) induced by fields along the crystallographic $\hat{a}$ and $\hat{b}$ (the solid curves are after Lebech and

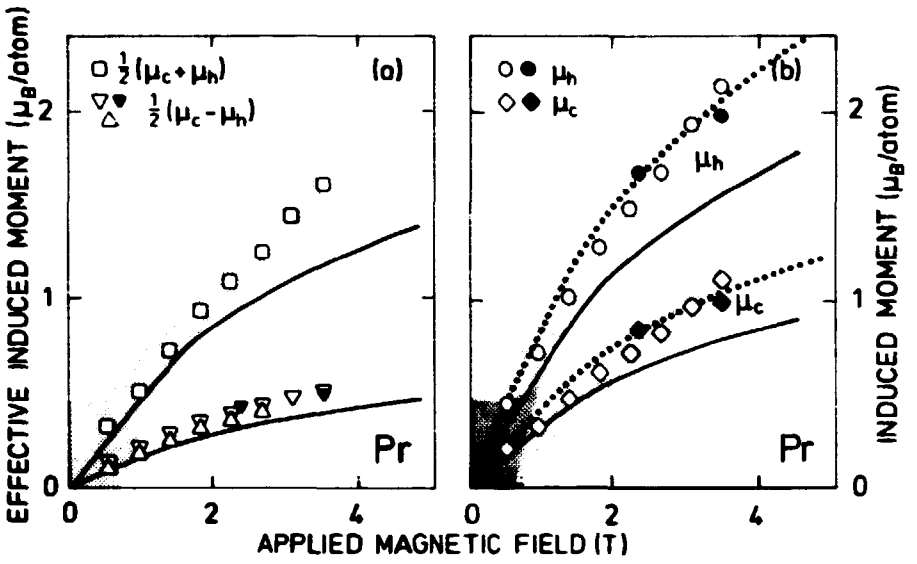

Fig. 3. (a) Sum and difference moment per Pr atom induced by magnetic fields applied along the $\hat{a}$ (filled points) or $\hat{b}$ directions (unfilled points). (b) Induced magnetic moments per Pr atom on the hexagonal and cubic sites for fields along $\hat{b}$ (o,◆) and $\hat{a}$ (●,◆). The data points in (b) are deduced from the data shown in (a). The hatched area illustrates the effect of up to ±5% error in the nuclear intensity of the (1,1,0) reflection.

Rainford (1971)). Within the accuracy of the present experiment, the basal plane anisotropy is neglible, and for fields along either the $\hat{a}$ or the $\hat{b}$ direction, $\mu_c \equiv 2\mu_h$. The absolute moments for fields in the basal plane are higher than those observed in the previous experiment (25% at 3 T). At the moment we have no explanation for this discrepancy.

1.4. Crystal field effects in $PrNi_5D_x$

J.K. Kjems, P.A. Alekseev* and I.P. Sadikov* (Kurchatov Institute, Moscow, U.S.S.R.)

The crystal field spectra of polycrystalline samples of $PrNi_5D_x$, $x = 0$, 0.28, 0.44 were studied on a triple axis neutron spectrometer. The aim was to obtain information about the position and the effective charge of the diffusing deuterium in the hexagonal lattice. Surprisingly, only very small changes in the crystal field spectra were observed which could be attributed to the

presence of deuterium. The changes were small energy shifts in the observed transitions and small changes in line width accompanied by changes in the relative intensities. Also the pure $PrNi_5$ sample showed some intrinsic line width and strong unexpected intensity at low energies, probably due to exciton branches. The data is analysed by comparison to crystal field calculations using different states of the deuterium atom. The preliminary results indicate that the charge on the deuterium is very effectively screened, thus explaining the very small pertubation of the crystal field spectra.

1.5. Crystal field effects in Pr(La)Al$_3$

(J. Kjems, P.A. Alekseev* and I.P. Sadikov* (*Kurchatov Institute, Moscow, U.S.S.R.))

The crystal field spectra of polycrystalline samples of $PrAl_3$ and $Pr_{0.5}La_{0.5}Al_3$ have been studied using a cold source triple axis neutron spectrometer. The $\Gamma_1 - \Gamma_6$ transition was studied in detail as a function of both momentum transfer and temperature. An asymmetric line broadening was found in $PrAl_3$ probably due to exchange interactions. However, the measurements on the diluted sample showed nearly the same overall line width of 1 meV at 40 K although without the asymmetry. Therefore more than one line-width mechanism may be contributing.

1.6. Influence of superconductivity on the crystal field transitions in $Tm_xLa_{1-x}Al_2$

(R. Feile*, K. Knorr* (*University of Mainz, Mainz, F.R.G.) and J.K. Kjems)

The study of dilute rare earth ions in crystals of $LaAl_2$ was continued with $Tm_{0.003}La_{0.997}Al_2$.

This crystal becomes superconducting below $T_c = 3.15$ K and detailed measurements of the $\Gamma_5 - \Gamma_4$ transition at $\hbar\omega = 0.75$ mV showed an anomaly in the observed energy-width near the transition. The width decreases as T_c is approached from above but,

unlike what was found for La(Tb)Al_2, it increases again as the temperature is lowered further. This may be explained by coupling to other levels or to degeneration of the ground state. The analysis is as yet in complete.

1.7. Correlation theory applied to the static and dynamic properties of EuO and EuS*

(P.-A. Lindgård)

In order to describe accurately the static and dynamic properties of a magnetic system, a generalization of the random phase approximation has been developed in which essential correlation effects are included self-consistently. In this correlation theory (CT) an attempt is made to provide a simple scheme to calculate the dynamic response in an approximate yet realistic way (i.e. yielding renormalization and damping of excitations) in terms of static properties like correlation functions, to be calculated self-consistently by exact relations using the dynamics. EuO and EuS represent ideal realizations of the 3-D Heisenberg model. The structure is fcc, S = 7/2 and the nearest neighbour (nn) and next nearest neighbour (nnn) exchange constants J_1 and J_2 are known from spin wave measurements (Als-Nielsen et al., 1976 and Bohn et al., 1980): for EuO J_1 = 0.625 K, $J_2 = +J_1/5$ and for EuS J_1 = 0.253 K, $J_2 = -2J_1/5$; thus the nnn-interactions are significant and have opposite signs. Extensive measurements of dynamic and static (Als-Nielsen et al., 1976 and Mook, 1981) properties for $T \gtrsim T_c$ have been performed in particular for EuO. It is interesting to test the range of validity of the theory versus these experimental results.

The theory (Lindgård, 1982) can be briefly summarized as follows: By the Mori projection-operator formalism the dynamical response $(S^z_q\ S^z_{-q})_\omega$ is related to the static susceptibility χ_q and fre-

*Work done partly as a visiting scientist at Oak Ridge National Laboratory, Tennessee, USA

quency moments $\langle\omega_q^n\rangle$, which are expressed as wave vector sums over the exchange and static correlation function e.g. $\chi_q\langle\omega_q^2\rangle = 4\Sigma_k(J_k-J_{k-q})\langle S_k^z S_{-k}^z\rangle$. For <u>small frequencies</u>, $\omega < 2S(J_o-J_q)$, the two-pole-approximation is expected to describe the line shape well:

$$(S_q^z S_{-q}^z)_\omega = \frac{\chi_q}{\pi\omega}\langle\omega_q^2\rangle \text{ Im } \{\frac{1}{(\omega-\alpha_q-i\beta_q)(\omega+\alpha_q-i\beta_q)}\} . \qquad (1)$$

This corresponds to assuming a Lorentzian line-shape for the random force response function $(S_q^z S_{-q}^z)_\omega$ for <u>small ω</u>, with the half width $2\beta_q$. The term $(S_q^z S_{-q}^z)_\omega$ is evaluated approximately in terms of products of $(S_k^z S_{-k}^z)_\omega$ using the mode-mode decoupling; β_q is self-consistently obtained at the half-width frequency ω_{HW} of $(S_q^z S_{-q}^z)_\omega$. Equation (1) yields χ_q and $\langle\omega_q^2\rangle = \alpha_q^2 + \beta_q^2$ self consistently, which suffices for a description of the static correlation function that is quite accurate, using

$$\langle S_q^z S_{-q}^z\rangle = \int \omega(S_q^z S_{-q}^z)_\omega/(1 - e^{\beta\omega})d\omega.$$

The obtained dynamical properties are qualitatively correct; i.e. a) diffusion for $q \to 0$ ($\alpha_q \to i\beta_q$) for $T > T_c$, b) dynamical scaling $\omega_{HW} \sim q^{5/2}$ at $T = T_c$, and c) development of spin-wave like peaks at high q ($\alpha_q > \beta_q$). It is, however, clear that Eq. (1) is invalid at high frequencies and must be cut off in order to give finite higher-order moments $\langle\omega_q^n\rangle$, $n > 2$. If a cut-off determined by $\langle\omega_q^4\rangle$ is introduced, the line width ω_{HW} increases in particular for q near the zone boundary. Writing $\beta_q = C + \Sigma_n a_n(J_o-J_q)^n$, where C and a_n are temperature dependent constants, one finds that $C \to 0$ for $T \to T_c$. This means that both $(S_q^z S_{-q}^z)_\omega$ and $(\dot{S}_q^z \dot{S}_{-q}^z)_\omega$ exhibit critical slowing down, and therefore the two-pole-approximation is not satisfactory very close to T_c.

Figure 4 shows a comparison between experiments and the results of the CT-calculation using no adjustable parameters. The agreement is good for $1.02\ T_c < T < \infty$ for the static properties. The same is true for the dynamic properties. Figure 5 shows the calculated dynamic properties for EuO and EuS. The calculated

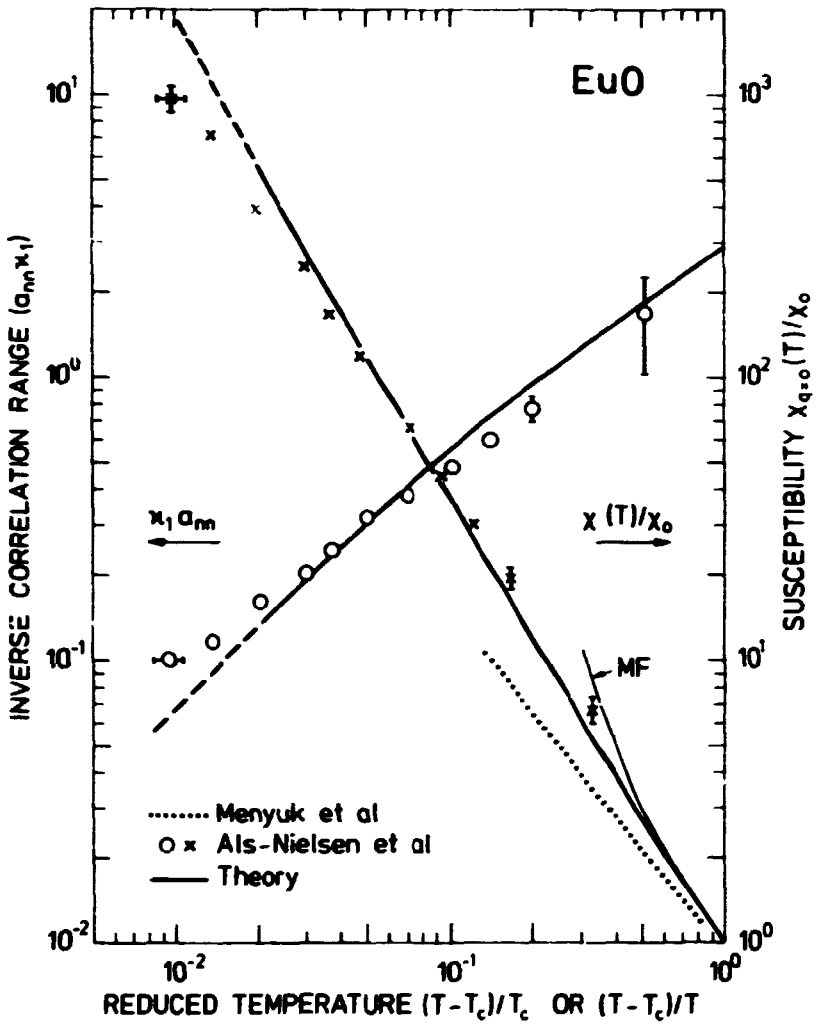

Fig. 4. The calculated inverse correlation range κ_1 times the nn distance for EuO. Agreement with experiment is obtained with no adjustable parameters for $0.02 < (T-T_C)/T_C$. For EuS, $\kappa_1 a_{nn}$ (not shown) is 15% smaller, because of the larger depression (Table 1) of T_C. When $J_2 < 0$, the difference is small and in agreement with the experimental trend. The susceptibility fits the neutron data similarily for $0.02 < (T-T_C)/T$. $\chi(CT)$ reduces to the mean field $\chi(MF)$ for $(T-T_C)/T \to 1$.

transition temperatures are given in Table 1. The contribution from the dipole forces may account for the difference of a few degrees Kelvin between $T_C(CT)$ and $T_C(exp)$.

Extension of the calculations to other Heisenberg magnets such as Gd, Fe, and Ni has also been performed. For Fe and Ni it is found that one needs strong ferromagnetic interactions to the first three groups of neighbours in order to obtain the correct

spin-wave dispersion and T_c. This in turn gives rise to extensive short-range correlation and therefore more pronounced spin waves for $T > T_c$ than in EuO. This is observed experimentally.

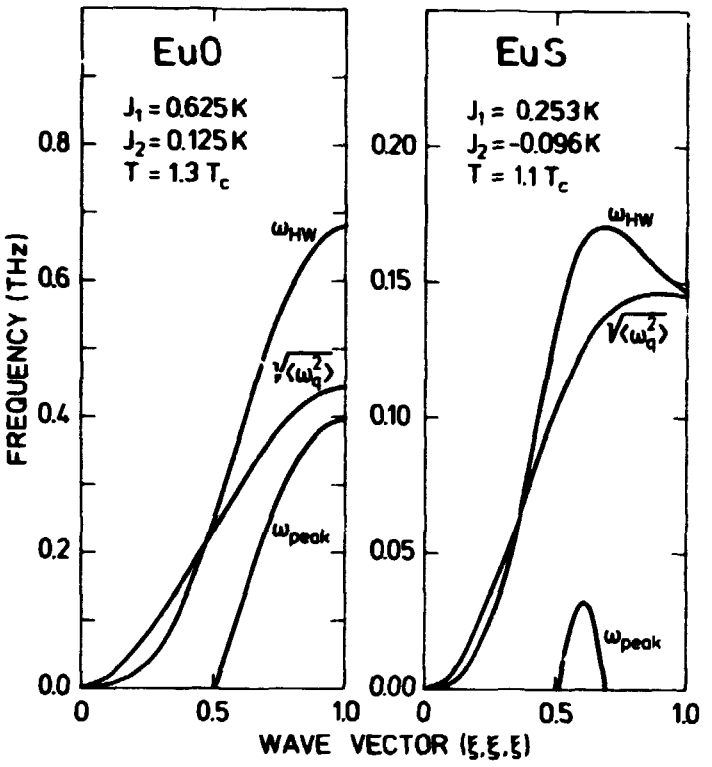

Fig. 5. Calculated half width ω_{HW}, peak position ω_{peak}, and second moment $\langle\omega_q^2\rangle$ for EuO and EuS. The influence of J_2 is evident when comparing the calculation of ω_{peak} for EuO ($J_2 = J_1/5$) and EuS ($J_2 = -2J_1/5$). In EuO a peak develops at $q > 0.5q_{zone}$ for $T > T_c$, whereas in EuS this happens only closer to T_c and in a limited q-range. As a function of temperature $\sqrt{\langle\omega_q^2\rangle_T}$ rises rapidly near T_c to a value $\approx 2\sqrt{\langle\omega_q^2\rangle_{T=\infty}}$ for $q = q_{zone}$ in EuO.

Table 1. Calculated transition temperatures for EuO and EuS.

	T_c(mean field)	T_c(CT)	T_c(exp)	T_c(CT)/T_c(MF)
EuO	86.6 K	66.6 K	69.1 K	0.768
EuS	25.8 K	14.1 K	16.6 K	0.662

1.8. Magnetic excitations in Ho_2Co_{17} and Ho_2Fe_{17}

(K. Clausen and B. Lebech)

The study by inelastic scattering of the microscopic magnetic interactions in Ho_2Co_{17} and Ho_2Fe_{17} has been concluded. The interpretation of the observed low energy (< 20 meV) magnetic excitations was based on a localised model, where only two different magnetic sites - one rare earth and one transition metal - have been assumed. This assumption was found to be justified by the experimental observations of a disordered structure and a single localised magnon mode. The interactions taken into account in the localised model were single-ion crystal-field anisotropy and isotropic exchange. The crystal-field parameters and exchange constants describing these interactions were determined by fitting the linear spin wave solution to the observed ground state magnon dispersion relations, and by a mean field analysis of the energy splittings of the four lowest Ho^{3+} levels (local modes).

In a previous analysis (Clausen 1981) only nearest-neighbour exchange, the B_2^0 and B_6^6 crystal-field parameters for the Ho site and the expansion parameter B_2^t for the anisotropy of the 3d-sublattice were taken into account. Using these approximations it was previously found that the 3d-3d exchange constant differed for the various high-symmetry directions. In the final analysis (Clausen and Lebech 1982) we have extended the Hamiltonian to include both nearest and next-nearest 3d-3d exchange and all four crystal-field parameters for the rare earth site.

In this more realistic analysis the linear spin-wave solution was found to give a good description of the ground-state spin wave branches observed in the three high symmetry directions. The analysis also led to a good agreement between the observed temperature dependence of the intensity of the scattering from the local modes and a mean-field calculation based on the derived exchange and crystal-field parameters. The very high magnetic ordering temperatures of the R_2T_{17} compounds are mainly determined by the 3d-3d exchange and for both compounds the observed values for T_c were found to be within the uncertainty of

estimates of T_C based on the 3d-3d exchange constants deduced in the analysis.

Point charge calculations (Greedan and Rao, 1973) which take only the more distant rare-earth neighbours into account predict two ground state local modes because one of the Ho sites would favour an easy basal plane and the other an easy c-axis. This would result in different level schemes for the two Ho^{3+} sites and lead to two non-degenerate local modes. However, only one ground-state local mode was observed. Hence, the single ion anisotropy of the two rare earth sites must be identical and therefore mainly determined by the charge distributions from the nearest-neighbour 3d-metal ions, which are almost identical at the two rare earth sites. The crystal-field anisotropy of the rare earth ions is of

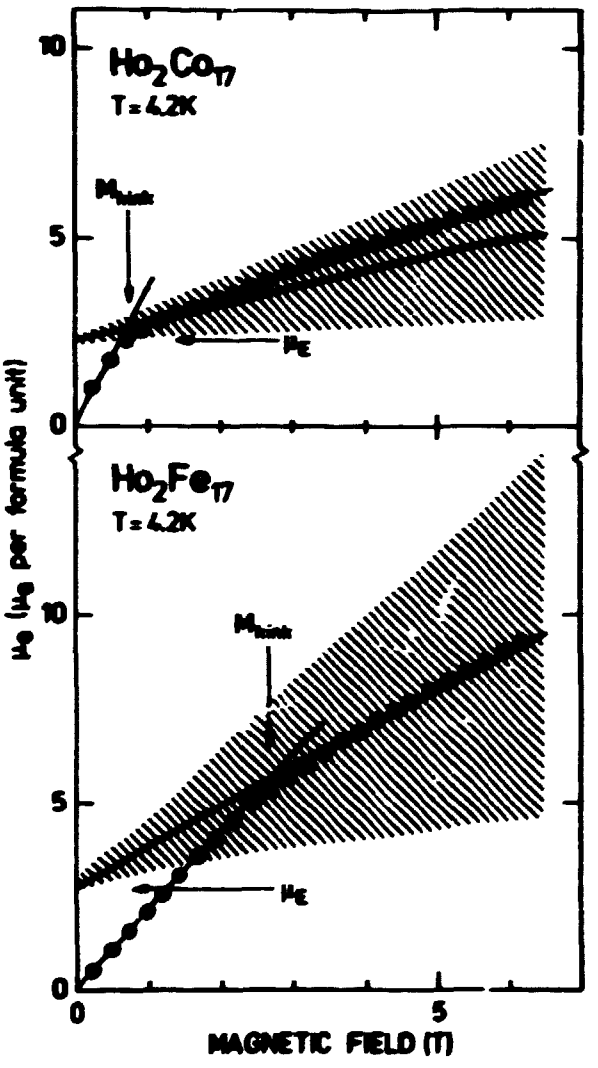

Fig. 6. The observed magnetic moment μ_θ induced along the applied internal field H_i oriented at an angle θ to the c-axis. For Ho_2Co_{17} $\theta = 16°$ and for Ho_2Fe_{17} $\theta = 9.5°$. The solid line is μ_θ as calculated from a two sublattice model, using the parameters derived from the microscopic measurements. The hatched areas represent the uncertainty of the calculations.

the same order of magnitude as found in the pure rare-earth metals. The single-ion crystal-field anisotropy for the transition metal site was found to favour an easy basal plane for both compounds, the anisotropy of the Co sublattice in Ho_2Co_{17} being about an order of magnitude larger than that of the Fe sublattice in Ho_2Fe_{17}.

In a previous study of the macroscopic anisotropy of Ho_2Co_{17} and Ho_2Fe_{17} (Clausen and Nielsen 1981) rigid uniaxial magnetic structures were assumed. The microscopic parameters, however, revealed that the rare earth - transition metal exchange was of the same order of magnitude as the anisotropy of the rare earth sublattice and hence deviations from collinearity are unavoidable. Using a two sublattice model and the microscopic parameters deduced from the spin wave data, the macroscopic anisotropy was calculated. The observed and calculated macroscopic anisotropy, as represented by the hard axis magnetisation and the anisotropy within the basal plane, agreed within the uncertainty of the calculation (see Fig. 6).

1.9. Soliton and two-magnon scattering in $CsNiF_3$

(K. Kakurai*, M. Steiner* (*Hahn-Meitner Institute, Berlin) and J.K. Kjem·)

The relative roles of two-magnon and soliton scattering in $CsNiF_3$ have been studied with a newly designed cryostat equipped with a movable permanent magnet. The inelastic spectra for vertical and horizontal fields were obtained under identical scattering conditions, which eliminates several sources of systematic errors. The results (Fig. 7) show that an apprecible contribution to the central peak of $CsNiF_3$ is due to correlations which are transverse to the field. This effect is expected only for soliton scattering. The longitudinal component of the central peak is dominant at low q and it may well contain both solition and two-magnon contributions because the scale of the two-magnon scattering can be determined independently from the observed peaks at $\hbar\omega_1 + \hbar\omega_2$ which are clearly seen in the spectra.

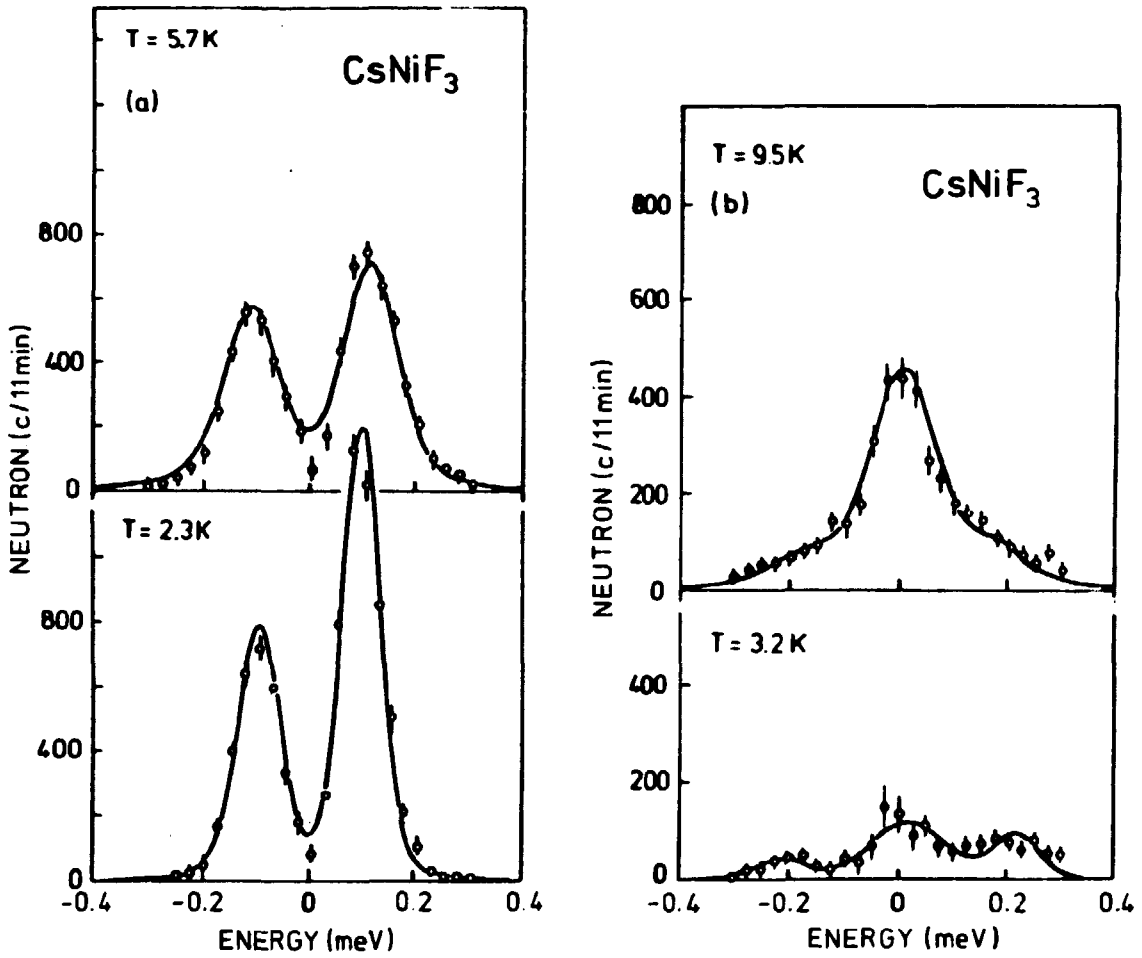

Fig. 7. The background corrected spectra of $CsNiF_3$ at q = (0.275,0,0) for (a) $\vec{H} \parallel \vec{q}$ and (b) $\vec{H} \perp \vec{q}$ at low and high temperatures.

1.10. Dynamical scaling in Rb_2NiF_4

(H. Ikeda (Ochanomizu University, Japan) and J.K. Kjems)

Rb_2NiF_4 is a model system for the studies of 2-D-phase transitions in the Ising universality class. The present experiment was aimed at clarifying the issue of dynamical scaling and it consisted of a inelastic neutron scattering study of the energy width of the critical scattering as function of temperature and wave vector. The preliminary analysis indicates a value of the critical exponent z close to 2. This exponent describes the relation between the energy width Γ and the wave vector, $\Gamma \propto q^z$, at the transition temperature, T_N. A value of $z \approx 2$ renders support to the theoretical treatment based on the 2-D kinetic

Ising model and it seems to conflict with the simple dynamical scaling concept which gives $z = D/2 = 1$.

1.11. Neutron scattering studies of the antiferromagnetic phase of $Cd_{1-x}Mn_xTe$

(T. Giebultowicz*, W. Minor* (*University of Warsaw, Warsaw, Poland) B. Buras, K. Clausen and B. Lebech)

Magnetic susceptibility and specific heat studies of mixed semiconductor crystals $Cd_{1-x}Mn_xTe$ indicate that: (i) for $x < 0.17$ the crystals are paramagnetic at all temperatures, (ii) for $0.17 < x < 0.60$ a spin glass and (iii) for $0.60 < x < 0.71$ an antiferromagnetic ordering are observed at low temperatures (Galazka et al., 1980). A preliminary neutron diffraction study using single crystals has shown that for $x = 0.70$ a magnetic ordering occurs at low temperatures and the observed reflections could be interpreted in terms of type III antiferromagnetic ordering of the f.c.c. sublattice.

The present experiments were made on single crystals with $x = 0.60$, 0.63, 0.65 and 0.70 (Giebultowicz et al., 1981). In all these compounds, magnetic reflections were observed at low temperatures and could be interpreted in terms of type III antiferromagnetic ordering as in the preliminary experiment quoted above. The temperature dependence of the integrated intensities of the magnetic reflections follows the square of the Brillouin function for $S = 5/2$ (Fig. 8), except close to the ordering temperature. This deviation is clearly seen for $x = 0.70$ in Fig. 8. From the Brillouin functions fitted to the data one obtains the following ordering temperatures: 37.0, 42.7, 45.7, and 49.0 K for $x = 0.60$, 0.63, 0.65 and 0.70, respectively.

The neutron study supports the conclusion made from measurements performed by means of the other techniques mentioned above. A quantitative comparison, however, can be made only for $x = 0.70$ because detailed data from susceptibility and specific heat measurements are available only for this composition

Galazka et al., 1980). For x = 0.70, The specific heat measurements give the ordering temperature (36±2)K while the neutron results give (49.0±0.6) K. However, the full width at half maximum of the diffraction peaks remains constant up to about 35 K and then begins to increase. This observation suggests the existence of clusters of magnetic correlations which develop well above 50 K and give rise to intensity which can be observed by neutron scattering (see the data for x = 0.70 in Fig. 8). At high

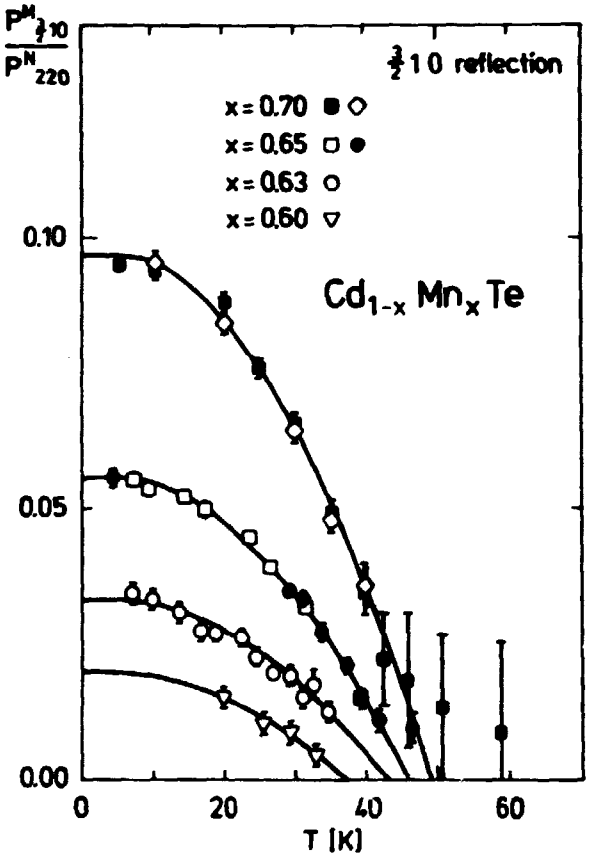

Fig. 8. Variation with temperature of the intensity of the antiferromagnetic reflection (2/3,1,0) of $Cd_{1-x}Mn_xTe$ normalized by the (2,2,0) nuclear reflection, for various Mn concentrations. The curves are the results of fits of the experimental data to scaled squares of the Brillouin function for S = 5/2.

temperatures (35 K < T < 50 K) the observed neutron scattering is mainly inelastic, i.e. the relaxation times are short. In the magnetic susceptibility measurements, the characteristic time scale is of the order of seconds. Therefore despite the existence of clusters of magnetic correlations, the susceptibility data exhibit paramagnetic behaviour at 50 K and somewhat below. As the temperature is lowered, the relaxation effects slow down and the cluster dimensions grow. Finally, at a certain temperature, $T_f \sim 35$ K, freezing of the clusters occurs. Below T_f the cluster

sizes do not change, the neutron scattering is then mainly elastic and the static magnetic susceptibility decreases slowly with decreasing temperature. This phenomenological description is supported by model calculations (Giebultowicz et al., 1982). Recently, we studied the temperature dependence of the magnetic reflections in a crystal having x = 0.60. This composition is close to the phase boundary for the antiferromagnetic to spin-glass transition. Down to 6 K, there was no evidence of the spinglass transition predicted theoretically by De Seze (1977).

1.12. High-temperature study of UO_2

(K. Clausen (Clarendon Laboratory, Oxford, U.K.), M.T. Hutchings (AERE, Harwell, U.K.) and J.K. Kjems)

UO_2 has an anomalous gradually increasing specific heat from 1800°C to the melting point ~ 3000°C. The origin of this feature is unknown and our study aimed at finding evidence for disorder in the oxygen lattice. The highest temperature obtained so far in the Risø furnace was 2000°C and no sign of disorder was detected. Some renormalization of the q = 0 optic phonons was observed. The study will be continued in a newly designed furnace at AERE Harwell which can reach ~ 2500°C.

1.13. Phonons in Mo_3Si

(A. Nørlund Christensen (University of Aarhus, Denmark) and B. Lebech)

Mo_3Si has the β-W or A15 structure. A number of compounds are known to have this structure. Some of them are superconductors with high transition temperatures (Nb_3Al: 18 K, Nb_3Pt: 10 K, Nb_3Ge: 8-17 K), and some of the compounds have low transition temperatures (Mo_3Al: < 1 K, Mo_3Si: < 1 K). Due to the extreme difficulty in producing large single crystals of almost all A15 compounds, the knowledge of the lattice dynamics of these compounds is limited. Measurements on a 1 cm^3 single crystal of Mo_3Si of the phonon dispersion relations are shown in Fig. 9. No soft modes were observed, and for lack of intensity it has

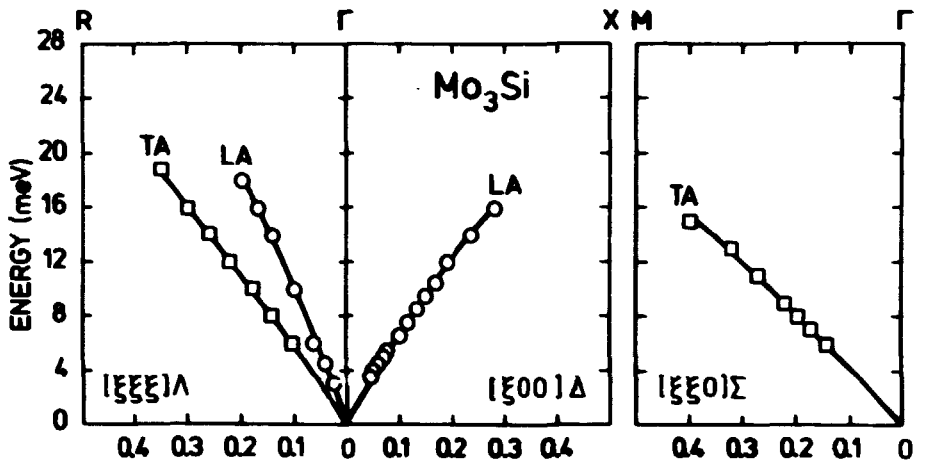

Fig. 9. Phonon dispersion relations along the three symmetry directions in Mo_3Si. The (o) correspond to longitudinal phonons and the (□) to transverse phonons. A 1 cm^3 single crystal of Mo_3Si was used.

not yet been possible to follow the phonon branches to the zone boundary.

1.14. Mode Grüneisen parameters in RbBr

(G. Ernst* and G. Quittner* (*Forschungszentrum Seibersdorf, Austria) G. Krexner (University of Vienna), W. Kress (Max-Planck-Institute, Stuttgart, F.R.G.), B. Buras and B. Lebech)

The measurement of microscopic Grüneisen parameters (mode γ's) is an experimental approach well suited to obtain information concerning anharmonic effects in lattice dynamics. For alkali halides only few data are available to give a fairly complete description over the whole Brillouin zone (Blaschko et al. 1975 and Farr et al., 1976) The occurrence of negative Grüneisen parameters over some branches appears to be a conspicuous and characteristic feature of these data.

In order to provide a broader experimental basis for understanding these phenomena, mode γ's Grüneisen parameters

$$\gamma(\vec{q},j) = -\left.\frac{d\ \ln\omega(\vec{q},j)}{d\ \ln V}\right|_T$$

of 45 acoustic phonons of RbBr in the symmetry directions $[00\zeta]$, $[\zeta\zeta 0]$ and $[\zeta\zeta\zeta]$ were determined (Fig. 10). The phonon frequency shifts were calculated by comparing two sets of measurements taken at atmospheric pressure and at 4 GPa, respectively. Figure 10 shows preliminary results: In the $[00\zeta]$ and $[\zeta\zeta 0]$ directions the transverse branches turn out to have rather constant and negative γ-values whereas the longitudinal branches exhibit a change from positive to negative γ-values near the X point. In

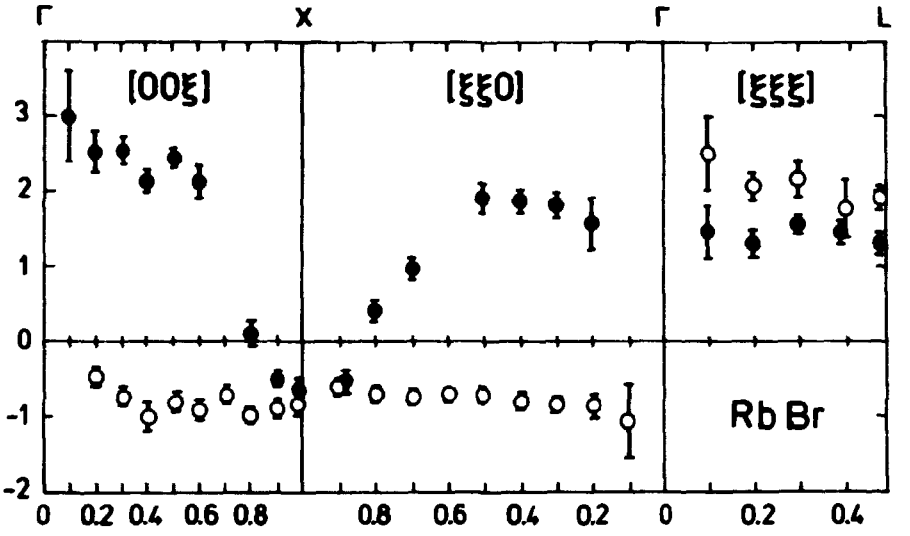

Fig. 10. Measured dispersion of the mode Grüneisen parameters in RbBr. o: transverse acoustic (TA) branches, •: longitudinal acoustic (LA) branches.

the $[\zeta\zeta\zeta]$ direction the γ's of both the longitudinal and transverse branches are positive and approximately constant. In general, the results are similar to those previously obtained for RbI. The data evaluation is made by using a breathing shell model. A comparison of the model parameters for RbBr with those of RbI should both contribute to a better understanding of the physical meaning of the parameters and provide further insight into the lattice dynamics of alkali halides.

1.15. Neutron scattering of the ionic conductor LiI·D_2O

(N. Hessel Andersen, J.K. Kjems and F.W. Poulsen (Metallurgy Department, Risø))

From structural studies of the ionic conducter LiI·D_2O it has been shown that the water molecule has significant influence on the Li-conduction process. In the high-temperature ionic-conducting α-phase quasi elastic diffuse neutron scattering data have established the presence of short range correlations in the orientations of the water molecules and between the orientation of the water molecules and the occupation of the available Li-sites (Fig. 11). These correlations are more strongly revealed at lower temperatures by the observation of a first-order struc-

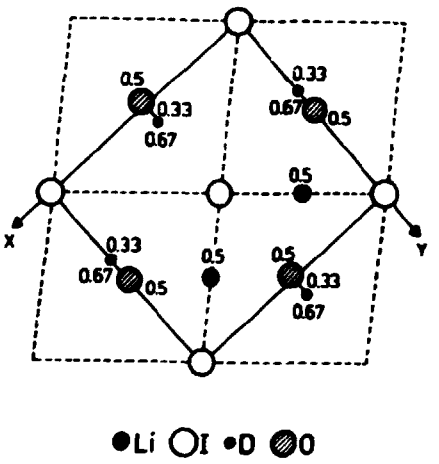

Fig. 11. Projection of the structure of ß-LiI·D_2O on the x-y plane. The full lines indicate the orthorhombic cell with two formula units. The broken lines indicate the unit cell which becomes cubic above the ß to α transition at -56°C. The fractional z-coordinates are given.

tural phase transition (at -56°C) which leads to an ordered state for both the orientation of the water molecules and the occupation of the Li-sites. The short range correlations between the Li-positions and the D_2O-orientations in the α-phase reduce the Li-diffusion and explain why a simple conductivity model fails to account for the observed data on LiI·D_2O.

1.16. Structural studies of lithium sulphate ionic conductors

(N. Hessel Andersen, J.K. Kjems and L. Nilsson (Chalmers Institute of Technology, Sweden))

The structural studies of the mechanisms which give rise to the high ionic conductivities of the high temperature cubic α-phases of lithium sulphate ionic conductors have been continued. Neutron powder diffraction studies of the fcc α-phase of $Li_{1.6}Ag_{0.4}SO_4$ confirm the picture developed for the isostructural Li_2SO_4, that high degrees of orientational disorder in the sulphate groups, rather than the mass and radius of the moving cations, are decisive for the high ionic conductivities observed in these systems. Similar investigations of bcc α-phase $LiAgSO_4$ and $LiNaSO_4$ support the conclusions that the disorder in the sulphate group system (probably dynamical) mediates the diffusion of the cations.

The attempts to study the diffusion mechanisms in the α-phase of these systems more closely by quasi-elastic diffuse neutron scattering were also continued. The method of in situ growing of the necessary single crystals from the highly corrosive melt has been developed for Li_2SO_4, but suitable orientation of the sample was not possible with the available experimental set-up.

1.17. Disorder scattering in $Ba_{1-x}La_xF_{2+x}$

(J.K. Kjems, N.Hessel Andersen and J. Schoonman, (University of Utrecht, The Netherlands))

Like almost all fluorites, BaF_2 can be heavily doped with trivalent ions, resulting in a high concentration of interstitial F^--ions. The ionic conductivity rises sharply with low doping concentration, but saturates in the range $x = 0.10 - 0.50$. Crystals with $x = 0.13$, 0.202, and 0.492 have been studied using neutron spectroscopy. Strong diffuse scattering was found which resembles the earlier results for thermally-induced defect clusters in CaF_2. However, at the highest concentrations the scattering shows a clear maximum near $\tau \pm (2/3,0,0)$; this indicates a tendency towards short-range ordering of the defect

clusters. No effect of lowering the temperature to 70 K was observed. The study will be continued with measurements on the 4-circle diffractometer (1.40) and with measurements at elevated temperatures.

1.18. Phase transitions in PdD_x

(J.K. Kjems, B.S. Bowerman* and D.G. Witchell* (University of Birmingham, U.K.))

The palladium-deuterium system provides an excellent example of a lattice gas where Pd establishes the periodic potential in which the deuterium diffuses. The phase diagram is not well understood in the ranges $0.60 < x < 0.7$, $50\ K < T < 70\ K$ where the system shows orderdisorder.

Single crystals with $x = 0.62$, 0.64, and 0.70 were investigated and the temperature evolution of the diffuse scattering was determined. All compounds showed a broad contribution centred at an incommensurate wave vector near (1/2,1,0). The intensity increased slowly with decreasing temperature. Below ~ 60 K a sharp commensurate component appears. Below 55 K this sharp component grows with a time constant of the order of hours, and below 50 K of the order of days.

The data is being analysed in conjunction with Monte Carlo computer calculations of the phase diagram performed at the University of Birmingham. The preliminary results indicate a change from a first to second order transition, i.e. the presence of a tricritical point in this composition range.

1.19. Refinement of the structure of $LiTb_{0.3}Y_{0.7}F_4$

(K. Kjær, F. Krebs Larsen (University of Aarhus, Denmark) and I. Laursen (Technical University of Denmark))

In the course of a study of the series of scheelite ($I4_1/a$) crystals $LiRE_xY_{1-x}F_4$, where RE is a rare earth ion, accurate nuclear structure factors have been obtained for the crystal $LiTb_{0.3}Y_{0.7}F_4$.

These structure factors provide an absolute scale for measurement of the spontaneous magnetization by neutron diffraction.

Intensities were determined for 1250 reflections at 295 K and at 175 K from a 4 mm spherical crystal of $LiTb_{0.3}Yb_{0.7}F_4$ using the Hilger-Ferranti four-circle diffractometer at the DR 3 reactor. The intensities were averaged to give 290 independent reflections with an internal R-factor of 2.7%. Starting from the reported structure for $LiTbF_4$ (Als-Nielsen et al., 1975), the extinction, thermal parameters and the fluorine positions were refined to give R-factors for F^2 of 3.7% at 295 K and 3.3% at 175 K. The fluorine positions obtained show small but significant differences from those reported for $LiTbF_4$ by Als-Nielsen et al. (1975).

1.20. The crystal structure of NdF_3

(B. Lebech, L. Nielsen*, R.G. Hazell**, R. Nevald* (*Technical University of Denmark) and F. Krebs Larsen** (**University of Århus, Denmark))

It is generally assumed that the four LnF_3 (Ln = La, Ce, Pr, and Nd) are isostructural with the mineral tysonite. Since 1931 (Oftedal, 1931), numerous attempts have been made to determine this structure. From x-ray studies the following four space groups have been suggested for tysonite: $D_{6h}^3(P6_3/mcm)$, $D_{6h}^4(P6_3/mmc)$, $C_{6v}^3(P6_3cm)$ and $D_{3d}^4(P3/C1)$. More recently (Nielsen, 1981), a fifth space group ($D_{3h}^2(P6C2)$) was suggested to explain the ^{19}F-NMR spectra of NdF_3.

In view of the controversy about the crystal structure of the chemically simple LnF_3 compounds, it was found worthwhile to attempt a determination of the crystal structure of NdF_3. Using the newly installed four-circle neutron diffractometer (1.40) a set of structure factors to be used for structure refinement was collected at room temperature, using incident neutrons of wavelength 0.8 Å on a ~ 6 mm diameter single crystal sphere of NdF_3.

A preliminary structure refinement of this data set has limited possible space groups from five to two, namely $C_{6v}^3(P6_3cm)$ and

D_{3d}^4(P3/c). For C_{6v}^3 the refinement, using anisotropic temperature factors, results in R(F) = 6.4% while D_{3d}^4 (with anisotropic temperature factors) gives R(F) = 14%. However, by introducing twinning of the D_{3d}^4 structure, the R-factor can be reduced to R(F) = 4.2%. Because the R-factor of D_{3d}^4 (twin) is slightly better that of C_{6v}^3, we suggest that the crystal structure of NdF_3 maybe the twinned trigonal structure described by the space group D_{3d}^4.

1.21. The crystal structure of YbD_2 and YbH_2

(B. Lebech, N. Hessel Andersen, S. Steenstrup, (University of Copenhagen, Denmark) and A. Schrøder Pedersen (Metallurgy Department, Risø))

It has been suggested that Yb in orthorhombic YbH_2 should undergo a transition at moderate pressure from the divalent to a trivalent state and that this transition might be followed by a change to the fluorite structure characteristic of the trivalent rare-earth hydrides. Recently, it was found by x-ray diffraction (Olsen et al., 1981b, see also 1.22) that a structural transition does indeed take place at ~ 14 GPa. However, the transition is from the othorhombic structure to a hexagonal close

Table 2. Atomic positions in YbD_2 and YbH_2. The structure is D_{2h}^{16}-Pnma and all atoms occupy (4c) positions.

Substance	Atom	X	Y	Z
	D(I)	0.3524	1/4	0.4282
YbD_2	D(II)	-0.0385	1/4	0.6843
	Yb	0.2472	1/4	0.1120
	H(I)	0.3429	1/4	0.4133
YbH_2	H(II)	-0.0033	1/4	0.6592
	Yb	0.2380	1/4	0.1100

packed structure. In order to achieve a better understanding of this transition and to establish the previously undetermined hydrogen position, neutron diffraction studies of YbD_2 and YbH_2 powder were made at room temperature. The neutron diffraction data were collected using incident neutrons of wavelength 1.43 Å

and a triple-axis spectrometer in the elastic mode. The data were analysed using a Risø version of the EDINP powder profile refinement program (Pawley et al., 1977). The analysis confirmed that at room temperature the structures of YbD_2 and YbH_2 are isostructural with orthorhombic CaH_2 (D_{2h}^{16}-Pnma) (Bergsma and Loopstra, 1962) in agreement with the suggestion of Warf and Hardcastle (1966). The results of a preliminary structure analysis are listed in Table 2. The hydrogen and deuterium positions are similar to those assumed for CaH_2 by Bergsma and Loopstra (1962). Figure 12 shows a comparison between the observed and calculated diffraction patterns for YbD_2.

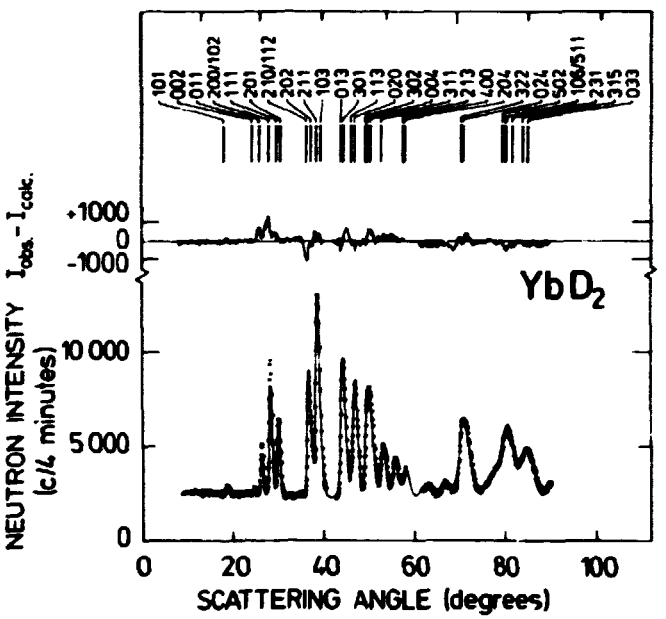

Fig. 12. Comparison between the observed (•) and calculated (solid curve) diffraction patterns of YbD_2. The solid curve in the upper part of the figure shows the difference between the observed and calculated patterns.

1.22. High pressure phase transformation of YbH_2

(J. Staun Olsen*, B. Buras, L. Gerward (Technical University of Denmark), B. Johansson (University of Aarhus, Denmark), B. Lebech, H. Skriver and S. Steenstrup* (*University of Copenhagen, Denmark))

In several rare-earth compounds and intermetallics the valence state of the rare-earth ion may be changed between the $4f^n (5d\ 6s)^2$ and $4f^{n-1} (5d\ 6s)^3$ configuration by chemical manipulation or by application of high pressure (see for example Jayaraman, 1979). Therefore, the structure of YbH_2 has previously (Buras et al., 1980) been studied at pressures up to 7 GPa and no phase transformation was found. Now we have extended the study, and used a diamond anvil high pressure cell capable of producing pressures up to about 30 GPa. The YbH_2 powder sample (200 μm in diameter and 80 μm thick) was enclosed in an Inconel gasket. A 4:1 methanol-ethanol mixture and a ruby were added to the powder to allow for hydrostatic pressure conditions and a proper pressure calibration, respectively.

The study was made at HASYLAB-DESY (Hamburg) using synchrotron radiation. The electron energy was 4 GeV and the time averaged electron current was between 20 and 40 mA. The white-beam energy-dispersive diffractometer (Staun Olsen et al., 1981a) and the triple-axis spectrometer (Als-Nielsen et al., 1980) working in the energy-dispersive mode were used. The exposure time was usually 500 s for each diffraction spectrum. The x-ray pattern, obtained at 28.2 GPa pressure, is shown in Fig. 13. (Note the absence of inconel lines which is due to the extreme collimation of the incident beam and to the precise remotely controlled movements of the diffractometer).

The structure of YbH_2 at atmospheric pressure is orthorhombic a = 5.898 Å, b = 3.576 Å, c = 6.765 Å D_{2h}^{16}-Pnma; but can be viewed as a distorted hexagonal structure (see 1.21).
As can be seen from Fig. 13, YbH_2 at 28.2 GPa has a different structure and the reflections can be indexed using a hexagonal close packed unit cell. Measurements at intermediate pressures show that the structural transformation occurs at about 15.0

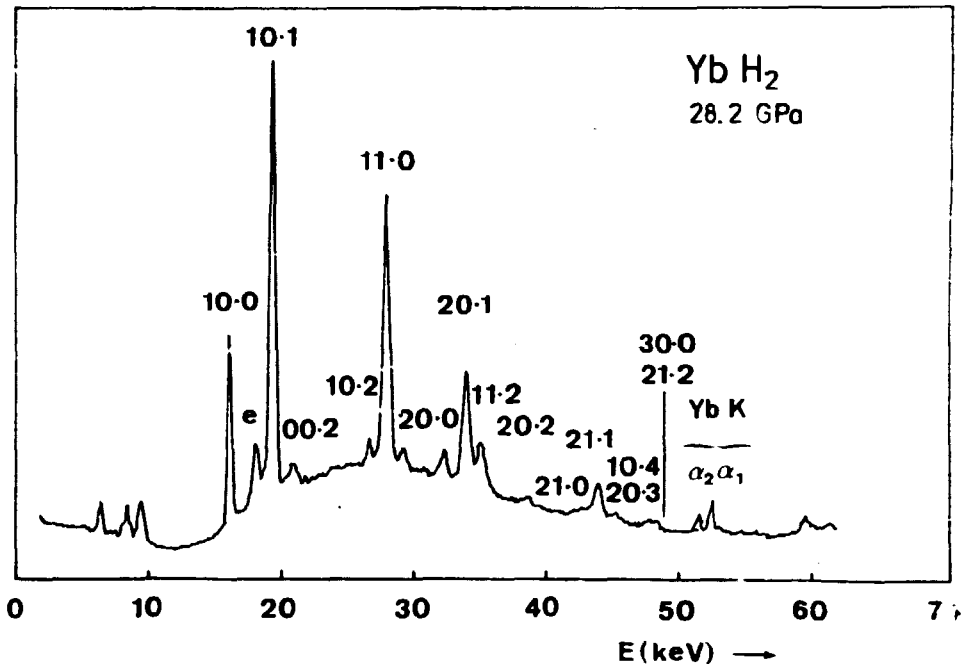

Fig. 13. X-ray energy-dispersive diffraction patterns of YbH_2 at atmospheric pressure and at 28.2 GPa ($2\theta = 14.5^{o}$). The data were taken at DORIS/HASYLAB. The beam parameters were: 4 GeV, 30 mA, 20 bunches.

GPa and at this pressure a = 3.614 Å and c = 4.848 Å. The transition is accompanied by a sudden decrease of the unit cell volume of about 5.4%. This may be caused by a valence change of the Yb-ion, an assumption that can be verified or rejected by absorption measurements which are under way. (For further details see Olsen et al., 1981b). This may be due to a change of the valence state of the Yb ion.

From a purely crystallographic point of view the transformation can be understood as a transition from a distorted hexagonal structure, mentioned above, to a hexagonal close-packed structure involving plausible movements of Yb and H ions. This interpretation is supported by the recent study of the YbH_2 structure at atmospheric pressure giving the positions of both the Yb and H ions (see 1.21).

Besides the physical results the study has clearly demonstrated the great advantage of x-ray energy-dispersive diffraction with synchrotron radiation for high pressure studies using a diamond cell.

1.23. Soft mode and structural phase transition in $Cs_2NaNdCl_6$

(G.P. Knudsen (Technical University of Denmark) and J.K. Kjems)

The materials $Cs_2NaLnCl_6$, where Ln is an element of the lanthanide series, crystallize in the face centered cubic elpasolite structure. The crystals with light lanthanide ions undergo a structural phase transition to tetragonal symmetry (Nevald et al. 1979, Knudsen et al. 1982). The transition temperature for the Nd-compound is 136 K.

The elpasolite structure is related to the perovskite structure and the antifluorite structure. Similar phase transitions are found in these materials (Lynn et al. 1978). The transition is caused by a condensation of the Γ_{25} mode (in this case corresponding to a rotation of the $LnCl_6^{3-}$ octahedra) either at the zone boundary or at the zone centre. It would be obvious to assume that a soft mode associates the phase transition in $Cs_2NaNdCl_6$ too.

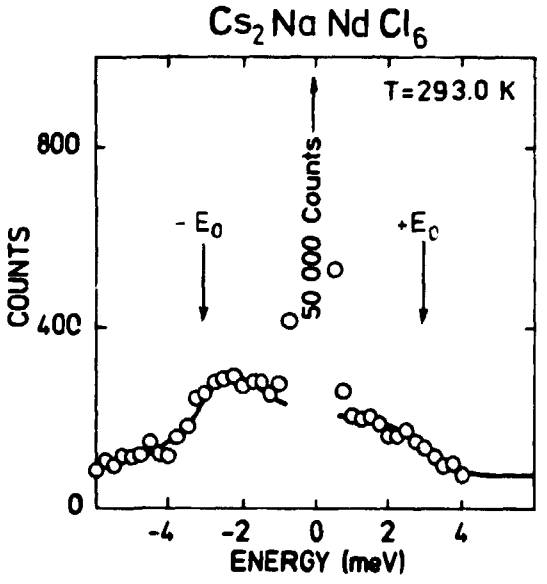

Fig. 14. Constant q scan at the zone centre at room temperature in $Cs_2NaNdCl_6$. The scattering centered at E = 0 is due to the (3,3,5) Bragg reflection. Two phonons (annihilation and creation) are observed at E_0 = ±3 meV, where E_0 is determined from fits (see 1.23) to the experimental data.

Neutron scattering measurements were carried out on the triple-axis spectrometer TAS I using 13.8 meV as incident neutron energy. With this energy it is possible to reach the reciprocal lattice point (3,3,5), around which the phonon structure factor

is relative large, and the energy resolution is still good enough. The result of a constant q scan is shown in Fig. 14. The two phonons (annihilation and creation) are damped. From fits damped phonons of the experimentally measured phonons at different temperatures, it is found that the square of the phonon energies follow approximately a Curie-Weiss law, except near the transition temperature of (136 K). Our measurements show that the phase transition in $Cs_2NaNdCl_6$ is driven by a zone centre soft mode. This mode is the rotation of the $NdCl_6^{3-}$ octahedra. We believe that the similar transitions observed in the elpasolite compounds formed by the other light lanthanides are caused by the same soft mode.

1.24. Smectic-A surface of the nematic and isotropic bulk phase

(J. Als-Nielsen, F. Christensen and P.S. Pershan (Harvard University, Massachusetts, USA))

The combination of a free surface and a parallel planar rigid surface with homeotropic alignment of the molecules will naturally expel mobile defects and may thus provide a dislocation-free smectic-A phase (Pershan, 1974). The fluid samples must be kept horizontal and the corresponding scattering geometry is shown in Fig. 15. The monochromatic beam of wave vector $\vec{k}$ is bent though the angle θ_s downwards by tilting the monochromator (a 3 bounce channel cut Si(1,1,1) crystal) by an angle $t = (k/\tau_{111})\theta_s$.

Horizontal smectic layers with layer spacing d will reflect this beam when $Q_o = (2\pi/d) = 2k\sin\theta_s \approx 2k\theta_s = 2\tau_{111}t$. Note that this Bragg condition is independent of wavelength for small angles. An analyzer symmetric with the monochromator gives a horizontal beam being detected in the position sensitive detector (PSD). A finite lateral correlation of the layers can be observed by rotating the analyser around a vertical axis, the limit of transverse correlation (15000 Å) being determined by the Darwin width of the monochromator and analyzer crystals.

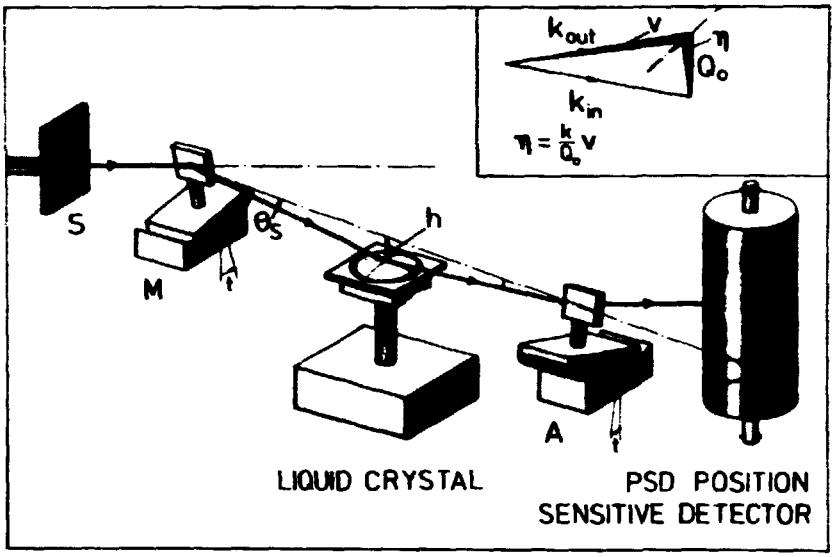

Fig. 15. Experimental set-up for study of the surface of a fluid, in this case the liquid crystal 8OCB. The inset shows the scattering geometry in reciprocal space.

We found that the boundary condition at the air surface interface is so strong that smectic layers, of a lateral extent larger than 15000 Å, are formed at the surface in the nematic phase. The penetration depth ξ_z grows as the temperature is decreased throughout the nematic phase and ξ_z diverges at the nematic to smectic-A transition temperature T_{AN}.

The temperature dependence of ξ_z may be understood from phenomenological Landau theory. In terms of the smectic order parameter the free energy density is of the form (de Gennes 1972):

$$F = A|\psi|^2 + \gamma[(\partial/\partial z - iQ_o)\psi]^2 + \ldots \qquad (1)$$

In the Landau theory A varies linearly with $(T-T_{AN})$ yielding a spontaneous smectic-A phase below T_{AN} and critical fluctuations above T_{AN} with a longitudinal correlation range $\xi_{11} = (\gamma/A)^{1/2}$. The divergence of ξ_{11} has been determined previously for bulk 8OCB (Litster et al., 1979) Assuming that the free surface is equivalent to a boundary condition of $\psi = \psi_o$ at $z = 0$, the z-dependence of ψ is found by minimatization of the volume integral of the free energy density:

$$\psi = \psi_0 \exp[-z(iQ_0 + \xi_z^{-1})] \quad , \quad \xi_z \ (\gamma/A)^{1/2} \qquad (2)$$

i.e. ξ_z is expected to be identical to $\xi_{||}$. Figure 16 shows that this is indeed the case.

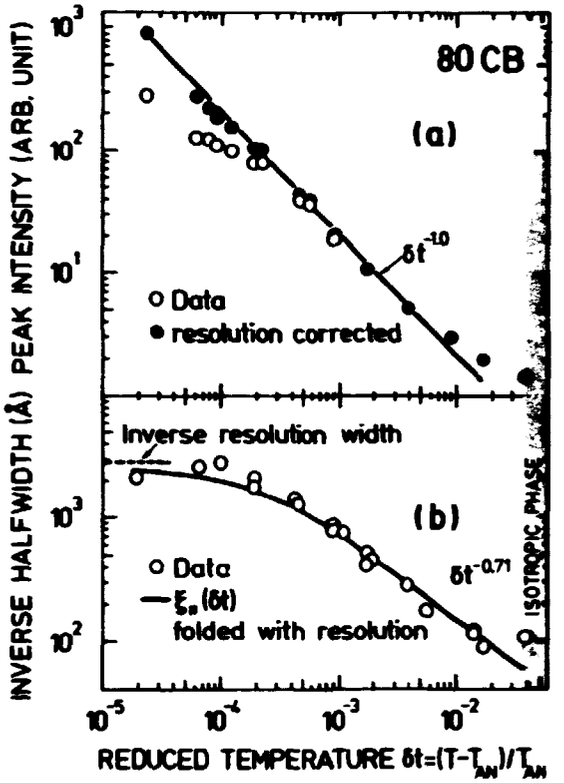

Fig. 16. Peak intensity (a) and inverse half-width (b) versus reduced temperature in 80CB. In (b), the penetration depth ξ_z is compared to the bulk longitudinal correlation range $\xi_{||}$ (Lister et al., 1979).

In the smectic-A phase we find that the layers are perfectly aligned, the Bragg reflection is specular, and dynamical rather than kinematical diffraction theory must be applied. Our present finding leads naturally to a number of future investigations:

(i) Measurement of the order parameter on an absolute scale by comparison with total relection intensities at smaller angles.

(ii) Detailed line shape studies of melting from the A to N phase.

(iii) Do smectic-A boundary layers occur in materials, which do not have a spontaneous smectic-A phase?

(iv) Studies of correlations <u>within</u> the smectic-A planes as the transition to the smectic-B phase is approached.

1.25. Hexagonal layer stacking in the smectic-B phase of 7O.7

(J. Collett*, P.S. Pershan* (*Harvard University, Massachusetts, USA) J.D. Litster (Massachusetts Institute of Technology, Massachusetts, USA) and J. Als-Nielsen)

It has been known for some time that good alignment of smectic layers can be obtained by freely suspended films (Young et al. 1978). Synchrotron x-ray studies on such films in a geometry described in Fig. 16a was first carried out by Moncton and Pindak (1980) at Standard Synchrotron Radiation Laboratory, California. Among other things their results showed very clearly that the smectic-B phase of 4O.8 was a crystalline one with ABAB ... stacking of layers. We have investigated stacking structures of the related compound 7O.7 with the chemical formula: $C_7H_{15}O$-Ø-CH = N-Ø-C_7H_{15}, where Ø denotes a benzene ring. The film is drawn like a soap bubble across a 7 mm diameter hole in a glass plate situated in a vacuum furnace. The film thickness is determined optically. The film can be rotated in its plane so one of the hexagonal axes is brought into the horizontal scattering plane. The incident wave vector k_{in} was obtained by Bragg reflecting the synchrotron beam from a (1,1,1) plane of a Ge crystal. The direction of the scattered beam with wave vector k_{out} was similarly determined by Bragg reflection from the (1,1,1) plane of a Ge analyzer crystal (Fig. 17a).

Figure 17b shows the ABAB ... hexagonal stacking, which can be thought of as two simple hexagonal sublattices displaced by: $\overrightarrow{O_AO_B} = (\vec{a}_1 + \vec{a}_2)/3$. The geometrical form factor given in Fig. 17b follows immediately, and the diffraction pattern in a $(1,0,\bar{1},1)$ scan at the upper right is indeed consistent with this structure when it is borne in mind that the intensities also involve the molecular form factor and the Debye-Waller factor. The cross hatched part of the spectrum is the thermal diffuse scattering. Note the logarithmic intensity scale spanning over five decades. (The value of h in Fig. 17c is not exactly 1 because the line-up was carried out at a different temperature where the size of a_1 was slightly larger).

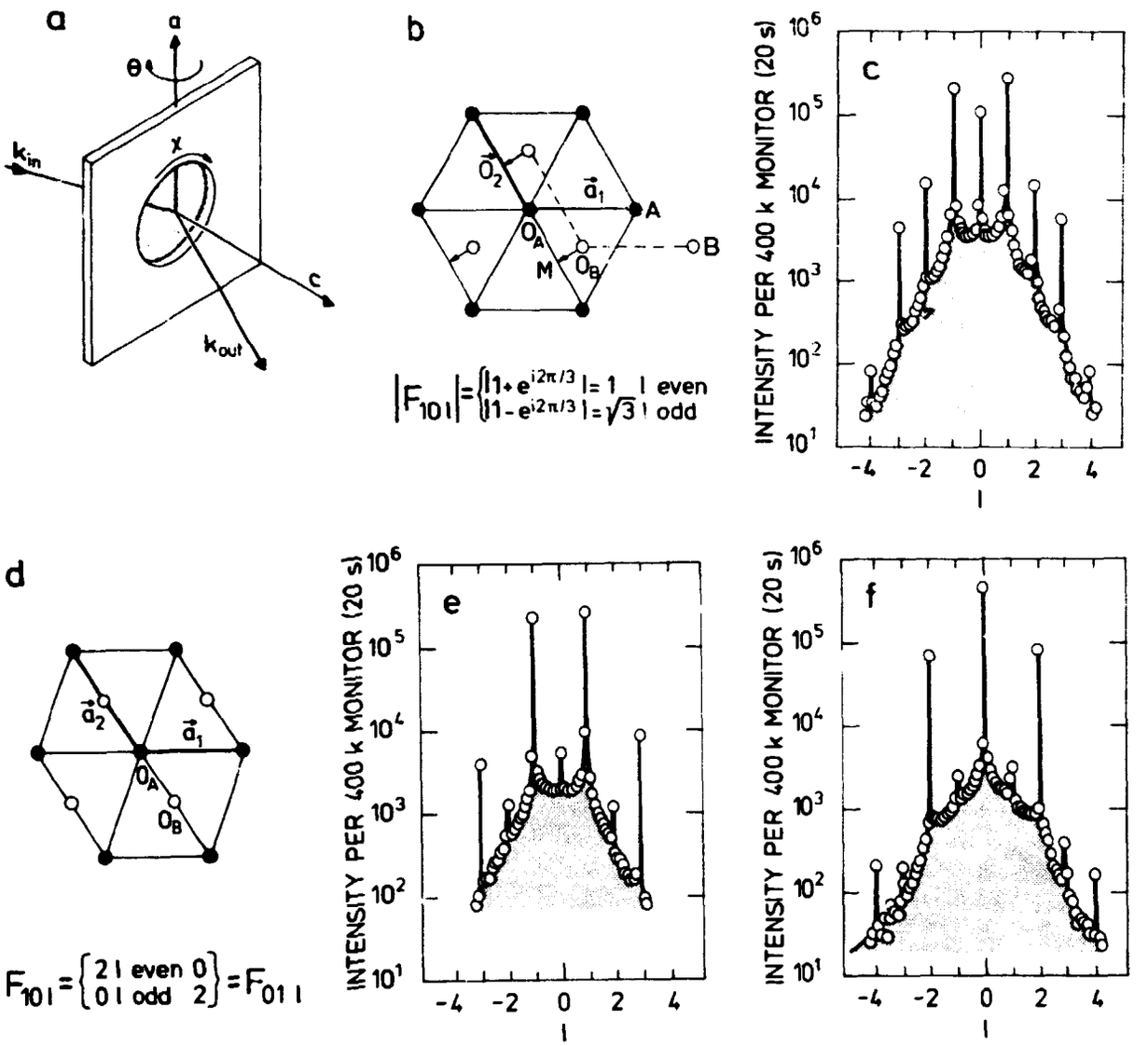

Fig. 17. Experimental details and results of the high resolution x-ray study of hexagonal layer stacking in the smectic-B phase of 70.7 (see 1.25 for details).

The lower part of Fig. 17 shows a different structure occurring at a lower temperature. The h = 1 ridge with Bragg peaks at all integral values of ℓ splits into a h > 1 ridge with only even-ℓ Bragg peaks and a h < 1 ridge with only odd-ℓ Bragg peaks. Note that the ridge-splitting is only $0.0013a^* \approx 0.002$ Å^{-1} and requires the resolution provided by the two perfect Ge-crystals in the triple-axis spectrometer to be seen. We interpret this pattern as a sliding of the B sublattice, so the origo O_B goes to the mid-position M between adjacent A lattice points. The hexagonal symmetry is thereby broken, as seen in Fig. 17d with

$|a_2| > |a_1|$. The geometrical structure factor, or the selection rules, are indeed consistent with the two diffraction patterns shown at the bottom right. The transition between the two structures was found to be of first order. Other structures were also found.

1.26. Pressure-induced commensurate-incommensurate transition in Kr-monolayers on graphite

(M. Nielsen, J. Als-Nielsen, J. Bohr, and J.P. McTague, (University of California, Los Angeles, California, USA))

In recent years thin films of physisorbed rare gases on graphite substrates have been studied extensively. They are model systems in studies of phase transitions in two dimensions. The solid phase may be commensurate with the underlying graphite honeycomb lattice as shown in the top part of Fig. 18 where the rare gas atom occupies every third carbon hexagon (the $\sqrt{3}\times\sqrt{3}$ R 30° structure) or incommensurate as shown in the bottom part of Fig. 18. In the case of Kr, a commensurate-incommensurate transition takes place versus coverage or applied two-dimensional pressure (see below). In 1.27 we describe a study of two-dimensional melting of rare gases physisorbed on graphite, primarily of Ar.

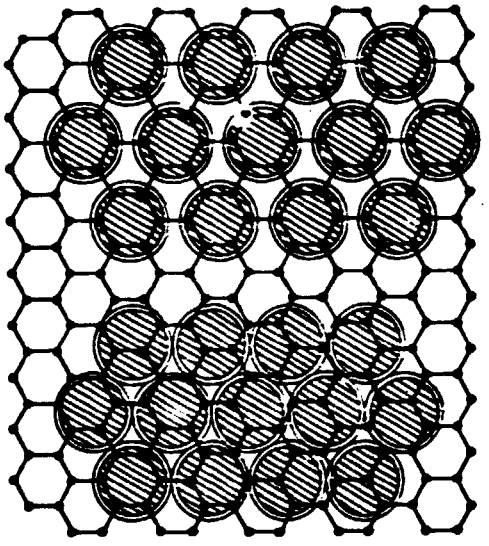

Fig. 18. Commensurate and incommensurate solid phases on graphite.

In 1.28 and 1.29 we describe diffraction studies of two-component mixtures and monolayers of CF_4. In all cases we used the set-up shown in Fig. 19. A double-crystal monochromator of 2 Ge(111) crystals is used in order to eliminate higher order contamination by misaligning the two crystals slightly. The graphite substrate, UCAR ZYX, has ideally flat surface areas of a linear extent of about 2000 Å. The angular spectrum of scattered radiation is recorded by a position-sensitive detector.

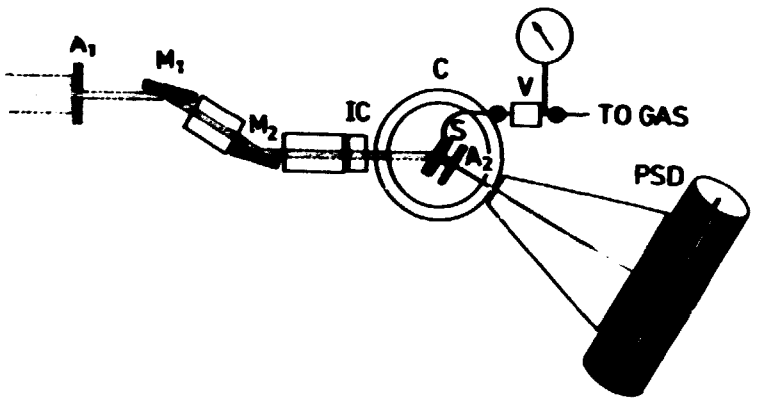

Fig. 19. Experimental set-up for the x-ray studies of physisorbed monolayers. Note that the spectrometer operates in the horizontal plane.

Sub-monolayers of Kr physisorbed on graphite have the commensurate $\sqrt{3}\times\sqrt{3}$ R 30° structure as shown in the top part of Fig. 18. When more Kr is adsorbed the film undergoes a commensurate-incommensurate transition to a structure with smaller lattice parameters. This phase transition has been subject of much experimental (Chinn and Fain, 1977 and Stephens et al., 1979) and theoretical (Villain, 1980) interest. LEED and x-ray diffraction measurements indicate that the transition is continuous at $T > 52$ K, although recent high-resolution synchrotron diffraction data show additional features (Moncton et al., 1982).

In order to extend the study to lower temperatures we have used a new technique to induce the transition and by synchrotron diffraction followed the structural change. By adding D_2 gas, which is insoluble in the Kr film we can apply a two dimensional

(2-D) spreading pressure, which can be controlled by adjusting the D_2 bulk vapour pressure. The D_2 gas pressure thus acts as a 2-D piston pushing on the Kr film. Later experiments using Ne instead of D_2 yielded identical results.

Figure 20 shows some results: three diffraction groups measured around the (1,0) Bragg position. A major result of our measurements is that the commensurate-incommensurate transition is proved to be of first order at low temperatures. In the upper two panels Fig. 20 shows profiles, which we interprete to be the sum of the scattering from the two components in the transition region where the phases coexist. The commensurate phase gives a

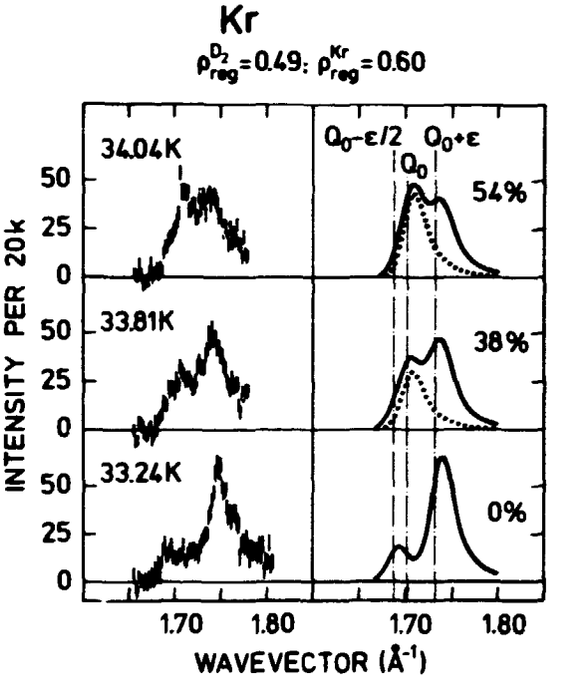

Fig. 20. Diffraction groups near the (1,0) reflection of Kr-monolayers adsorbed on graphite measured in the coexistence region of the commensurate-incommensurate transition. The coverages, ρ, of Kr and D_2, are given in units of a monolayer of the commensurate structure. The curves to the right are calculated. The relative intensity of the commensurate peak, shown by dots, is given in percentage.

single peak centered at the wave vector position $Q = 1.703$ Å^{-1}. The incommensurate phase gives a dominant peak at $Q = 1.733$ Å^{-1}. In addition it has a smaller "satellite" at a smaller value of

Q, which originates from a modulation in the layer density imposed on the adsorbed film from the substrate atoms.

The lowest part of Fig. 20 shows the response when the transition is completed, and we have a pure incommensurate phase. The curves in the right-hand part of the Fig. 20 show calculated profiles assuming that the transition occurs through coexisting phases. In the case shown, the spreading pressure of the D_2 gas on the Kr-film is varied by changing the temperature while keeping the gas fillings constant. With increasing temperature, the spreading pressure decreases as some of the adsorbed D_2 molecules desorbe.

As another typical first-order characteristic, the commensurate-incommensurate transition showed distinct hysteresis. This is illustrated in Fig. 21, where the intensity of the (1,0) Bragg peak of the commensurate component alone, is plotted for increasing and decreasing spreading pressure going through the tran-

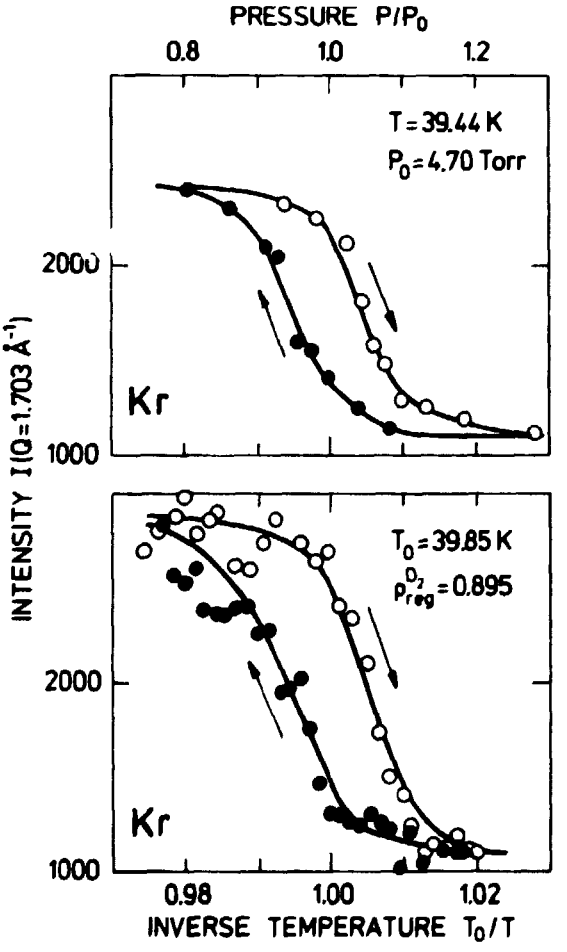

Fig. 21. Hysteresis loop of the commensurate-incommensurate transition in Kr-monolayers adsorbed on graphite. The intensity of the commensurate phase peak at Q = 1.703 $Å^{-1}$ is monitored (at constant temperature) as function of increasing and decreasing spreading pressure.

sition region. D_2 gas was chosen in these measurements as the pushing gas, rather than H_2, because this allows us to make complementary measurements with neutron scattering looking at the state of the adsorbed D_2 molecules. Such studies are in progress.

1.27. Melting of two-dimensional crystals

(M. Nielsen, J. Als-Nielsen, J. Bohr and J.P. McTague
(University of California, Los Angeles, California, USA))

In short we expect the following behaviour of an ideal two dimensional (2-D) system: At low temperatures the atoms will crystallize in an ordered structure observable through diffraction peaks at the 2-D reciprocal lattice positions. These peaks are not delta-functions in character as for 3-D crystals but have broad wings. The transitions from the 2-D solid to an isotropic 2-D fluid may occur either through a single first order melting process, as for 3-D systems, or through a second order transition to a new phase called hexatic followed (at a higher temperature) by a first order hexatic to isotropic fluid transition. This is described in the Kosterlitz-Thouless-Halperin-Nelson (KTHN) theory (Halperin and Nelson 1979). The hexatic phase is a 2-D fluid with an orientational ordering of the bond directions between the atoms; its diffraction signature is fluid-like scattering functions but centred around reciprocal lattice positions.

All rare gases have the simple triangular (or hexagonal) structure at low temperatures in the adsorbed phase on graphite. For Kr-monolayers the two lattices are in registry as shown in Fig. 18 Ar-monolayers are about 8% too concentrated and Xe-monolayers about 8% too dilute to fit this registry. Physically the two kind of monolayers are very different, the commensurate Kr-layers are laterally locked to the substrate whereas the incommensurate Ar- and Xe-layers are free floating, and to a first approximation we expect that they melt like ideal 2-D systems.

Figures 22 and 23 show some of our results. We follow the diffraction group at the (1,0) position of the films as a function

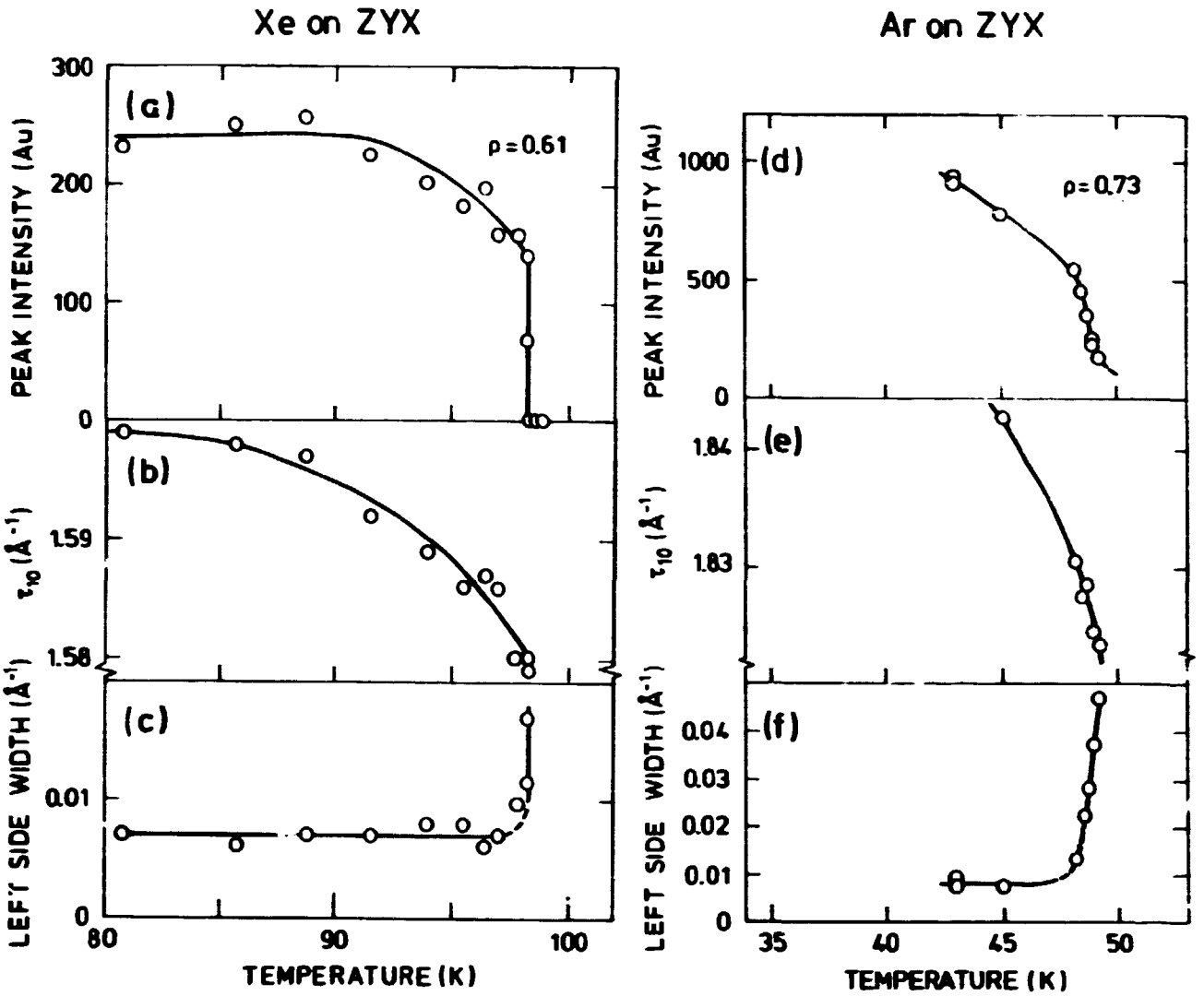

Fig. 22. Disappearance of the (1,0) Bragg peak with increasing temperature for adsorbed sub-monolayers of Xe and Ar on graphite. a, b, d and e show intensities and positions of the Bragg peak, c and f the widths of their left-hand sides.

of temperature. Our main conclusion is that for Ar-monolayers, with coverages less than one complete monolayer, the groups continuously lose peak intensity and get broader around 48 K, whereas for Xe-films (of the same coverage) the diffraction groups discontinuously disappear at T = 98 K. The interpretation of this is that the observed Ar-transition is continuous, melting presumably to a hexatic phase, and the Xe-transition is first order melting to an isotropic fluid. We are unable, to give the final proof of this, however, because it must include a detailed analysis of the measured line shape as described in the KTHN theory in order to check the temperature dependence

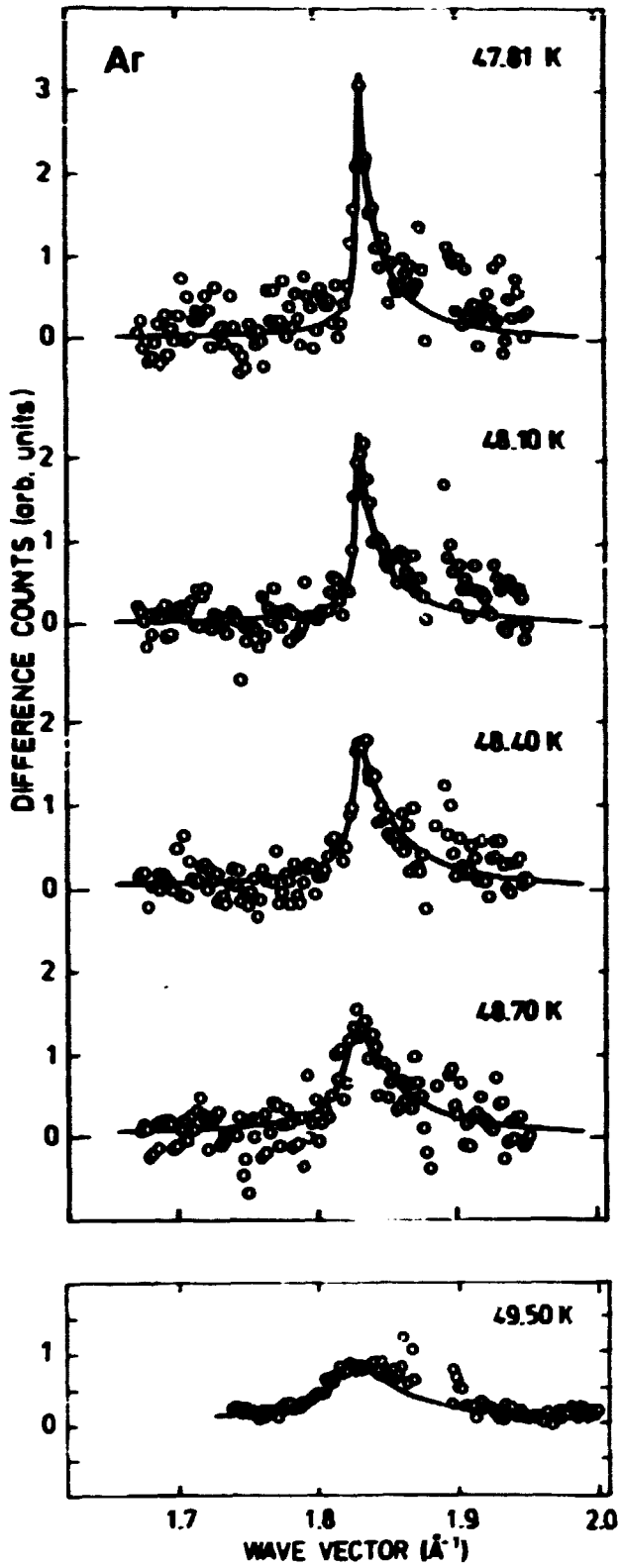

Fig. 23. Measured Bragg peak profiles at the (1,0) reflection of Ar monolayers on graphite. The upper four panels show the results obtained with synchrotron x-rays and with the average Ar-layer density = 0.83. The lower panel data were measured with a rotating x-ray source and with ρ = 0.93. The curves are calculated line shapes.

of the parameters involved. To do this we need still higher intensity. The fundamental question is: Why do the sub-monolayers of Ar and Xe, both having a typical incommensurate structure, melt in a qualitatively different way.

1.28. Two-component mixtures in the physisorbed monolayers on graphite

(J. Bohr, M. Nielsen and J. Als-Nielsen)

With the same diffraction technique as described in 1.26 we have studied the 2-D structures of the mixtures: Ar + Xe, Kr + Xe and CH_4 + Xe adsorbed on the ZYX-substrate. Data were taken in the coverage range (1/3 to 2 monolayers) as functions of composition and temperature.

Our main interest in this study is a search for fundamental phase transitions like ordering-disordering of the 2-D alloys or phase separation in the mixtures. The basic feature of our results is a large tendency to form $\sqrt{3}\times\sqrt{3}$ R 30° commensurate alloys, but no evidence for ordered alloys has been observed for temperatures down to 11 K. Also, incommensurate alloys are observed and these show the same lack of ordering down to 11 K. The commensurate-incommensurate transitions are of first order and distinct coexisting phases are found. From incommensurate monolayers with densities approaching the commensurate density the diffraction show strong satelites originating from domain super-structures. This suggests that fluctuations in chemical composition follow the domain formation. Melting of the 2-D alloys is studied in the Ar + Xe system. Near the 50-50% alloy the melting takes place through strongly correlated liquid structures.

1.29. Structure of CF_4 monolayers on graphite

(K. Kjær, J. Bohr, M. Nielsen, H.J. Lauter (Ill, Grenoble, France) and J.P. McTague (University of California, Los Angeles, California, U.S.A.))

With the same technique as described in 1.26 we have studied the structures of different phases of CF_4 monolayers on graphite. At low coverages they have a (2×2) registered structure below the melting temperature and two new phases at lower temperatures. The (2×2) structure has one CF_4 molecule per four carbon hexagons of the graphite surface. Furthermore the adsorption sites are

above the vertex points of the honeycomb structure, where the symmetry differs from that at the centre of hexagons. Both factors influence the nature of the commensurate-incommensurate and melting transitions.

We have so far mapped out the solid part of the phase diagram of the monolayers and identified four different ordered structures. Of particular interest is the commensurate-incommensurate transition from the (2×2) structure, which seems to be continuous and involves an uniaxial distortion.

1.30. Neutron scattering from ^{4}He physisorbed on (0,0,2) graphile surfaces

(K. Carneiro, L. Passell[+], W. Thomlinson[+] ([+]Brookhaven National Laboratory, New York, USA) and H. Taub (University of Missouri, Missouri, USA))

In continuation of earlier studies of neutron diffraction from a single atomic layer of ^{4}He adsorbed on grafoil (Carneiro et al., 1976), several layers were studied (Fig. 24). In agreement with specific heat studies (Bretz, 1973) it is demonstrated that the first layer solidifies in a dense triangular lattice, whereas the second crystallises in a less-dense lattice only when some ^{4}He is present in a third layer. The third and subsequent layers do not solidify. Unfortunately the details of the interplay between the first and second atomic layers cannot be resolved due to the limited number of Bragg peaks that can be observed.

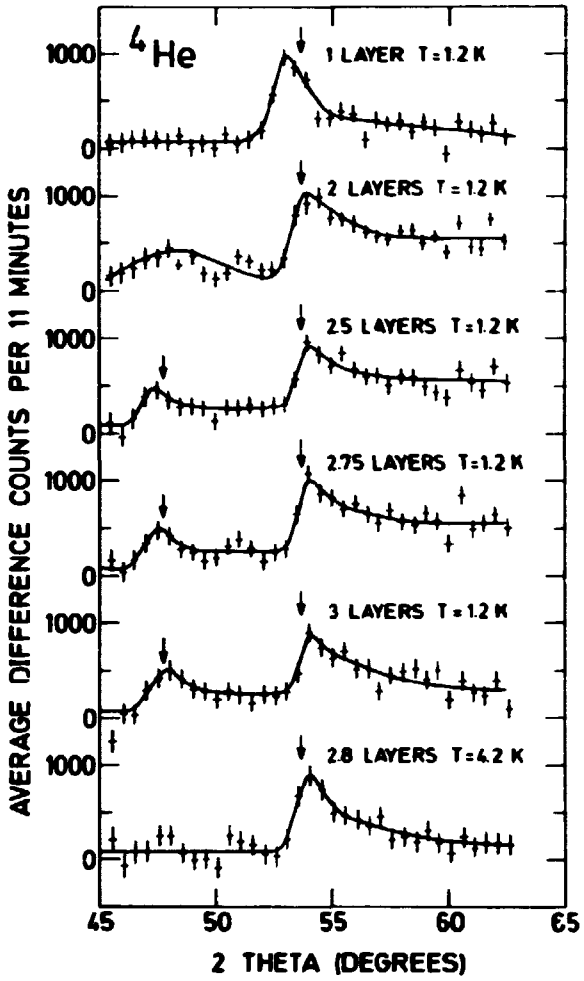

Fig. 24. Coverage dependence of difference diffraction profiles from ^{4}He films adsorbed on grafoil. The arrows identify peak positions expected from heat capacity determinations of the layer densities. The heat-capacity data indicate that the second layer is melted at 4.2 K. The solid lines are guides to the eye.

1.31. Dynamic texture measurements using neutron diffraction

(D. Juul Jensen, J. Kjems, T. Leffers* and N. Hansen*
(*Metallurgy Department, Risø))

The development of a facility for dynamic texture measurements, e.g. recrystallization kinetics, was continued. At present, the equipment is a modified triple axis spectrometer where the sample table is replaced by an Euler goniometer, which offers the possibility of setting the sample in any desired orientation under automatical control. The analyser part is replaced by a linear position sensitive detector placed in the Debye-Sherrer plane ($2\theta = 90^{o}$) covering an angle of 51 degrees.

The preferred orientations of the crystallites in a textured material is commonly described by a stereographic projection refered to as a pole figure. The pole figure is a map of the

statistical distribution of the normals to given {h,k,l}-planes. With the counter fixed at a scattering angle 2θ corresponding to the plane under investigation, the intensity in any point of the pole figure is proportional to the volume of the crystallites with the corresponding orientation. The procedure for investigation of dynamical properties is simply to record a number of pole figures while a dynamic process is taking place.

With a Cu-sample (~ 2 cm^3), a quarter of a pole figure based on 61×19 sampling points, each covering a solid angle of $8 \cdot 10^{-4}$ steradians, can be recorded in fourteen minutes with a typical accuracy due to counting statistics of 2-3%. Out of these fourteen minutes only three are spent counting while the remaining eleven minutes are used to change the sample orientation.

The study of recrystallization kinetics requires a rapid change of temperature. For this purpose a heating system has been developed, whereby the sample is heated by a jet of hot air. With a distance of 1 cm between the sample and "hot-air-blower", 250°C can be reached within one minute and the temperature kept constant within 1°C. Because of the fast heating rate, the system is well suited for kinetic investigations.

The first recrystallization experiments were carried out with samples of fine (~ 35 μ) and coarse grained (0.5-1 mm) 99.99% pure copper. Both materials were rolled to 95% reduction, i.e. the thickness of the Cu plate has been reduced to 5% of its original value. There are some quantitative differences between the rolling texture of the fine- and the coarse-grained material. (see Fig. 25) which is in agreement with earlier observations (Leffers, 1974). The two materials behave differently during recrystallization, and they develop quite different recrystallization textures, as shown in Fig. 24. The fine-grained material, shows a fairly strong cubic texture, whereas the texture is less pronounced for the coarse-grained material.

On the basis of the {2,0,0} pole figures recorded during recrystallization, we have analyzed the temporal evolution of the pole-densities PD(t) (normalized intensities) integrated over the

areas shown in Fig. 25. PD(t) is fitted to the following expression:

$$PD(t) = k_1 - (\exp - k_2 t^{\beta}) ,$$

where k_1, k_2 and β are fitting parameters, and t is the time. The resulting β-values are close to one. This means that even though the recrystallization processes in the two materials lead to quite different recrystallization textures (see Fig. 25), they have very similar kinetics.

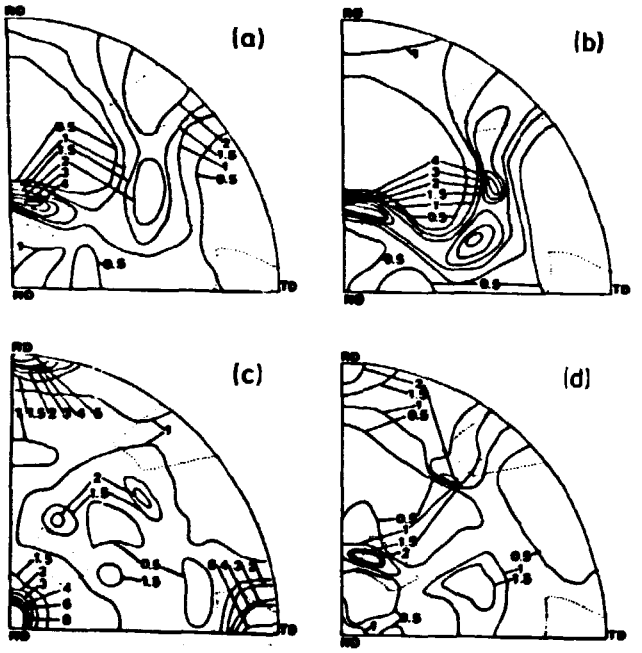

Fig. 25. Quarter {2,0,0} pole figure for Cu/roled to 95% (a and b) and recrystallized Cu (c and d). Fine (a and c), coarse-grained material (b and d).

1.32. EXAFS investigations of hydro-desulfurization catalysts

(B.S. Clausen,* H. Topsøe,* R. Candia,* J. Villadsen*
(*Haldor Topsøe Research Laboratories, Lyngby), B. Lengeler
(IFF, Jülich, F.R.G.), J. Als-Nielsen and F. Christensen)

By analyzing the extended X-ray absorption fine structure (EXAFS) of the Mo absorption edge, we have obtained structural information about both calcined and sulfided Mo/Al_2O_3 and

Co-Mo/Al_2O_3 catalysts. The calcined catalysts show only one strong backscatter peak in the radial distribution function, which indicates that Mo is present in highly disordered structures. When the catalysts are sulfided, an ordering of the resulting Mo-containing phase takes place, as evidenced by the observation of a contribution from a second coordination shell as well. From a comparison with EXAFS data for well-crystallized MoS_2, it is concluded that the Mo atoms in the sulfided catalysts are present in MoS_2-like structures. Furthermore, from an analysis of the amplitudes of the peaks, it is concluded that the MoS_2-like structures are ordered in very small domains. The results show for both the calcined and the sulfided states that the surroundings of the Mo atoms are not greatly influenced by the presence of the Co promoter atoms.

1.33. The structure of the Cu and Zn sites in yeast superoxide dismutase

(R. Bauer, J.C. Phillips (EMBL/DESY, Hamburg, F.R.G.), J.C. Dunbar* and J.T. Johansen* (*Carlsberg Laboratory, Copenhagen))

Extended x-ray absorption fine-structure (EXAFS) spectra have been recorded at the Cu and Zn edges in native yeast superoxide dismutase and at the Cu and Cd edges in the yeast superoxide dismutase derivative where Zn has been substituted by Cd. Two different metal ligand distances in the range 1.9-2.0 Å and 2.3-2.4 Å are determined for the Cu and Zn sites. For Cd at the Zn site, again two different metal ligand distances are detected in this case about 2.2 Å and 2.6 Å, respectively. Two radial distances in the range, 3.7-3.9 Å and 4.2-4.4 Å could in addition be determined for the Cu and Zn sites. The striking feature is the similarity between the amplitudes and radii determined for both the Cu and Zn sites. The increased distances for Cd can be explained by the increased ionic radius of Cd relative to Cu and Zn. We further conclude that the ligand histidine residues must be in an unusually bent position compared to smaller metal complexes with histidines or imidazole. Based upon these EXAFS results we propose an average Zn geometry

of two histidine and one aspartic acid metal ligand at about 2.3 Å and one water molecule and one histidine ligand per enzyme molecule (i.e. a half histidine per metal site) at about an average distance of 1.9 Å. For Cu we propose the same geometry except that the aspartic acid is substituted with a histidine at 2.3 Å.

1.34. Structural information concerning the catalytic metal site in horse liver alcohol dehydrogenase

(I. Andersson (Swedish Agricultural University, Uppsala, Sweden), R. Bauer and I. Demeter (Central Research Institute for Physics, Budapest, Hungary))

Perturbed angular correlation spectra on horse liver alcohol dehydrogenase measured on ^{111}Cd inserted specifically in the catalytic site have been obtained under various conditions. Spectra have been obtained in the pH range 6-9 and in the presence of coenzyme and/or pyrazole or trifluoroethanol. No ionization at the metal site could be detected between pH 6 and 9 irrespective of whether NAD^+ is present or not. From this we conclude that a water molecule ligated to Cd(II) must have a pK of ionization higher than 9.5. Both coenzyme, pyrazole and trifluoroethanol affect the spectra of Cd incorporated in the catalytic site of alcohol dehydrogenase. The interpretation of the present data is consistent with a four coordinated nearly tetrahedral metal geometry, both with and without the coenzyme bound to the enzyme. The effect of the coenzyme on the metal coordination can best be explained by a reduction of the two cysteine metal bond lengths. From an analysis of the data we conclude that both pyrazole and trifluoroethanol enter as a fifth ligand not displacing the solvent ligand to the metal.

1.35. Direct observation of the unstable substrate enzyme complex of ^{111}Cd carboxypeptidase A_α

(R. Bauer and J. Johansen (Carlsberg Research Center, Copenhagen, Denmark))

The active centre of Cd(II) carboxypeptidase during catalysis has been examined by perturbed angular correlation γ-ray spectroscopy. Addition of the substrate Bz-Gly-Gly-L-Phe induces a dramatic change in the coordination sphere of Cd(II). The pseudo-substrate Gly-L-Tyr do also change the coordination sphere of Cd(II) but very differently from the effect of Bz-Gly-Gly-L-Phe. Interpretation of the nuclear quadrupole coupling parameters for Bz-Gly-Gly-L-Phe using the angular overlap model infers that the substrate binds to the metal via a charged oxygen liqand displacing the solvent ligand from the fourth coordination site.

1.36. Evidence for two types of binding sites in Cd metallothionein

(M. Vazák (University of Zürich, Zürich, Switzerland) and R. Bauer)

The metal-binding sites in rabbit metallothionein have been probed by perturbed angular correlation of γ-ray spectroscopy (PAC) using excited ^{111}Cd. The presence of two distinct frequencies, $\omega_1 \sim 120$ and $\omega_2 \sim 580$ MHz, is consistent with the existence of two different coordination geometries for Cd binding in this protein. The 120 MHz frequency is comparable to the 65 MHz frequency displayed by excited ^{111}Cd when substituted for Zn in the slightly distorted tetrahedral structural metal site of horse liver alcohol dehydrogenase. Judged from the greater amplitude of the 120 MHz signal, it would appear that this symmetry type applies to about 80% of all metal-binding sites in metallothionein. The 580 MHz frequency is close to the 880 MHz frequency calculated for the square planar Cd $(Cys\text{-}S)_4^{2-}$ complex and, hence, it could arise from an extremely distorted tetrahedron. Less likely, it could originate also from an octahedral-type complex having two axial carboxylate ligands and yielding a frequency of 640 MHz.

The two frequencies are observed both in partially and fully complexed metallothionein and are, thus, independent of the degree of metal-binding site occupation. Hence, the clustering of the metals in metallothionein, as proposed from homonuclear ^{113}Cd-decoupling experiments and from magnetic studies of the Co(II)-derivative, does not measurably alter the basic coordinative feature of the metal environment.

1.37. Identification of Cd binding sites within living human cells

(A. Bakka*, D.Ø. Eriksen (University of Oslo, Blindern, Norway), H.E. Rugstad* (*National Hospital, Oslo, Norway) and R. Bauer)

For the first time, the spectroscopic technique of perturbed angular correlation of γ-rays (PAC) has been applied to a study of binding modes of Cd(II) in living cells. This method needs only trace amounts of species to obtain structure information about metal binding sites. The cells studied were human epitheloid cells designated HE_{100}, with a high content of the protein metallothionein (MT). PAC studies of MT-bound Cd(II) have successfully been done using pure MT isolated from rabbit liver. The purposes of the present study were to test if it is possible with the PAC technique to get information about Cd(II) binding within living cells with the PAC technique and, if so, to determine which cell components Cd(II) is bound to. The results showed that (i) the PAC technique is capable of giving significant information about the number and types of Cd(II) binding sites available in living cultured cells, (ii) the cellular Cd is mainly bound to MT, and (iii) the Cd-containing MT molecules are freely suspended in the cell cytoplasma.

1.38. Assignment of partial nuclear quadrupole interaction frequencies to various biologically important metal ligands

(R. Bauer and E. Larsen (Royal Veterinary and Agricultural High School, Copenhagen, Denmark))

A series of perturbed angular correlations of γ-rays on various Cd complexes including amino acid and peptide complexes has been taken. For all these Cd complexes the three-dimensional structure is known from x-ray diffraction measurements. The nuclear quadrupole interaction from the various Cd complexes is calculated within the angular overlap model. In order to match these calculations with the experimental nuclear quadrupole interactions, one has to fit partial nuclear quadrupole frequencies for each type of metal ligand. Analysis of all the Cd complexes shows that the partial frequencies derived for the various metal ligands can be transferred from one Cd complex to another within 10%. This constitute a proof that the angular overlap model is applicable to reliable nuclear quadrupole interaction calculations for Cd complexes. Partial nuclear quadrupole frequencies for the following series of Cd ligands have been determined; water, chloride, sulphate, pyridine (nitrogen), thiourea (sulphur), imidazole (nitrogen), carboxyl groups thiosemicarbazide (nitrogen and sulphur).

At present these data are used in a structural analysis of the metal site in four different Zn enzymes using the experimental nuclear quadrupole interactions obtained under various circumstances for these four enzymes.

1.39. The small-angle neutron-scattering instrument, SANS

(J. Kjems, J. Linderholm, L.G. Jensen, B. Breiting, H. Bjerrum Møller and R. Bauer)

The small angle neutron scattering instrument, SANS, is now installed in the neutron house. During the spring of 1982 test runs will be performed in order to document the scientific standard of the instrument. Details of the instrument are shown in Figs. 26 and 27. From the left (Fig. 26) the instrument

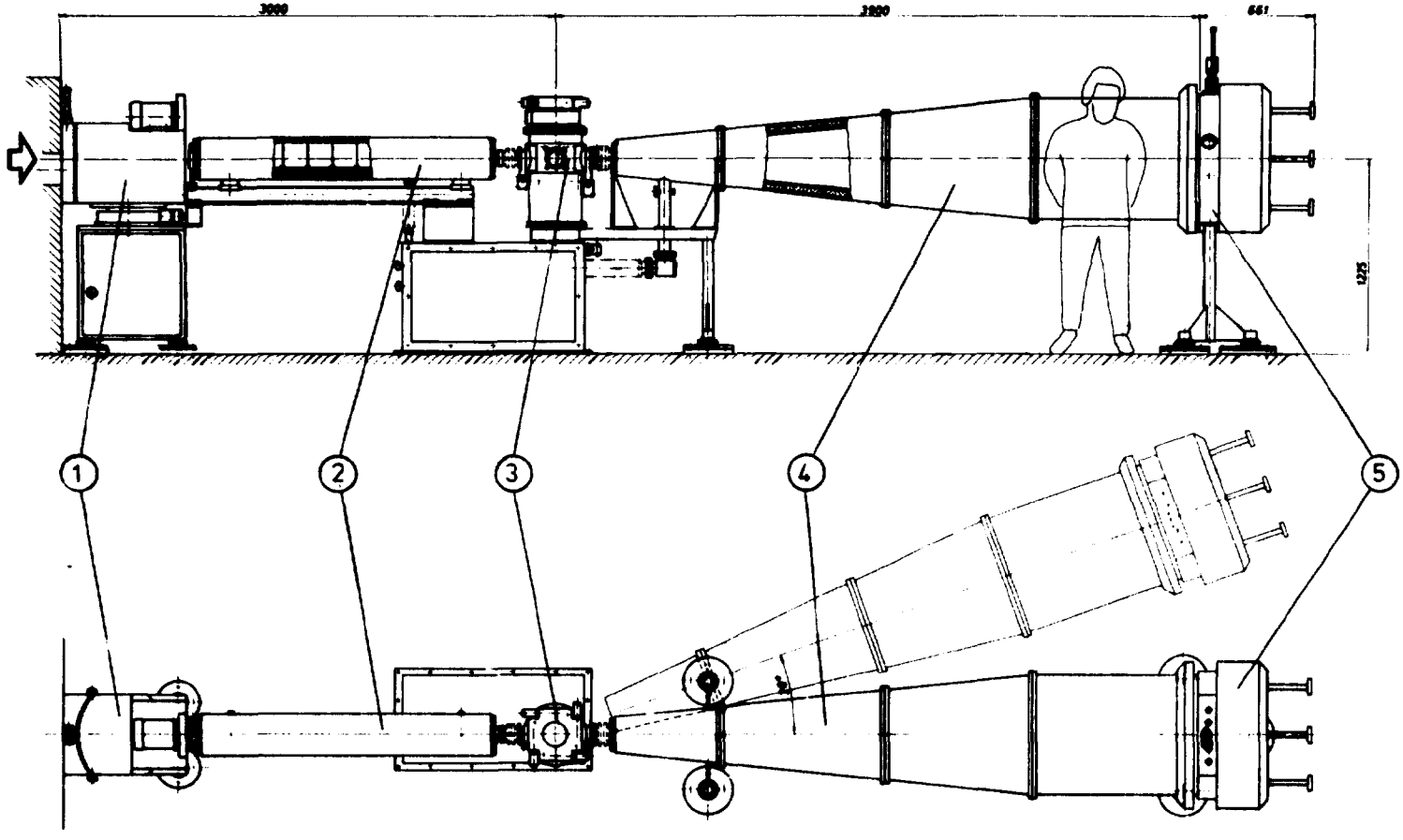

Fig. 26. Drawing of SANS. (1) Mechanical velocity selector, (2) collimator, (3) sample chamber (see Fig. 27), (4) flight path and (5) neutron area-sensitive detector.

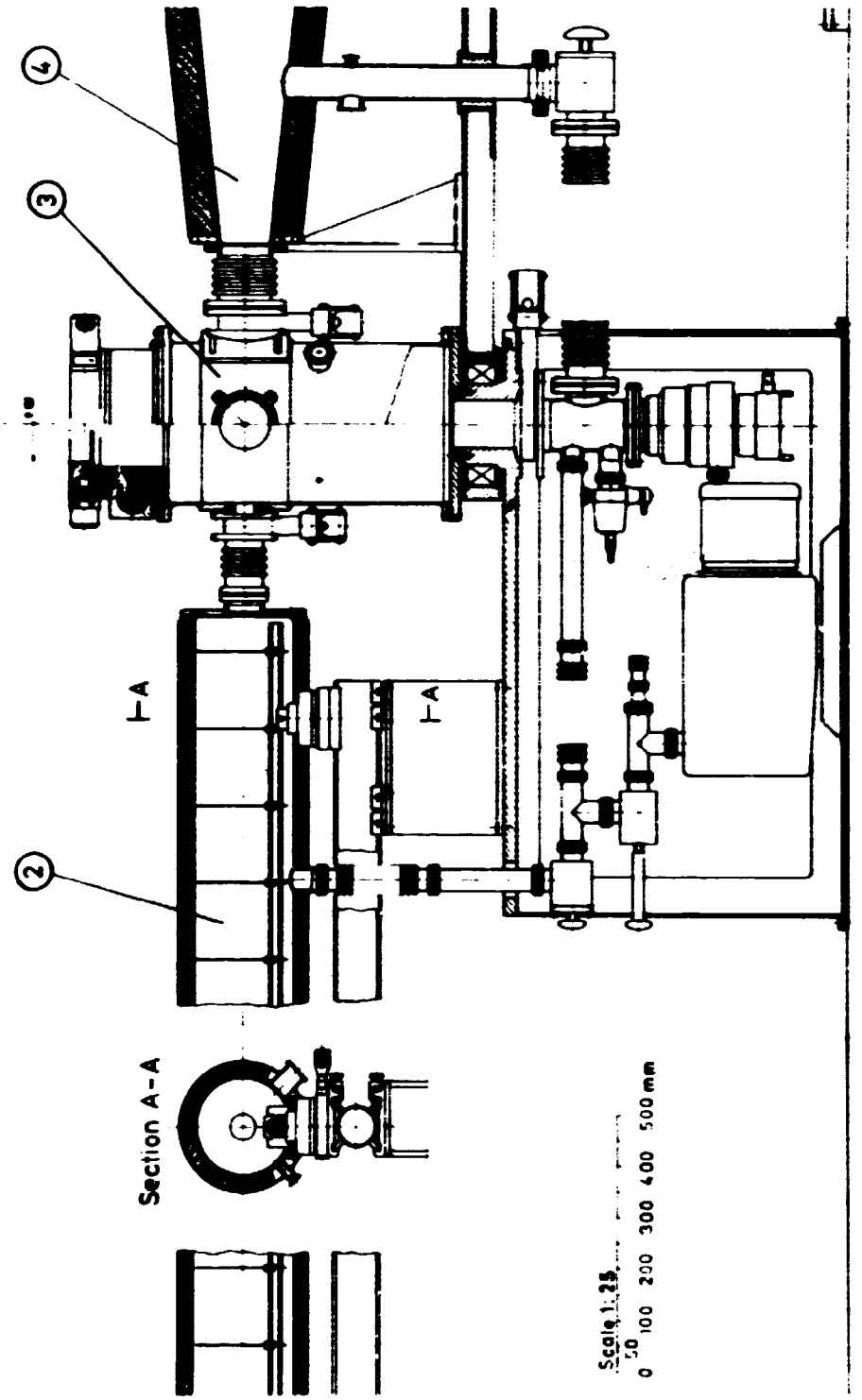

Fig. 27. Detailed drawing of SANS. (2) Collimator, (3) sample chamber and (4) flight tube.

consist of (1) mechanical velocity selector (2) collimating tubes, (3) sample chamber, (4) flight path, and (5) neutron area-sensitive detector. Below we outline some details of the various components:

Mechanical velocity selector: Consists of a rotating drum (max. 5000 rpm) with tilted slits for passage of neutrons. The spectral properties after passage through the monochromator are characterised by $\lambda = 7920 \times \theta / \nu$ (Å) and $\Delta\lambda/\lambda = 3168/(\nu \times \lambda)$, where θ is the tilt angle in deegree and ν is the rotation of the drum in rpm. For the peak position of the cold neutron source $\lambda = 3.3$ Å and $\nu = 5000$ rpm we have $\Delta\lambda/\lambda = 0.19$ and an intensity of about 10^6 n/s cm^2.

Collimators: Consist of a 2 m evacuated tube with slits at both ends. The slits decreases the angular divergence at the sample position from 45' to 26'.

Sample chamber: An evacuated cylinder with a sample holder inset designed for biological application. The sample holder can accomodate up to 6 different quartz cuvettes of thickness 1,2 or 5 mm containing liquid samples. A motor-driven horizontal translation system can position the sample with an accuracy of 0.1 mm. In addition the samples can be kept at temperatures controlled between 0^oC to 60^oC via a peltier heating system. Slits can be inserted as close as 1 cm before and after the sample, in order to ensure that only scattering from the sample is detected by the area sensitive detector.

Flight path: A 3.5 m evacuated conically-shielded tube leading from the sample chamber to the detector. The flight tube can be turned 20^o off the incident beam direction.

Detector: A 40 by 40 cm^2 area-sensitive detector which functions as a proportional gas counter. The detector gas consists of 2 atm Ar containing 5% CO_2 and 1 atm He^3. The latter gas is used to produce ionised hydrogen and tritium from the reaction $n + He^3 \rightarrow p + H^3 + 764$ keV. The electrons from the ionization tracks in the gas, drift toward the anode and are multiplied near the

64-wire anode grid at +3.6 kV. The resulting currents are also picked up by the two parallel coupled cathode grids with each 128 wires held at a potential of about +1700 V. Both anode and catode grids are used to determine the position of the above-mentioned neutron reaction impact via the difference in arrival times for the current pulse at the ends of the grids. The cathode wires are chosen to have a total delay of 2.4 μs (T = RC). The anode grid has small 200 Ω resistors interconnecting the wires and giving a similar delay. By measuring the arrival times at each end of the grids the neutron signal can be converted to an (x,y) position by standard electronic circuitry. The resolution is 6 mm full width at half maximum.

Computer system: A two parameter 64×64 channel analyser is used to store the x and y coordinates corresponding to the neutron events in the detector. The two-dimensional spectra can be displayed either as a contour plot or as a three-dimensional overview. By means of a PDP 11-23 computer on line with the dual parameter-system, it is posible to convert the spectra into (kx,ky) space coordinates and thereafter to analyse the data in various ways. The computer is also linked to a CAMAC-system which, among other features, controls the (X,Y) translation of the sample holder, the velocity of the velocity-selector drum and the temperature of the sample. In addition the computer will be equipped with a 512×512 pixel colour graphic screen and a sixteen-colour plotter for graphical data analysis. The instrument is in, particular, designed for molecular biological studies of large molecules such as proteins, DNA virus, and membranes.

1.40. The four-circle neutron diffractometer

(P. Krebs Larsen*, B. Lebech, M. Lehmann (ILL, Grenoble, France), M.H. Nielsen* (*University of Århus, Denmark), J. Bundgaard** and P. Skaarup**, (**Electronics Department, Risø))

The four-circle paper-tape-controlled Ferranti neutron diffractometer, which has been operated at Risø since 1967 by the Chemi-

cal Institute of the University of Århus on behalf of the Danish National Committee for Crystallography, has been replaced by a modern instrument (Fig. 28) to be described below. The new instrument was partly financed through a grant from the Danish Natural Sciences Research Council. It has been in operation since August 1981 and serves all Danish Crystallographers.

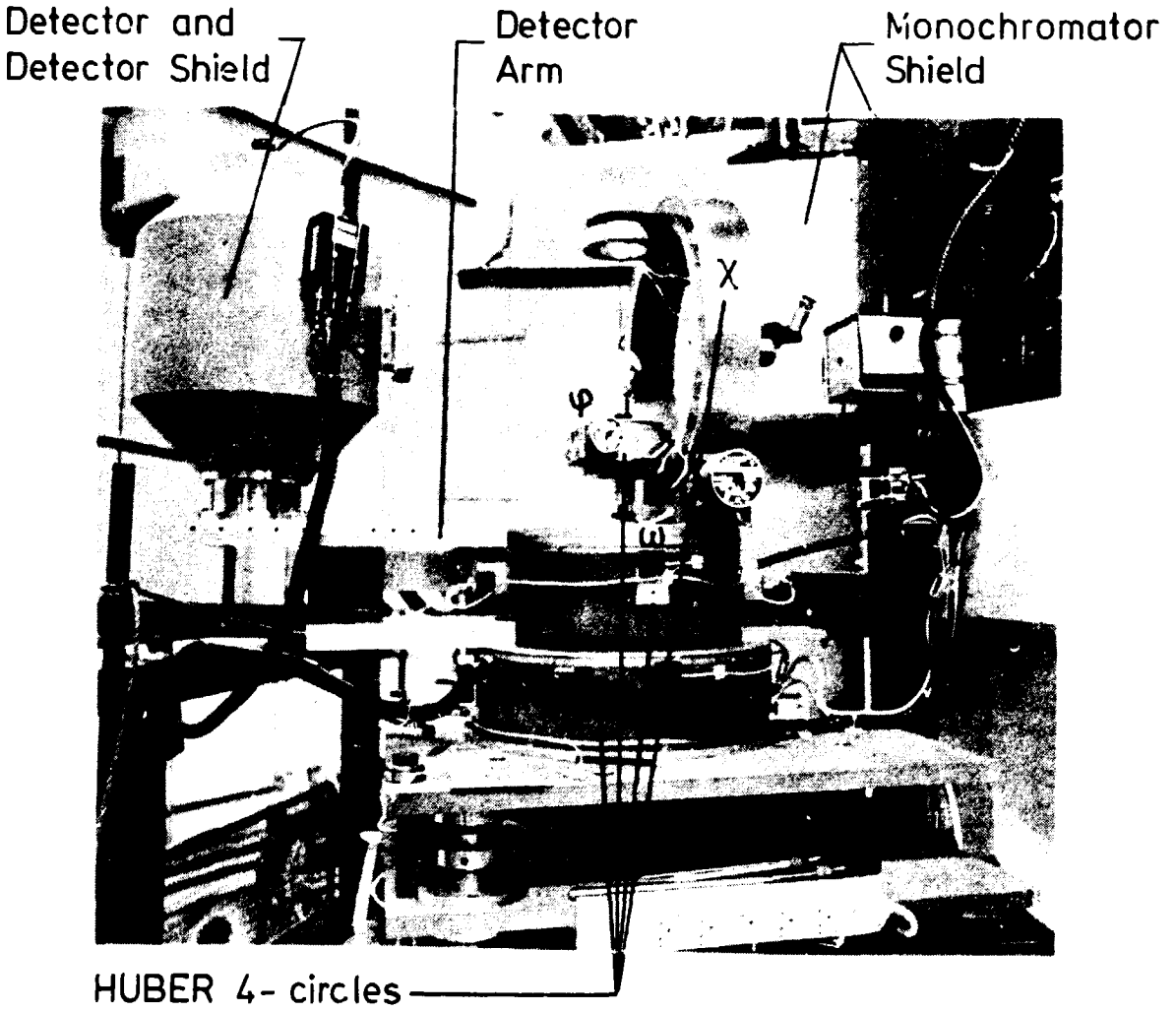

Fig. 28. The four-circle neutron diffractometer.

The mechanical part of the diffractometer consists of a monochromator part which allows an easy change of incident neutron wavelength and a four-circle HUBER goniostate consisting of an Euler cradle (HUBER 512) and two horizontal goniometers (HUBER 440 and HUBER 430). The goniostate is computer controlled by a PDP 11/34 interfaced via CAMAC modules. The PDP-11/34 computer

has a 128 k byte memory, two hard magnetic disc stations, a fast DEC-writer terminal and a screen terminal. The diffractometer can be operated remotely via modem and telephone line connections from remote stations such as the University of Århus and ILL, Grenoble. Minor parts of the software used to control the diffractometer were developed at Risø while the major parts of the control and data reduction software were a generous gift to Risø from College 5, the diffraction group, at the Institute Laue-Langevin, Grenoble, France.

Thanks to this gift from the ILL, the instrument has already proven to be a flexible and powerful tool in solving several crystallographic problems such as, for instance the structure of TiC, NdF_3 (see 1.20) and a determination of the hydrogen positions in the nearly planar molecyle nitromalonamid (Simonsen and Thorup, 1979 and Thorup et al., 1982).

1.41. PDP-11 spectrometer control software for triple-axis spectrometers

(D. Juul Jensen)

A new software system has been developed for spectrometers controlled by a PDP-11 computer. The program is written in BASIC and all commands (data input/output etc.) are specified by two letters which in most cases are followed by an "=" and some numbers (separated by commas).

When the computer is ready to accept input from the terminal, the program allows:

(i) Changes of variables, e.g. wavelength, lattice parameters, etc.
(ii) The setting up of scans in reciprocal space and/or energy transfer scans. It is possible to set-up ten different scans at one time.
(iii) The performance of a specified number of scans.
(iv) The changing of temperature or magnetic field.
(v) The use of a number of fast routines, e.g. scan with one or more motors, or go to a particular reciprocal point.

The measured data are optionally stored on standard floppy discs, which can be used at any PDP-11 computer for data analysis and plotting of the data. The system is flexible and is equally well suited for both for crystal alignment and more extended time consuming scans.

1.42. Technical improvements of the triple-axis x-ray spectrometer

(J. Als-Nielsen, J. Bohr, E. Dahl Petersen*, S. Jørgensen, J. Linderholm, J. Munck, P. Skaarup*(*Electronics Department, Risø))

The location of a synchrotron beam will change between different fillings of the storage ring and it can also vary within one filling period. It is therefore important to relocate the instrument to the new beam position without having to both realign the spectrometer and monitor the beam position continuously. The latter aspect was obtained by an ionization chamber with a common cathode but four separate anodes monitoring respectively, the right, left, top, and bottom part of the beam.

The vertical setting of the spectrometer was obtained by moving the entire platform by simultaneous rotation of three spindle legs by three stepping motors with a precision of better than one micron per step. The horizontal setting is less critical and was funished by a manual translation of the spectrometer.

As mentioned in 1.25-1.29 we have used a position-sensitive detector extensively. An on-line plotting of the multichannel analyzer data was done on the DECWRITER equipped with a special graphic option so the discrete steps of the printed characters are much reduced and the paper can be rolled backward and forward by the plotting program.

1.43. High-resolution powder diffraction using synchrotron radiation

(B. Buras and F. Christensen)

A preliminary test of high-resolution powder diffraction was made using the triple-axis x-ray spectrometer (Als-Nielsen et al., 1980) installed at the D4 beam line at DORIS working at 3.185 GeV and about 80 mA. A monochromatic x-ray beam of a wavelength of 1.54 Å produced by the (1,1,1) reflection from a perfect Si crystal was used. This beam diffracted by a flat thick powdered naphthalene sample in symmetric position was again reflected by a similar perfect Si crystal acting as a collimator. The slit defining the beam was 2.5 mm wide and about 3 mm high. Figure 29 shows, as an example, the (1,1,1) reflection from naphthalene in the case of a non-dispersive setting. A good fit was obtained with a modified Lorentzian

$$C[1 + [k(\theta - \theta_o)]^2 + k' [k(\theta - \theta_o)]^4\}^{-1}$$

resulting in a full-width-at-half-maximum (Δd) of $24 \cdot 10^{-3}$ = 86 seconds of arc. This width corresponds to a "resolution" $\Delta d/d$ = $2.5 \cdot 10^{-3}$ at a scattering angle $2\theta \cong 19^{o}$, i.e. the resolution is much better than one could obtain with a conventional x-ray source. This preliminary test indicates that synchrotron radiation could be very useful for high-resolution powder diffraction. The methodological study will be continued.

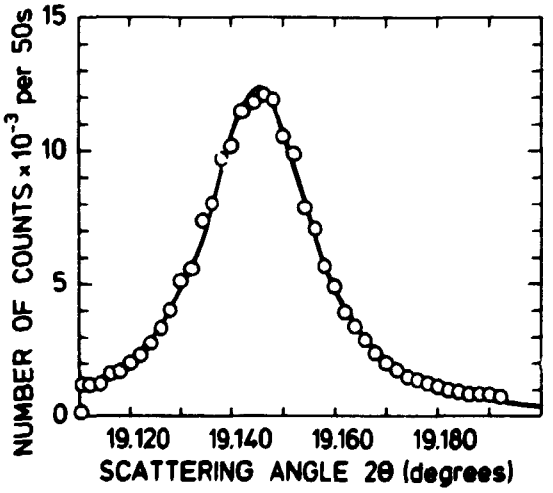

Fig. 29. The (1,1,1) reflection from a powdered naphthalene sample obtained with a triple-axis spectrometer. The FWHM is 86" corresponding to $\Delta d/d = 2.5 \cdot 10^{-3}$.

1.44. References to Chapter 1

ALS-NIELSEN, J., DIETRICH, O.W. and PASSELL, L. (1976). I-III Phys. Rev. B14, 4897-4945.

ALS-NIELSEN, J., HOLMES, L.M., KREBS LARSEN, F. and GUGGENHEIM, H.J. (1975), Phys. Rev. B12, 191-197.

ALS-NIELSEN, J., LINDERHOLM, J., JØRGENSEN, S., SKAARUP, P., DAHL PETERSEN, E. and BURAS, B. (1980). In: Risø R-441, 62-67.

BERGSMA, J. and LOOPSTRA, B.O. (1962). Acta Cryst. 15, 92-93.

BLASCHKO, O., ERNST, G., QUITTNER, G., KRESS, W. and LECHNER, R.E., (1975). Phys. Rev. B11, 3960-3965.

BOHN, H.G., ZINN, W., DORNER, B. and KOLLMAR, A. (1980). Phys. Rev. B22, 5547-5552.

BURAS, B., GERWARD, L., JOHANSSON, L., LEBECH, B., OLSEN, J. STAUN, SKRIVER, H. and STEENSTRUP, S. (1980): In: Risø-R-441, 34-35.

CARNEIRO, K., ELLENSON, W.D., PASSELL, L., McTAGUE, J.P., TAUB, H. (1976). Phys. Rev. Lett. 37, 1695-1699.

BRETZ, M. (1973). Phys. Rev. Lett. 31, 1447-1451.

CHINN, M.C. and FAIN Jr., S.C. (1977). Phys. Rev. Lett. 39, 146-149.

CLAUSEN, K. (1981). Risø-R-426.

CLAUSEN, K. and LEBECH, B. (1982). Magnetic Excitations in Ho_2Co_{17} and Ho_2Fe_{17}. Accepted for publication in J. Phys. C.

CLAUSEN, K. and NIELSEN, O.V. (1981). J. Magn. Mag. Mat. 23, 237-240.

DASH, J.G. (1978). Films on Solid Surfaces (Academic Press, New York).

DASH, J.G. (1980). In: Ordering in Two Dimensions. Proceedings of the International Conference at Lake Geneva, Wisconsin, U.S.A. Edited by S.K. Sinha (North Holland, New York - Amsterdam).

DE SEZE, L. (1977). J. Phys. C10, L353-356.

FARR, M.K. and TEVINO, S.F. (1976). Proceedings of the Conference on Neutron Scattering, Gatlinburg, U.S.A. 237-

GENNES, P.G. de (1972). Solid State Comm. 10, 783- .

GALAZKA, R.R., NAGATA, S. and KEESOM, P.H. (1980). Phys. Rev. B22, 3344-3355.

GIEBULTOWICZ, T., KEPA, H., BURAS, B., CLAUSEN, K. and GALAZKA, R.R. (1981). Solid State Commun. 40, 499-501.

GIEBULTOWICZ, T., MINOR, W., KEPA, H., GINTER, J. and GALAZKA, R.R. (1982). A phenomenological description of the antiferromagnetic transition in Cd_{1-x} Mn_xTe, to be published.

GREEDAN, J.E. and RAO, V.U.S. (1973). J. Solid State Chem. 6, 387-396.

HALPERIN, B.I. and NELSON, D.R. (1979). Phys. Rev. B19, 2457-2484.

JAYARAMAN, A. (1979). In: Handbook of the Physics and Chemistry of Rare Earth, Vol. 2, Ed. by A. Gschneider Jr. and L.R. Eyring (North Holland, Amsterdam).

JOHANSSON, T., McEWEN, K.A. and TOUBORG, P. (1971). J. Phys. (Paris) 32, C1 372-374.

KNUDSEN, G.P., VOSS, F.W., NEVALD, R., AMBERGER, H.-D. (1982). To be published in Volume 3 of The Rare Earths in Modern Science and Technology.

LEBECH, B. and RAINFORD, B.D. (1971). J. Phys. (Paris) 32, C1 370-371.

LEFFERS, T. (1974). Met. Trans. 5, 2110-2112.

LINDGÅRD, P.-A. (1980). Proceedings of the International Conference on 4-f systems, Philadelphia, U.S.A. November 1979 (Plenum Press), 153-164.

LINDGÅRD, P.-A. (1982). J. Appl. Phys. 53, 1861-1863.

LITSTER, J.D., ALS-NIELSEN, J., BIRGENEAU, R.J., DANA, S.S., DAVIDOV, D., GARCIA GOLDING, F., KAPLAN, M., SAFENYA, C.R. and SCHAETZING, R. (1979). J. Phys. (Paris) Colloq. 40, C3-337.

LYNN, J.W., PATTERSON, H.H., SHIRANE, G., WHEELER, R.G. (1978). Solid State Commun. 27, 859-862.

MONCTON, D.E. and PINDAK, R. (1980). In: Ordering in Two Dimensions. Proceedings of the International Conference at Lake Geneva, Wisconsin, U.S.A. Edited by S.K. Sinka (North Holland, New York, Amsterdam).

MONCTON, D.E., STEPHENS, P.W., BIRGENEAU, R.J., HORN, P.M. and BROWN, G.S. (1981) Phys. Rev. Lett. 46, 1533-1536.

MOOK, H.A. (1981). Phys. Rev. Lett. 46, 508-512.

NEVALD, R., VOSS, F.W., NIELSEN, O.V., AMBERGER, H.-D. and FISCHER, R.D. (1979). Solid State Commun. 32, 1223-1225.

NIELSEN, L. (1981). Investigation of the crystal structure of NdF_3 by means of neutron diffraction and ^{19}F-NMR. (In Danish) Thesis. The Technical University of Denmark.

OFTEDAL, I. (1931). Z. Phys. Chem. B13, 190-200.

OLSEN, J. STAUN, BURAS, B., GERWARD, L. and STEENSTRUP, S. (1981a). J. Phys. E14, 1154-1158.

OLSEN, J. STAUN, BURAS, B., GERWARD, L., JOHNSSON, B., LEBECH, B., SKRIVER, H. and STEENSTRUP, S. (1981b). In: Physics of Solids under High Pressure. Edited by J.S. Schilling and R.N. Shelton (North-Holland Publishing Company), 305-309.

SIMONSEN, O. and THORUP, N. (1979). Acta Cryst. B35, 433-435.

PAWLEY, G.S., MACKENZIE, G.A. and DIETRICH, O.W. (1977). Acta Cryst. A33, 142-145.

PERSHAN, P.S. (1974). J. Appl. Phys. 45, 1590- .

STEPHENS, P.W., HEINEY, P., BIRGENEAU, R.J. and HORN, P.M. (1979). Phys. Rev. Lett. 43, 47- .

THORUP, N., SIMONSEN, O. and KREBS LARSEN, F. (1982). The structure of intromalonamid determined by neutron diffraction, to be published.

VILLAIN, J. (1980). In: Ordering in two Dimensions. Proceedings of the International Conference at Lake Geneva, Wisconsin, U.S.A. Edited by S.K. Sinha (North Holland, New York - Amsterdam).

WARF, J.C. and HARDCASTLE, K.I. (1966). Inorg. Chem. 5, 1736-1739.

YOUNG, C.Y., PINDAK, R., CLARK, N.A. and MEYER, R.B. (1978). Phys. Rev. Lett. 40, 773-776.

2. PLASMA PHYSICS

The Plasma Physics Section operates under a contract of association between Risø National Laboratory and Euratom, and some staff members participate as members of, or consultants in several of the committees concerned with the Euratom fusion programme. The research activities are centred on research in basic plasma physics (2.1-2.11) and on studies of technology of interest for future fusion reactors (2.12-2.27). In addition, a design of a single-point Thomson-scattering system for JET was carried out under a contract with JET (2.28).

The activities within basic plasma physics, including experimental as well as theoretical investigations, were mainly concentrated on non linear phenomena. The experimental studies of strong electrostatic double-layers in the Q-machine plasma were continued. These investigations are part of an international collaborative programme between Risø, Tohoku University, Sendai, Japan, and Innsbruck University, Austria, on the study of laboratory double-layers. Investigations of the formation of three-dimensional double-layers sustained by an electron beam of finite radial extension were among the studies.

Construction of the new experimental device - the DP-machine - was completed in the summer. The DP (Double Plasma) -machine has a total volume of 0.2 m^3. It is divided into two chambers (driver and target chamber) separated by a fine mesh grid and electrically insulated from one another. The unmagnetized plasma is produced by discharge between hot filaments and the chamber walls. When biasing the driver chamber, beams may be injected into the target plasma, making the machine well suitable for studying, e.g. ion-beam plasma interactions. Measurements of the basic plasma properties show densities in the 10^8 - 10^9 cm^{-3} range, and temperatures $T_e \sim 5$ eV, $T_i < 0.2$ eV. Because of this high electron-to-ion temperature ratio and the

relatively low density, this plasma is suitable for investigations of electrostatic waves. Furthermore, due to the large plasma volume, the effects of boundaries on wave propagation are negligibly small. Preliminary experiments with non linear ion-acoustic waves appeared promising.

The theoretical studies were concerned mainly with non linear wave phenomena, covering both analytical and numerical investigations. Included were subjects such as the propagation of transient signals, generations of harmonics, evolution of solitons, formation and stability of electron and ion phase space vortices (holes), and numerical simulation of non linear electron plasma waves.

The desire to strengthen the more direct fusion-oriented research resulted in an initiation of studies on Electron Cyclotron Resonance Heating (ECRH) of tokamak plasmas. Additional heating of fusion plasmas from temperatures of a few keV, which is the upper limit of ohmic heating, to a temperature of above 10 keV is necessary to achieve ignition of the fusion fuel. One of the most promising candidates is absorption of microwave power at the cyclotron resonance of the electrons gyrating around the magnetic field lines of the tokamak. However, the strength of the magnetic field in the large experimental tokamaks is so high that the necessary high-power microwave sources do not, at present, exist. The recent development of the gyrotron provides confidence in utilizing ECRH in the future. More intensive research of the capabilities of ECRH in Europe has been recommended recently by the JET joint undertaking.

The technological aspects of plasma physics are studied with one of the possible refuelling schemes for fusion reactors in mind. In this particular scheme, the fuel will be injected as high velocity pellets of solid hydrogen isotopes. Investigations of fundamental processes in the interaction between charged particles of different energies and solid hydrogen isotopes are therefore of great interest. These studies have been concerned mainly with the interaction between films of hydrogen, deuterium, or mixtures of different hydrogen forms and

beams of electrons and light ions of different energies. Measurements of the emission coefficients for positive and negative particles from solid HD and H_2-D_2 mixtures bombarded with keV electrons and hydrogen ions, ranges and stopping powers of hydrogen and deuterium ions incident on H_2 and D_2 targets, and erosion of films of D_2 by keV light ions and electrons were the main results obtained.

The direct interaction between pellets of deuterium and a plasma is studied in the "Dante" tokamak. A new pellet injector producing small pellets (cylindrical in shape, 0.4 mm long and 0.4 mm in diameter) was installed at Dante, and experiments with these pellets were initiated. The pellets are fed to the tokamak through a 5 m long guide tube. The guide tube technique was improved in order to inject the pellets in a well-defined manner. By using a special launching unit, the angular spread of the injected pellets was minimized ($< 1^o$). The Ruby-laser Thomsen-scattering system was installed and measurements of the electron temperature were in agreement with measurements using soft x-rays. The Thomsen-scattering system has the capability of making a double temperature measurement with short time difference.

Studies of problems with the handling, acceleration, and injection of pellets of relevance for large plasma and fusion experiments were continued. Among other things, a pellet injector for use at the tokamak (TFR) at CEN Fontenay-aux-Roses, Paris, is under construction. These projects were partially supported by a grant from the Danish Ministry of Energy.

2.1. Electron-cyclotron resonance heating

(J.P. Lynov and P. Michelsen)

Calculations of the various cut-off and resonance surfaces for electromagnetic waves in a plasma with parameters typical of the Dante tokamak were performed.

The results showed that in order to achieve an effective absorption of the microwave power it is necessary to use either mode conversion at the fundamental frequency (18-20 GHz) or direct absorption at the second harmonic. Since high power oscillators above 18 GHz are very expensive, we concluded that an experiment on Dante will have to utilize the mode conversion at 18 GHz. The basic feature of the mode conversion scheme is the conversion of an extraordinary, electromagnetic wave at the upper hybrid resonance layer into an electrostatic electron Bernstein wave, which in turn is effectively absorbed in the plasma. The extraordinary wave can either be launched from the inner, high-field side of the tokamak or it can be generated by an additional mode conversion of an ordinary wave launched from the outer, low-field side at the plasma frequency layer.

In order to obtain more detailed information about how electromagnetic waves propagate, are mode converted, and finally absorbed in a plasma, an extensive computer program is in preparation. Concerning near-field problems of the antenna system, contact with the Electromagnetic Institute (EMI) at the Technical University of Denmark was made. EMI has many years of experience in this field and has developed computer programs suitable for these problems.

2.2. Data acquisition and processing system

(J.P. Lynov and P. Michelsen)

A computer program, GANDALF (Generally Applicable Numerical Data Acquisition Laboratory Facility), has been implemented at the Q-machine laboratory at Risø on a HP-9825 computer. GANDALF is designed for different types of data acquisition, e.g. for A/D numerical input, it has flexible data processing functions, and it can produce various kinds of data output on the HP-9872A four-colour-plotter, in addition to lineprinter listing on the HP-9866B storage, on floppy disks by a HP-9885M, and D/A output by a HP-59303A.

2.3. Formation of three-dimensional double layers in a laboratory plasma

(D. Jovanović (Institute of Physics, Beograd, Yugoslavia), J.P. Lynov, P. Michelsen, H.L. Pécseli, J. Juul Rasmussen and K. Thomsen)

The formation of three-dimensional double-layers was investigated in the Q-machine plasma. The double-layers were produced when an electron beam of radius R_b was injected along the magnetic field lines into the Q-machine plasma of a larger radius R_p. The three-dimensional plasma potential distribution, which was axially symmetric, was measured by means of simple electron emissive probes movable in axial and radial directions. Stationary double-layers were found for a broad range of plasma parameters, beam energies, and for magnetic field magnitudes ranging from almost unmagnetized ions (ion-Lamor-radius, $\rho > R_b$) to strongly magnetized ions ($\rho << R_b$). (The electrons are always strongly magnetized, $\rho_e << R_b$). In Fig. 30, we show typical plasma potential contours for strong (Fig. 30a, ρ = 0.22 cm) and weak (Fig. 30b, ρ = 0.74 cm) magnetic fields, respectively. The beam radius R_b = 0.4 cm, the plasma radius R_p = 1.5 cm, and the beam energy E_b = 30 V. The plasma potential contours are U-shaped, with the U bending towards the low potential region, as expected for a stationary double-layer in a plasma with a magnetic field (Block, 1981). This effect is especially pronounced in the cases with strong magnetic fields, where the ions are also confined within the beam region and the radial transport is negligible. In these cases, the potential jump of the double-layer is confined within the beam region. For lower magnetic fields, $\rho > R_b$, the ions are drawn radially into the beam region and thus force the potential of the surrounding plasma down. Consequently, the potential contours "open" and the potential jump is felt over the whole width of the plasma column. The change in the axial electron distribution function measured at different radial and axial positrons clearly demonstrates the acceleration and reflection of the electrons by the double-layer. Measurements of the potential fluctuations showed the existence of low-frequency (< 50 kHz) noise of relatively small amplitude, mainly within

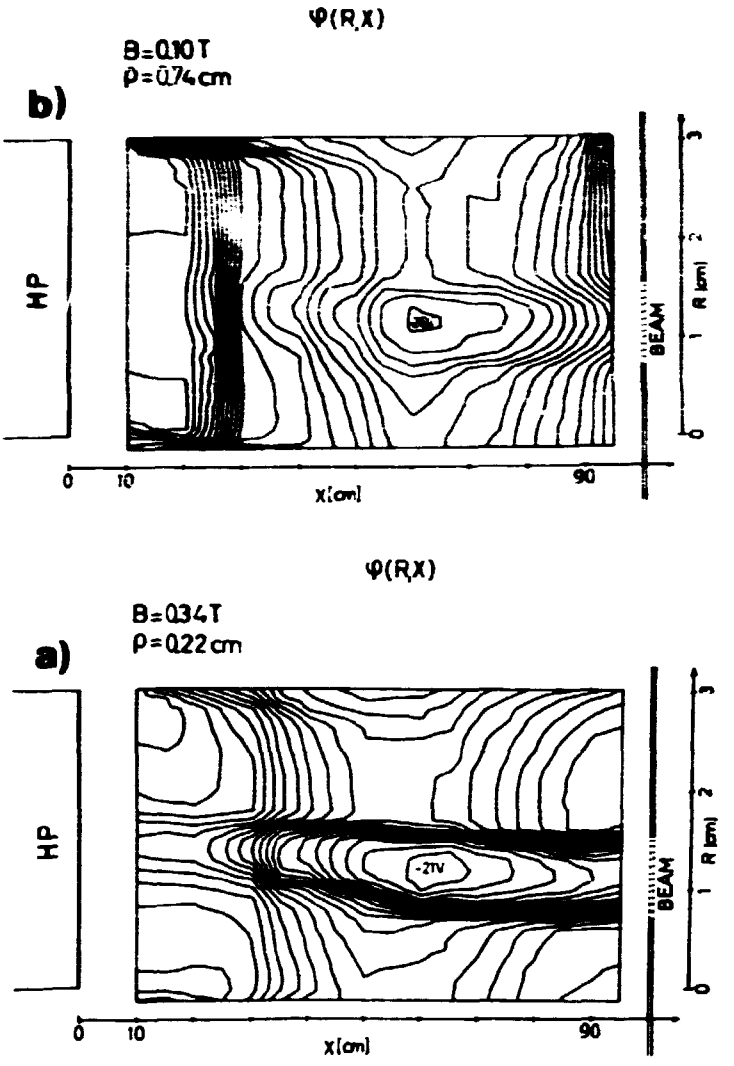

Fig. 30. Contours of constant plasma potential for the case of (a) high magnetic field (B = 0.34 T and (b) a low magnetic field (B = 0.10 T). The minimum potential is indicated on the inner contour. The potential difference between two adjacent contours is 1 V. The electron beam with energy 30 V is injected 100 cm from the hot plate (HP).

the beam region. These fluctuations do not seem to disturb the gross properties of the double-layer. The formation of the double-layer by the electron beam is ascribed to the non linear evolution of the Pierce instability of a beam with finite radial extension (see 2.4). A similar mechanism was suggested for the formation of planar double-layers in the unmagnetized plasma (Iizuka et al., 1979).

Finally, it should be mentioned that the observed U-shaped double-layers resemble many features suggested for the double-

layer formation above the auroral arc (e.g. Block, 1981; Kan et al., 1979). At least our experimental results show that such configurations can exist self-consistently when sustained by an electron beam.

2.4. The influence of beam boundaries and velocity reduction on the Pierce instability in laboratory plasmas

(D. Jovanović (Institute of Physics, Beograd, Yugoslavia))

The influences of the beam-plasma boundary and of weak non-linearities on the Pierce instability (Pierce, 1944) were investigated. It was shown that the finite width of the beam had negigible influence on both the stability of the system and its growth rate. The instability was confined to the beam region and the transverse scale length of the growing field was much shorter than the longitudinal scale length.

The non linear evolution of the instability was studied using a perturbation method. As a result of second-order non linearities, the wavelength of the unstable mode was found to decrease and the wave potential was enhanced close to the beam inlet boundary. The relationship between this effect and the formation of double-layers was discussed.

2.5. Numerical simulation of non linear plasma waves

(J. Juul Rasmussen and K. Thomsen)

The investigations of the non linear propagation properties of electron plasma waves using numerical simulations (Lynov et al., 1980a) were continued. Special interest was paid to the effects of wave-particle interaction on the propagation of strongly non linear waves. By extending the simulation model we could follow the temporal evolution of the frequency shift $\delta\omega(t) = \omega(t) - \omega_L$ (ω_L is the linear frequency) and the damping rate, $\gamma(t)$. A typical evolution of $\delta\omega(t)$ and $\gamma(t)$ is shown in Fig. 31. The frequency shift is normalized with Ω_o, which is a measure of the asymptotic frequency shift (Morales and

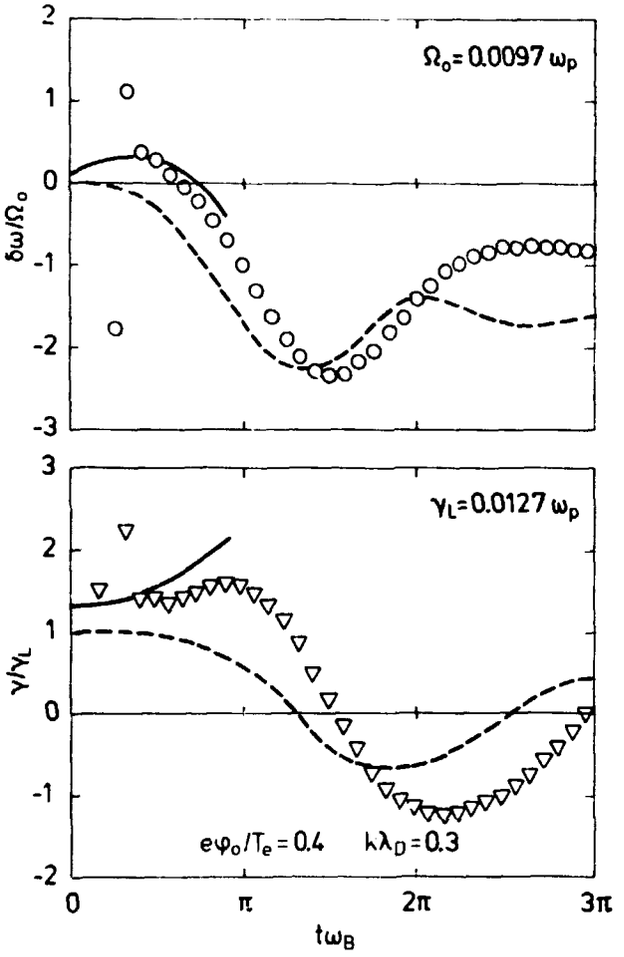

Fig. 31. The evolution of the frequency shift, $\delta\omega$, and damping rate, γ, for a non linear electron plasma wave with initial amplitude $e\phi_o/T_e^o = 0.4$ and wave number $k\lambda_D = 0.3$ (λ_D is the Debye length, γ_L is the linear damping rate and Ω_o is explained in Section 2.5). The results from the numerical simulation ($\delta\omega$:o, γ:▽) are compared with theoretical results of Morales and O'Neil (1972) (broken line) and Sugihara and Yamanaka (1979) (full line).

O'Neil, 1972). The solid curves are the theoretical results of Sugihara and Yamanaka (1979) which are claimed to be valid for arbitrary ϕ_o and v_p in the initial phase $0 < t < \pi/\omega_B$; where ω_B is the bounce frequency ($\omega_B = k\sqrt{e\phi_o/m}$). The positive frequency shift and the increasing damping rate predicted by the theory is clearly reproduced by the simulation results for $t < \pi/\omega_B$. For larger times $\delta\omega$ becomes negative and follows the evolution predicted by Morales and O'Neil (1972) qualitatively. Their results, being valid only for small amplitudes $e\phi_o/T_e << (v_e/v_p)^2$ are shown in Fig. 31 as the broken curve. (ϕ_o is the initial wave amplitude, T_e the electron temperature, $v_e = (T_e/m)^{1/2}$, and v_p is the phase velocity). Also the damping rate changes sign for $t > \pi/\omega_B$, indicating a regrowth of the wave as predicted by Morales and O'Neil (1972). It should be noted that we have verified the results of Morales and O'Neil (1972) quantitively for waves with sufficiently small amplitudes ($e\phi_o/T_e < (v_e/v_p)^2$) and with weak initial damping, i.e.

$v_p/v_e > 4$. For smaller phase velocities where the linear damping is stronger, the long term evolution of the wave amplitude followed the theoretical predictions of Pocobelli (1980) in which the contributions of all electrons (untrapped, detrapped, and trapped) are included self-consistently. For larger amplitudes the initial behaviour was in close agreement with the theory of Sugihara and Yamanaka (1979), as seen in Fig. 31, (see also Lynov et al., 1980a), while no theoretical predictions for $t > \pi/\omega_B$ exist up until now. However, our simulation results showed persistent amplitude oscillations which did not damp out due to phase mixing of the trapped electrons as predicted for small amplitude waves (Morales and O'Neil, 1972).

2.6. Non linear transient signal propagation in homogeneous plasmas

(D. Jovanović (Institute of Physics, Beograd, Yugoslavia), H.L. Pécseli and K. Thomsen)

The non linear transient evolution of a suddenly applied monochromatic wave in a homogeneous plasma was considered, with particular emphasis on the magnetized case, where $\vec{B}$-normal incidence of ordinary and extraordinary electromagnetic waves were treated. Two important features were described: First, the penetration of the wave front was shown to be accompanied by "radiation" of low frequency wave types, where ion-cyclotron and lower hybrid waves were considered here. Figure 32 shows the results of a numerical solution to our full set of non linear equations (Yu and Shukla, 1977; Dysthe et al., 1978) giving the variation of density, and modulus and argument of the complex envelope of the high-frequency wave field as a function of position for various times. A characteristic feature of these results is the development of a modulational instability behind the propagating wave front.

Secondly, our analysis predicted the presence of a non linear second harmonic precursor containing two natural modes of oscillation, one with exactly twice the frequency of the fundamental, and the other being a slightly frequency-shifted contribution.

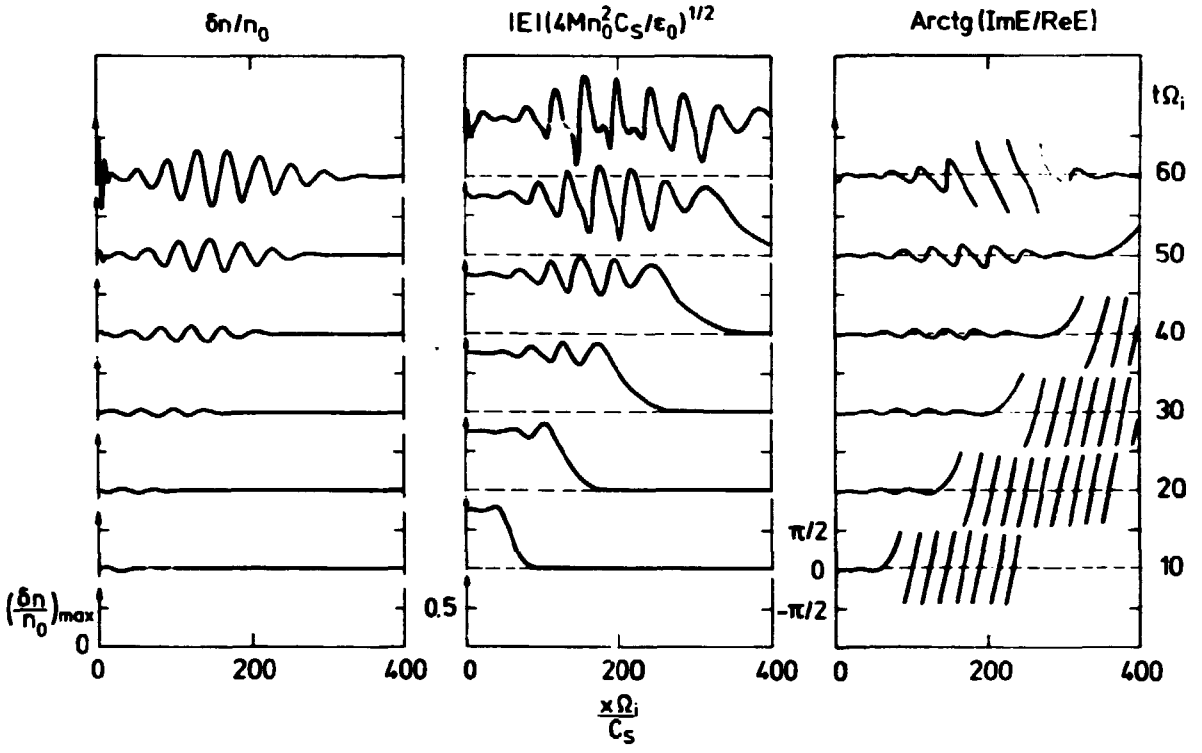

Fig. 32. Relative density perturbation associated with the low-frequency wave type, modulus and argument of the envelope of the high-frequency wave train as a function of normalized spatial variable. C_s is the ion sound speed, while Ω is the ion-cyclotron or lower hybrid frequency, depending on the wave types considered. $(\delta n/n_0)_{max} = 0.21$.

2.7. Investigations of plasmas by means of the quasi-linear theory

(D. Jovanović (Institute of Physics, Beograd, Yugoslavia))

As an example of the studies by means of the quasi-linear theory, second-harmonic generation in cold non-homogeneous magnetoactive plasma was investigated. It was demonstrated that the generation from the upper-hybrid layer, where the pump field has a second-order singularity, is negligible compared with the contribution of the wave-number matching region $k(2\omega_0) = 2 \cdot k(\omega_0)$, which can exist in the case of the extraordinary polarized pump wave. Numerical results were presented, predicting the energy transfer efficiency ~ 10%.

Another example is the use of the non linear current formalism of the quasi-linear theory to obtain an integro-differential

equation describing the diffusion of the self-generated magnetic field from the critical layer $\varepsilon = 0$, both to the over dense and the corona region. Analytical estimates in the case of p-polarized pump wave predicted a magnetic field of the order of several hundred tesla.

2.8. Non linear harmonic generation in a magnetized plasma waveguide

(J. Jørgensen, J.P. Lynov, H.L. Pécseli, J. Juul Rasmussen and K. Thomsen)

The properties of non linear Trivelpiece-Gould waves (Trivelpiece and Gould, 1959) were investigated with particular emphasis on the generation of second harmonics. In the case of a harmonically oscillating fundamental wave ω_o, k_o following the approximate normalized dispersion relation

$$\omega(k) \approx k(1 + k^2)^{-1/2} , \qquad (1)$$

we found two second harmonic waves generated by the non linearities, namely $(2\omega_o, 2k_o)$ which corresponds to a forced oscillation, and $(2\omega_o, k(2\omega_o))$, which is a natural mode of oscillation. If the fundamental wave is a long, but finite wave train, the natural mode will lag behind the fundamental since it has a smaller group velocity, according to Eq. (1). (We consider only cases where $\omega_o < 0.5$). This non linear "postcursor" was investigated analytically by a non linear model-equation and by a particle in cell simulation code (Turikov, 1978) modified to reduce the shot noise usually present in such codes (Trulsen, 1980). Also solitary waves were investigated, and the results of various models were compared.

2.9. Interaction of Langmuir solitons with resonant particles

(J.P. Lynov, H.L. Pécseli, J. Juul Rasmussen, K. Rypdal (University of Tromsø, Norway) and K. Thomsen)

The effect of resonant ions and electrons on the propagation of a Langmuir soliton was studied. The evolution of the Langmuir soliton is generally governed by the Zakharov equations (Zakharov, 1972), which may be reduced to the non linear Schrödinger equation in certain limiting cases. Perturbation terms for the Zakharov equations and the non linear Schrödinger equation were derived in the two limits $t \ll \tau_B$ and $t \gg \tau_B$, where τ_B is the bouncing time for a particle reflected from the soliton (Rypdal, 1981). The perturbed non linear Schrödinger equation was studied using Karpman's (1979) perturbation theory, and the main effect was found to be an exponential deceleration of the soliton without any deformation of its shape. The perturbed Zakharov equations were investigated using a simple technique based on the conservation laws. In the limit $|E|^2/4\pi nT \ll m_e/m_i$ the same result as for the non linear Schrödinger equation was obtained. ($|E|$ is the amplitude of the soliton, n the density, T the electron temperature, and $m_{e,i}$ electron and ion masses, respectively). In the opposite limit, however, the Zakharov equations yielded a weaker deceleration than the non linear Schrödinger equation, and there was a formation of flat ion-sound shelves radiated from the soliton in both directions.

These analytical results were compared with direct numerical integration of the perturbed non linear Schrödinger equation and those of Zakharov. In both cases, the agreement was found to be quantitatively very good for a broad range of soliton parameters as long as the perturbation was not too large. In Fig. 33 we show a typical evolution pattern for the perturbed Langmuir soliton as solution to the Zakharov equations. The deceleration of the soliton in agreement with the analytical results (Fig. 33b) and the formation of the ion-sound shelves (Fig. 33c) are clearly seen.

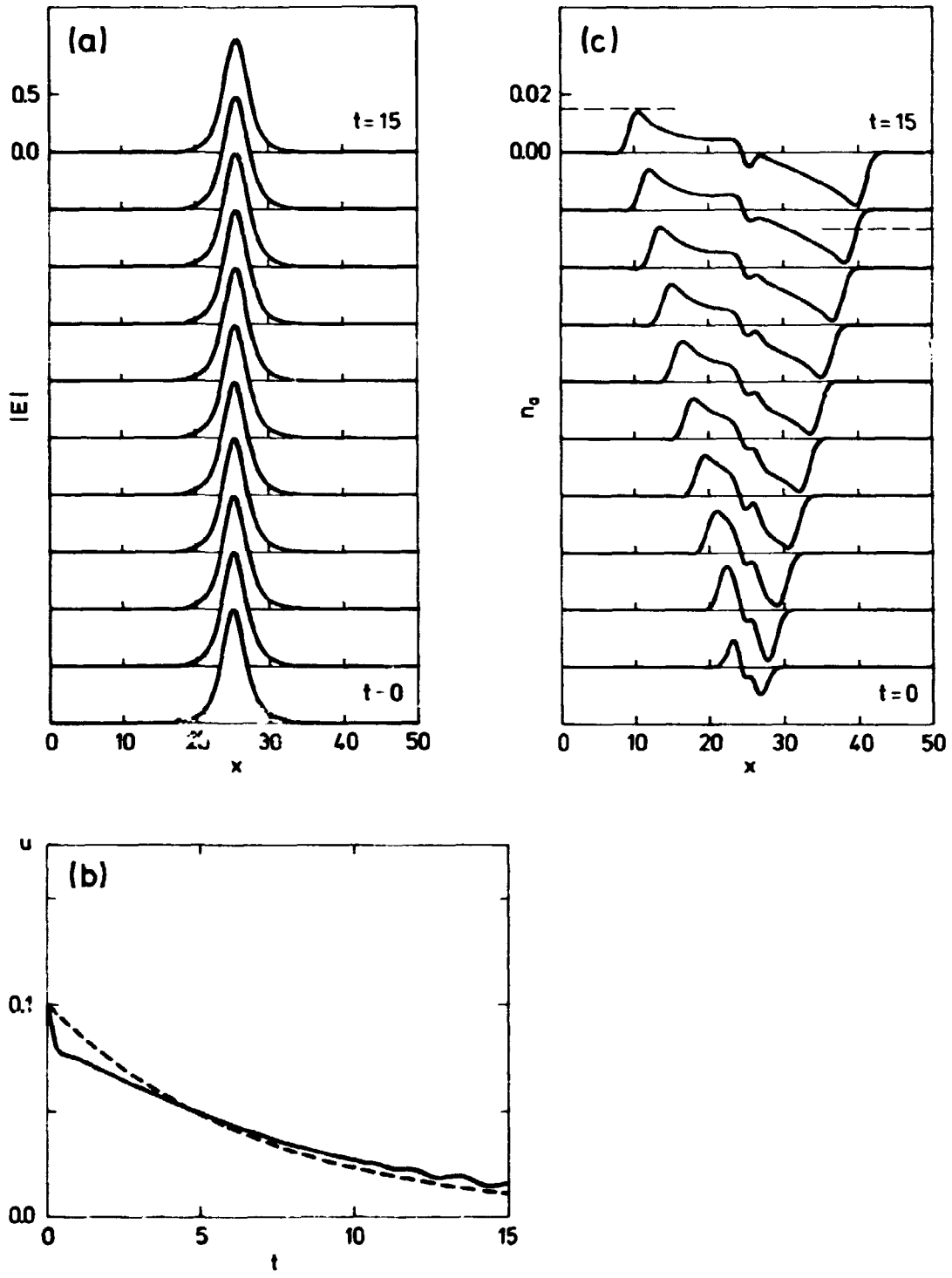

Fig. 33. The evolution of the perturbed Langmuir soliton. a) The electric field amplitude. b) The variation of the soliton velocity (full line) compared with theory (broken line). c) The ion-sound emission calculated as the difference between the total ion-density response and the soliton part; broken lines indicate the theoretical level of ion sound radiation.

2.10. Langmuir wave collapse in weakly magnetized plasmas

(P.L. Christensen*, P.S. Lomdahl* (*Technical University of Denmark) J.P. Lynov, H.L. Pécseli, J. Juul Rasmussen and K. Thomsen)

Most treatments of wave collapse in weakly magnetized plasmas concentrate on the influence of the magnetic field $\vec{B}$ on the high frequency waves (e.g. Goldman et al., 1981). It is well-known, however, that the equation for the variation of the plasma on the slow time scale has to be modified similarly (e.g. Dysthe et al., 1978) due to the appearance of new low-frequency wave types (ion-cyclotron or lower hybrid waves) propagating essentially perpendicular to $\vec{B}$. For collapse along $\vec{B}$, these waves are obviously immaterial. It is also well known that one-dimensional systems do not exhibit Langmuir wave collapse, so the direction perpendicular to $\vec{B}$ must play a role. Moreover, a recent theoretical work (Giles, 1981) actually predicts collapse of upper hybrid waves into $\vec{B}$-field-aligned filaments, and in this case a modification of the low-frequency equation may play a crucial role.

In order to elucidate the effect of the low-frequency wave types already mentioned, we considered a two-dimensional system in a plane perpendicular to $\vec{B}$. For simplicity, we treated only cases having cylindrical geometry and used a set of equations

$$\left[i\frac{\partial}{\partial\tau} - \frac{1}{r^2} + \frac{1}{r}\frac{\partial}{\partial r} + \frac{\partial^2}{\partial r^2}\right] E = \left(\frac{\omega_{UH}}{\omega_o}\right)^2 nE \qquad (1)$$

$$\left[\frac{\partial^2}{\partial\tau^2} + \Omega^2 - \frac{1}{r}\frac{\partial}{\partial r} - \frac{\partial^2}{\partial r^2}\right] n = \left[\frac{1}{r}\frac{\partial}{\partial r} + \frac{\partial^2}{\partial r^2}\right]|E|^2 \quad , \qquad (2)$$

in normalized units, where Ω represents the ion-cyclotron frequency or lower hybrid frequency, depending on the problem at hand, while ω_{UH} is the upper hybrid frequency. We solved the self-consistent set of Eqs. (1) and (2) numerically, and found that $\Omega \neq 0$ may indeed stabilize a collapse provided $2\pi/\Omega$ is smaller than a characteristic time scale for the initial stage of the collapse. The stabilization is brought about by "radi-

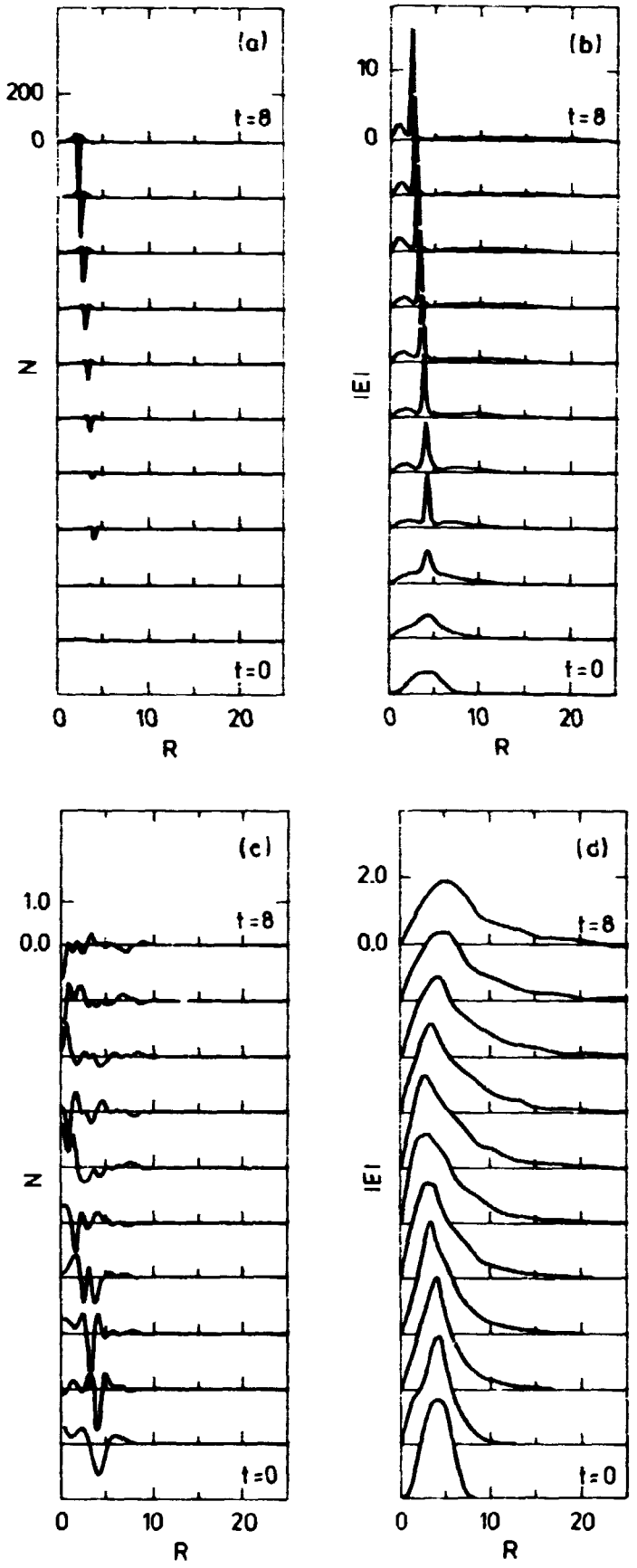

Fig. 34. Wave collapse in unmagnetized case, ((a) and (b)) and with Ω = 20 (c) and (d)), showing density N and modulus of the electric field |E|.

ation" of low-frequency modes, which inhibit the formation of a density cavity containing a localized high-frequency electric wave field of high intensity. Figure 34 demonstrate this effect, showing an unmagnetized case for reference (Fig. 34a and b), and a case where $\Omega = 20$ (Fig. 34c and d).

2.11. Non linear evolution of the transverse instability of plane envelope solitons

(P.A.E.M. Janssen (Royal Netherlands Meteorological Institute, De Bilt, The Netherlands) and J. Juul Rasmussen)

The non linear evolution of the transverse instability of plane envelope solitons was investigated. The starting point was the non-linear Schrödinger equation for the slowly varying envelope of a wave train. In two spatial dimensions the non linear Schrödinger equation, derived in many branches of physics, may take the form

$$\left(i\frac{\partial}{\partial t} + \frac{\partial^2}{\partial z^2} + \alpha\frac{\partial^2}{\partial x^2} + |A|^2\right) A = 0 \ . \qquad (1)$$

The constant α depends on the linear dispersion of the wave and may have either sign. A plane envelope soliton solution to Eq. (1) is unstable with respect to long wavelength transverse (x-direction) perturbations for both positive and negative α (Zakharov and Rubenchik, 1973). In the case of positive α there exists a critical value of $\alpha = \alpha_c$, above which the envelope soliton is stable for a given perturbation wavelength, while the soliton is unstable for $\alpha < \alpha_c$. For negative α such a critical value cannot be found and the investigations were confined to the case of positive α. By applying the multiple time scale method, the dynamical equation for the transverse instability was found to be given by the Duffing-like equation:

$$\left(\frac{\partial^2}{\partial t^2} - \gamma^2 - \beta^2|\phi|^2\right)\phi = 0 \ , \qquad (2)$$

where ϕ is the complex amplitude of the unstable mode with wave number slightly below the critical value, and γ and β are real

coefficients. From Eq. (2) it is seen that the non linear term tends to enhance the growth rate of the linearly unstable mode, leading to collapse of the envelope soliton. This result is in qualitative agreement with numerical investigations of the two-dimensional stability of Langmuir solitons (Pereira et al., 1977).

2.12. Modified Maxwellian model of a solitary electron hole

(J.P. Lynov, P. Michelsen, H.L. Pécseli, J. Juul Rasmussen, S.H. Sørensen and K. Thomsen)

In a previous work (Lynov et al., 1980b), our experimental and numerical observations of electron holes (Saéki et al., 1979; Lynov et al., 1979) were compared with a simple, theoretical description of an electron hole (Lynov, 1981) based on the single waterbag model. Although the theoretical results from this analysis concerning the hole width as a function of its amplitude were in good qualitative agreement with the numerical results, they were approximately 30% too small.

In order to improve the theoretical predictions, a more sophisticated model based on a modified Maxwellian distribution (Schamel, 1979) was applied. It was found that the modified Maxwellian model imposes restrictions on the hole velocity and amplitude, results that are in agreement with our previous waterbag calculations. When applied to the calculations of the hole width versus amplitude, the modified Maxwellian model completely removed the quantitative discrepancy between the theoretical predictions and the numerical observations which were obtained with the waterbag model. In contrast to previous predictions by others, we found in our numerical simulations, as well as our theoretical calculations with both the models mentioned, that the general trend is that the larger the hole amplitude the greater the width.

2.13. Non linear evolution of the ion-ion beam instability

(H.L. Pécseli and J. Trulsen (University of Tromsø, Norway))

A previous study (Armstrong et al., 1980) indicated that the formation of ion phase space vortices was associated with the non linear development of the ion-ion beam instability. We have pursued this hypothesis by deriving a non linear equation for the initial evolution of the instability in question, and obtained the equation

$$2\frac{\partial^2 e\phi}{\partial t^2} - 2\frac{\partial^4 \phi}{\partial x^2 \partial t^2} - V_o^2\frac{\partial^2 e\phi}{\partial x^2} + V_o^2\frac{\partial^4 \phi}{\partial x^4} =$$

$$2\frac{1}{V_o}\frac{\partial^2}{\partial t^2}(V_o^2 - 2\phi)^{1/2} - V_o^3\frac{\partial^2}{\partial x^2}(V_o^2 - 2\phi)^{-1/2}$$

$$+ V_o\frac{\partial^2}{\partial t^2}(V_o^2 - 2\phi)^{-1/2} \qquad (1)$$

where ϕ is the electrostatic potential normalized to T_e/e, V_o is the velocity (normalized to C_s, the ion sound speed) of the two counter-streaming ion beams, where for simplicity we assume that they have identical densities. Finite ion temperature effects are ignored. In Fig. 35 we show a numerical solution of Eq. (1). We note the development of positive spikes, or cusps, in the potential. These are necessarily associated with an increase in ion density, i.e. a decrease in the ion beam velocity. When fully developed, i.e. when the local ion velocity goes to zero, two adjacent cusps thus encircle an ion phase space vortex. This

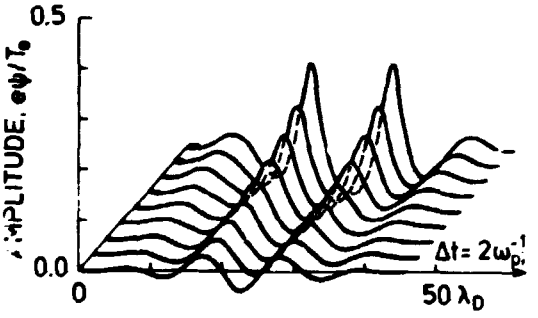

Fig. 35. Solution for the electrostatic potential as a function of position for various time. The normalizing quantities are Debye length λ_D and ion plasma period ω_{pi}^{-1}.

very final stage of the evolution of the ion beam instability is, however, not correctly accounted for by a cold ion model. Using a simple waterbag model, we argue that finite ion temperatures are important for the saturation of the instability, and a numerical particle simulation code (Trulsen, 1980) supports our interpretation, but verifies that the results of Eq. (1) are indeed accurate for the initial evolution.

2.14. Wave reflection and the Fermi acceleration problem

(K.B. Dysthe*, H.L. Pécseli and J. Trulsen* (*University of Tromsø, Norway))

The propagation of almost monochromatic plasma-wave packets in a well between oscillating, perfectly reflecting boundaries was considered. A simple set of difference equations was derived (using a dispersion relation of the form $\Omega^2 = \omega_o^2 + (kV)^2$ for the parameters of the wave packet after a reflection:

$$K_{n+1} = K_n + 2\,U(T_{n+1}) \quad , \tag{1}$$

$$T_{n+1} = T_n + 1/K_n \quad , \tag{2}$$

$$E_{n+1} = E_o(1 + K_n^2)^{1/2}/(1 + K_o^2)^{1/2} \quad , \tag{3}$$

where K is the normalized wave number of the carrier wave, E the corresponding wave energy, and T the normalized time. The function U accounts for the movement of the reflecting boundary. We found that both the basic idea of the problem and the set of equations applied for its mathematical description were conceptually very similar to those of the standard Fermi acceleration problem (e.g. Lichtenberg and Lieberman 1980). Figures 36 and 37 summarize our initial results. First, we allowed one reflecting boundary to oscillate periodically and depict the motion of one wave packet in a suitably defined phase space specified through the coordinates K_{n+1}, $1/K_n = (T_{n+1} - T_n)$, i.e. the wave number after the (n+1)-th reflection and the corresponding transit time for the wave packet. For a given initial condition, we observed a transition from regular to apparently chaotic motion

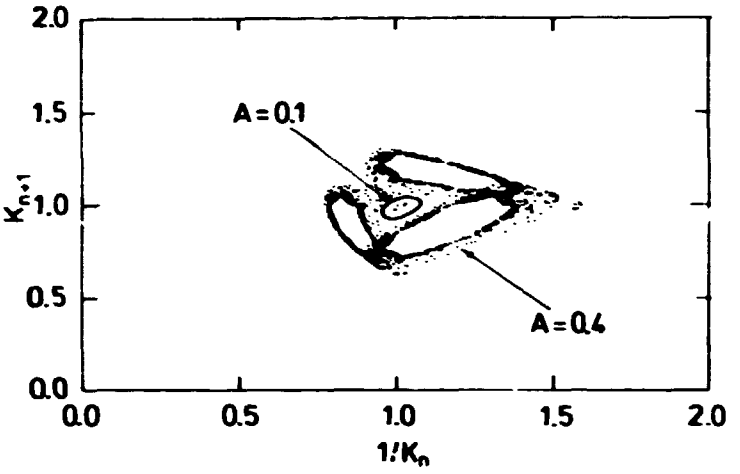

Fig. 36. Motion of a wave packet in a K_{n+1}, $1/K_n$ plane, where n is the number of reflections from a harmonically oscillating reflecting boundary, for two different amplitudes.

of the wave packet in phase space, (see Fig. 36). The amplitude 0.4 was chosen to be slightly above the critical value that leads to the chaotic behaviour. Secondly, if the phase of the oscillating boundary is chosen randomly at impact, we find, as expected, that the motion is stochastic for arbitrary oscillation amplitudes of the reflecting boundary (see Fig. 37). Ultimately, the carrier frequency exceeds the cut-off frequency and escapes from the well. We are currently investigating the behaviour of

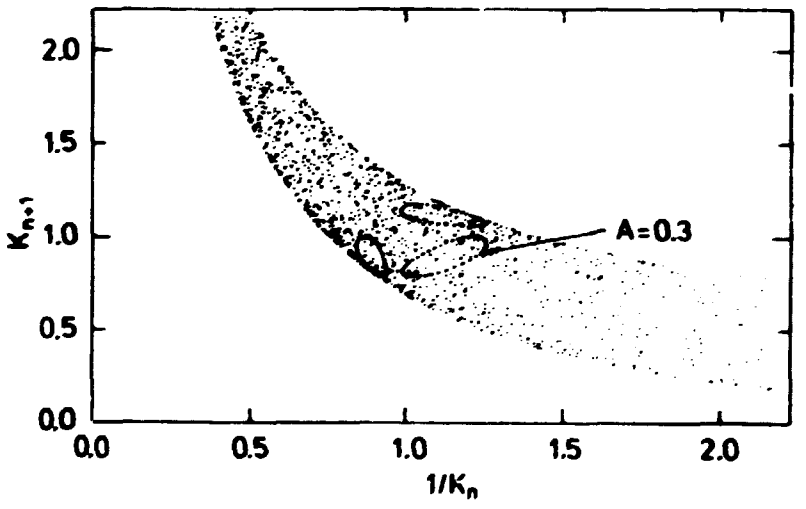

Fig. 37. Fig. 36 but with a random phase included in the oscillation. The regular curve corresponds to Fig. 36.

a full wave spectrum, under the conditions described here, by representing it by a superposition of wave packets randomly distributed in real space with a given distribution of carrier wave numbers.

2.15. Relative diffusion in turbulent plasmas

(S.E. Larsen, T. Mikkelsen and H.L. Pécseli)

The expansion of a cluster of ionized particles released in a turbulent plasma was considered. We assumed that the time scale of the turbulent fluctuations was well below the ion-cyclotron period and let the fluctuations in velocity be given by $\vec{E} \times \vec{B}_o/B_o^2$, where $\vec{E}$ is the fluctuating electrostatic field and $\vec{B}_o$ the externally applied stationary magnetic field. Following Smith (1959) we obtained a set of equations governing the expansion rate for the width $\sigma(t)$ of the cluster. Assuming that the power spectrum for the $\vec{E}$-field fluctuations is of the form $k^{-\beta}$, we find three basically different cases:

(i) for $1 < \beta < 3$. $\sigma(t) \sim t^{2/(3-\beta)}$,

(ii) $\beta = 3$, $\sigma(t) \sim e^{\alpha t^2}$,

where α is a constant determined by the turbulent spectrum,

(iii) $\beta > 3$, $\sigma(t) \sim [\delta t^2 + \gamma]^{-1/(3-\beta)}$,

leading to an explosive growth of the cluster. (Obviously the divergence does not conform to physical reality since the power law $k^{-\beta}$ ultimately breaks down).

We find it particularly interesting that experimental and analytical results (Mikkelsen and Pécseli, 1978; Tchen et al., 1980) give a k^{-3} subrange for two-dimensional gradient-driven electric field fluctuations. Our results are relevant for the diffusion of material deposited in a turbulent plasma by, e.g. barium cloud releases in the ionosphere or pellet refuelling in fusion experiments (Chang et al., 1980).

2.16. Laboratory investigation of electron Bernstein waves in inhomogeneous magnetic fields

(R.I. Armstrong*, Å. Frederiksen*, H.L. Pécseli, K. Rypdal* and J. Trulsen* (*University of Tromsø, Norway))

The basic properties of electron Bernstein waves in inhomogeneous magnetic fields were investigated. The magnetic field was produced by two Helmholz-coils placed at an angle (typically ~ 30°) and the waves were excited by a shielded antenna (Armstrong et al., 1981) and propagated essentially along the symmetry axis of the two coils. The phase fronts curve as the wave propagates, due to the inhomogeneity of the $\vec{B}$-field. (The phase velocity decreases with increasing $|\vec{B}|$). The angle between the wave normal and $\vec{B}$ thus changes locally, leading to enhanced wave damping as predicted by theory (e.g. Muldrew anc Gonfalone, 1974). However, as the wave propagates into regions of varying $|\vec{B}|$, its group-velocity v_g changes. Conservation of wave energy flux leads to a corresponding variation in wave amplitude, in addition to the one caused by wave damping. The effect of a locally varying group velocity is most easily observed as the wave propagates towards a resonance (i.e. $k \to \infty$) since a WKB-approach remains valid throughout the whole region (in contrast to the behaviour close to cut-off). Wave reflection following a cut-off was also investigated. This phenomenon, however, seems to require extremely homogeneous $\vec{B}$-fields locally in the cut-off region. By carefully shaping the magnetic field, a geometric focussing of electron Bernstein waves seems feasible.

2.17. Highly supersonic ion pulses connected with the temporal evolution of a current-driven potential relaxation instability

(R. Schrittwieser (Innsbruck University, Austria) and J. Juul Rasmussen)

The initial transient response of a collision-less plasma to a high positive voltage step was investigated in the Q-machine at Innsbruck University, Austria. Four different pulses were observed. An electron plasma wave pulse was followed by an ion burst. The latter was overtaken and absorbed by a highly super-

sonic ion pulse. Thereafter, an ion rarefaction pulse with roughly the ion-acoustic velocity propagated into the other direction. The supersonic pulse was tentatively explained as being the result of a transient Buneman instability. Together with the rarefaction pulse, it formed the first cycle of an instability which is customarily considered a current-driven ion-acoustic one, but is, in fact, a potential relaxation instability (Iizuka et al., 1980).

2.18. Stopping of 0.3-10 keV/amu ions in solid H_2, D_2, and N_2

(P. Børgesen and H. Sørensen)

The electronic stopping cross section S_e of hydrogen ions in solid H_2 and D_2 was found by two independent methods to be the same as in gaseous targets, whereas a very large difference was found between solid and gaseous targets of N_2 by three independent methods (phase effect).

The ranges R_L of hydrogen ions in solid H_2, D_2 and N_2 were determined as described earlier (Børgesen et al., 1979) and compared to Ionization Extrapolated Ranges (IER) measured by a similar method in gaseous targets (Cook et al., 1953). Very good agreement was found for hydrogen targets, whereas the ranges in solid N_2 were considerably larger than in N_2-gas.

The corresponding S_e were measured by a back-scattering method. The energy spectrum of positive ions back-scattered from a thick layer of solid Xe was measured with an electrostatic analyzer (Børgesen et al., 1980) at an angle of 45° to the surface. Deposition of a thin film of D_2 or N_2 on the Xe would cause the Xe-signal to be shifted towards lower energies because of the energy loss of the ions passing in and out through the film. Very few ions were back-scattered from the film. S_e could then be evaluated from the film thickness ΔX and the energy shift ΔE of the Xe-signal. For various experimental reasons, these measurements could be made only within a quite small energy interval.

For both D_2- and N_2-targets, the measured S_e were in very good agreement with the corresponding ranges R_L, while S_e for solid N_2 was only about half of that measured independently in N_2-gas (Dose and Sele, 1975). Thus, we conclude that for hydrogen targets the stopping is essentially independent of the phase, but that there is a phase effect for N_2 targets.

The phase effect in N_2 was further investigated by a method developed for that particular purpose: For projectiles of energy E incident on a target material A the secondary electron emission coefficient δ_A may be expressed as (Schou, 1979)

$$\delta_A = \Lambda_{exp}(A) \cdot S_e(E,A) \ . \qquad (1)$$

If we assume the stopping cross section in solid H_2 to be well established (see above), we may then determine $S_e(E,N_2)$ from measurements of secondary electrons via the following expression

$$S_e(E,N_2) = \frac{\delta_{N_2}}{\delta_{H_2}} \frac{\Lambda_{exp}(H_2)}{\Lambda_{exp}(N_2)} S_e(E,H_2) \ . \qquad (2)$$

Although the experimental "material parameter" Λ_{exp} depends somewhat on projectile and energy (Schou, 1979), it may be shown that at the presently used energies, the ratio $\Lambda_{exp}(H_2)/\Lambda_{exp}(N_2)$ is the same for incidence of electrons as for protons. In Eq. 2 this ratio is determined from independent experiments with electrons (Sørensen, 1977, Sørensen and Schou, 1978, Schou and Sørensen, 1978). The above approach, used for justifing the existence of a phase effect reducing S_e in solid N_2 to about half of that in N_2-target, is rather uncertain, because it is based on many assumptions. However, the conclusion that a phase effect exists agrees with other independent observations. A similar effect was not found for incidence of electrons (Sørensen and Schou, 1978).

2.19. Erosion of solid H_2, D_2, N_2, Ne, and Ar by 1-3 keV electrons

(P. Børgensen and H. Sørensen)

For thin films on an Au-substrate both the electron reflection coefficient η and secondary electron emission coefficient δ vary with film thickness ΔX. Thus, in bombarding even a very thick film with an electron beam of known intensity, we may determine the time it takes to erode the film completely by continuously monitoring η or $(\delta+\eta)$.

Figure 38 shows initial film thickness ΔX versus the incident beam dose D necessary for complete film erosion, for 2-keV electrons incident on D_2-films. Films were eroded with biases of -45 V (▽) and +45 V (●) on a grid around the target, and the

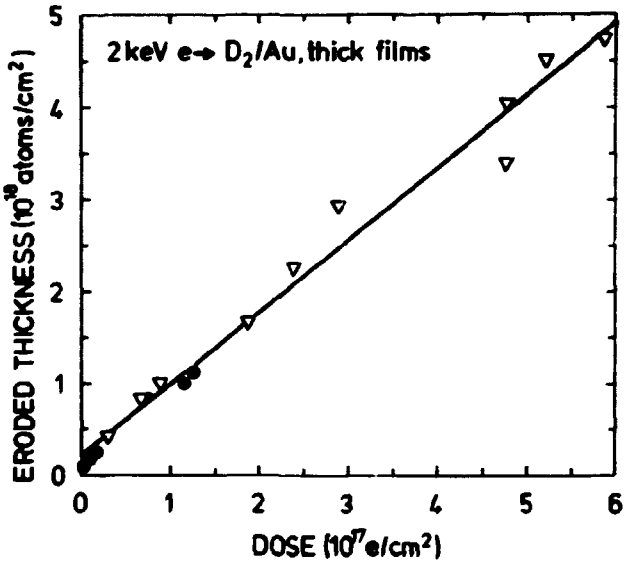

Fig. 38. Initial film thickness X_o vs. total dose D_o of erosion. Thick films. Results with bias -45 V (▽) and +45 V (●). Solid line: Fit through (D_o, X_o)-points for $X_o > 4 \cdot 10^{17}$ at/cm^2.

agreement between the two sets of points proves that the erosion is not significantly influenced by a small bias. This was not the case for Ne-targets: a positive bias of only +30 V was seen to strongly inhibit the erosion of Ne-films, suggesting perhaps that the erosion is somehow related to an ionization of the target atoms. This behaviour seems to be unique for Ne.

For thin films the erosion rate was found to depend on the instantaneous film thickness, whereas for thick films a linear relation between thickness ΔX and beam dose D indicates a constant erosion rate (see Fig. 38). The thickness-dependent region seemed to be a material constant, quite unrelated to the projectile range. A bulk erosion yield was determined by fitting a straight line to the thick film results. Table 3 shows the bulk erosion yields determined until now. We note that preliminary measurements (Børgesen et al., 1980) gave typical yields of ~ 800 atoms/atom for incidence of 2-keV protons on bulk H_2, i.e. protons are almost two orders of magnitude more efficient than electrons in the eroding solid H_2.

Table 3. Erosion of bulk targets by 1-3 keV electrons

Target	Energy [keV]	Yield [atoms/electron]
H_2	2	~ 15
D_2	1	6.9
	2	7.8
	3	7.8
Ne	1.2	20.8
	2	14.7
	3	10.5
N_2	2	~ 1
Ar	3	~ 0.6

2.20. Secondary electron emission from mixtures of solid hydrogen isotopes

(H. Sørensen, J. Schou, Chen Hao-Ming (Tsing Hua University, Peking, China) and P. Børgesen)

The data analysis of the previously obtained results (Børgesen et al., 1980) has continued. For all binary mixtures of solid hydrogen, deuterium, or tritium, the following expression for the secondary electron emission coefficient δ has been determined:

$$\delta = \frac{\delta_x \delta_y}{c_x \delta_y + c_y \delta_x} \quad ,$$

where δ_x is the secondary electron emission coefficient for the pure isotope, and c_x is the atomic concentration. The agreement between this formula and the experimental results is encouraging.

2.21. Nuclear stopping power of hydrogen for primary electrons

(J. Schou)

The nuclear stopping power for primary electrons in hydrogen isotopes has been evaluated on the basis of the Born approximation. This stopping power is usually neglected because of the small energy loss, but is nevertheless important for the broadening of the energy distribution in hydrogen pellet material.

The stopping power for primary energies above 100 eV in all hydrogen isotopes is given by

$$-\frac{dE}{dx} = N\pi\frac{me^4}{ME}\ln\frac{1.302\ E}{I} \quad ,$$

where N is the atomic density, m and M the mass of the electron and the nucleus, respectively, -e the electron charge, E the primary energy, and I the mean ionization potential (= 15.0 eV for atomic hydrogen). Then, the average energy loss for a 2 keV electron penetrating a monolayer of molecular hydrogen is approximately 0.1 meV. Thus, it is hardly possible that a direct knock-on mechanism is responsible for the erosion yield of 15 atoms/electron at 2 keV (see 2.18).

2.22. Secondary ion emission from NbV-alloys

(J. Schou, G. Plentje*, W.O. Hofer* and U. Linke* (KFA, Jülich, F.R.G.))

Secondary ion emission from a series of NbV-alloys by ion bombardment has been studied in a follow-up of a more comprehensive work on cluster emission (Schou and Hofer, 1982). It turned out that there is almost no relative difference in Nb- or V-ion yields, in spite of large differences in surface morphology.

2.23. Vaporization mode and state of the ablatant of a hydrogen pellet in tokamak discharges

(C.T. Chang)

In the original neutral-shielding model of Parks and Turnbull (1978), the system of equations describing the ablated flow was analyzed by using the following boundary condition at the pellet surface: $q_p/q_* = 0$ and $T_v/T_* = 0$, i.e. the energy flux q_p of the incident electrons and the temperature T_v of the ablatant near the pellet surface are considerably lower than their respective values of q_* and T_* at the sonic surface. This boundary condition is physically unsatisfactory in two aspects: The solution of the problem depends explicitly on the plasma temperature alone and is universally valid for arbitrary plasma electron density and pellet radius. The condition of $q_p/q_* = 0$ does not conform with the requirement of energy conservation.

By comparing the ablation time of a hydrogen pellet in tokamak discharges with the time required for the sublimation process, it is shown that the evaporation of the pellet is a dynamic phase transition, instead of being a slow sublimation; i.e. the transport of heat is due to the propagation of an evaporation front. Based on this finding, an alternative boundary condition is formulated thus

$$\frac{\gamma}{2}\left(\frac{\gamma+1}{\gamma-1}\right) > \frac{q_p - q_s}{\dot{n}\, kT_v} > \frac{1}{\gamma-1}$$

where γ is the ratio of specific heats of the evaporate, T_v the temperature of the evaporate at the pellet surface, q_p the energy of the incident electron at the pellet surface, and $q_s = \dot{n}\epsilon'$ the energy carried away by the evaporate due to the sublimation energy ϵ'.

Using this boundary condition, the state of the ablatant and the scaling law of the pellet ablation rate were analyzed numerically. The results showed that compared to the result obtained using the previous condition of $q_p/q_* = 0$, the ablatant near the pellet surface is hotter and less dense. The scaling law of the pellet ablation rate is unaffected by this change of the boundary condition.

2.24. Theoretical study of the H_α-line emission from a hydrogen pellet in tokamak discharges

(C.T. Chang)

Currently, the in-situ ablation rate of a refuelling pellet was inferred mainly from the H_α-line emission of the ablatant.

Based on a simplified collisional-radiative model (Bates et al., 1962) that all upward transitions of excitations and ionization by electron impact are from the ground state and neglecting recombination processes, the rate of H_α-photons emitted per unit volume is related to the ionization rate by a function (see Fig. 39).

$$G = \frac{dn_{H_\alpha}}{dt} / \frac{dn_i}{dt} .$$

Using the neutral-shielding model (Parks and Turnbull, 1978), computer studies of the correlation between the spatial variation of the total H_α-photon emitted, dn_{H_α}/dx and of the pellet particle ablated, dn_p/dx, were undertaken for given plasma temperature and density profiles. The results indicate that when perturbation of the background plasma is absent, good correlation between the rate of the pellet ablation and of the H_α-emission

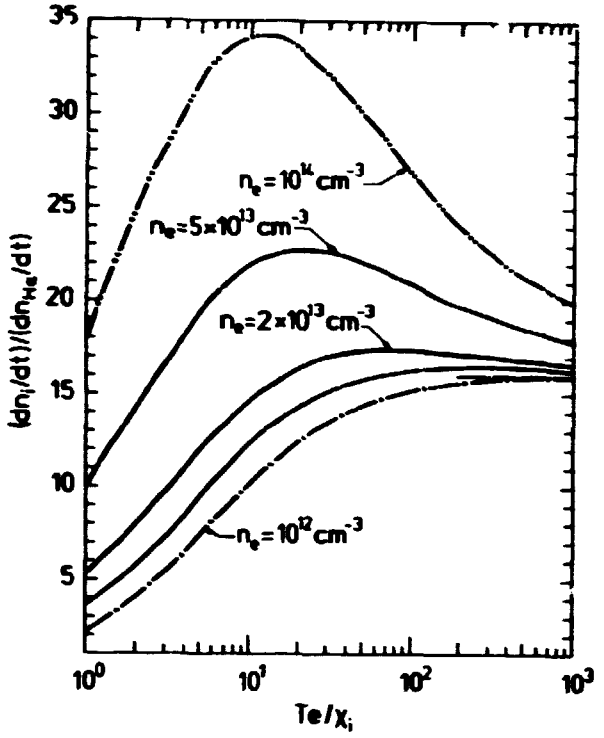

Fig. 39. Variation of the function $1/G = (dn_i/dt)/(dn_{H_\alpha}/dt)$ vs. the normalized electron temperature T_e/χ_i, where χ_i is the ionization potential.

is obtained provided there is no strong influx of charged particles and very low electron temperature at the plasma edge. Since the plasma edge temperature is likely to be around 10 eV or beyond in most tokamak discharges, and the total charged particle influx is unlikely to exceed the total number of particles, N, contained originally in the torus, good correlation between the rate of H_α-emission and that of the pellet ablation is to be expected for the injection of a small pellet, e.g. the total particle N_p contained in the pellet does not exceed a few percent of the total number of particles N contained in the torus.

2.25. Dante (Danish Tokamak Experiment)

(V. Andersen, H. Bejder, M. Gadeberg, P.B. Jensen and P. Nielsen)

Work with the guide tube technique has continued in order to inject the frozen deuterium pellets into the plasma in a well defined manner. Problems with the angular spread of directions of the pellets leaving the guide tube have been overcome by development of a special launching unit, giving the pellets a well-

defined orbit. Figure 40 shows the angular spread of the pellets leaving the bare guide tube, and Fig. 41 shows the angular spread using the launching unit. In both cases, the target is an aluminum foil of 14 cm in diameter. The free flight distance of the pellets is 60 cm.

New measurements of the ablation of relatively large (2 mm × 0.6 mm (diameter)) pellets in the hot plasma have been performed in a plasma discharge with fewer run away electrons. This showed a drastic decrease in the ablation rate, giving an ablation of approximately 10% of the pellet. This is in much better agreement with the theory than the previous results. Yet the measured ablation is still higher than the result given by the theory, which may indicate that we have some runaway electrons left.

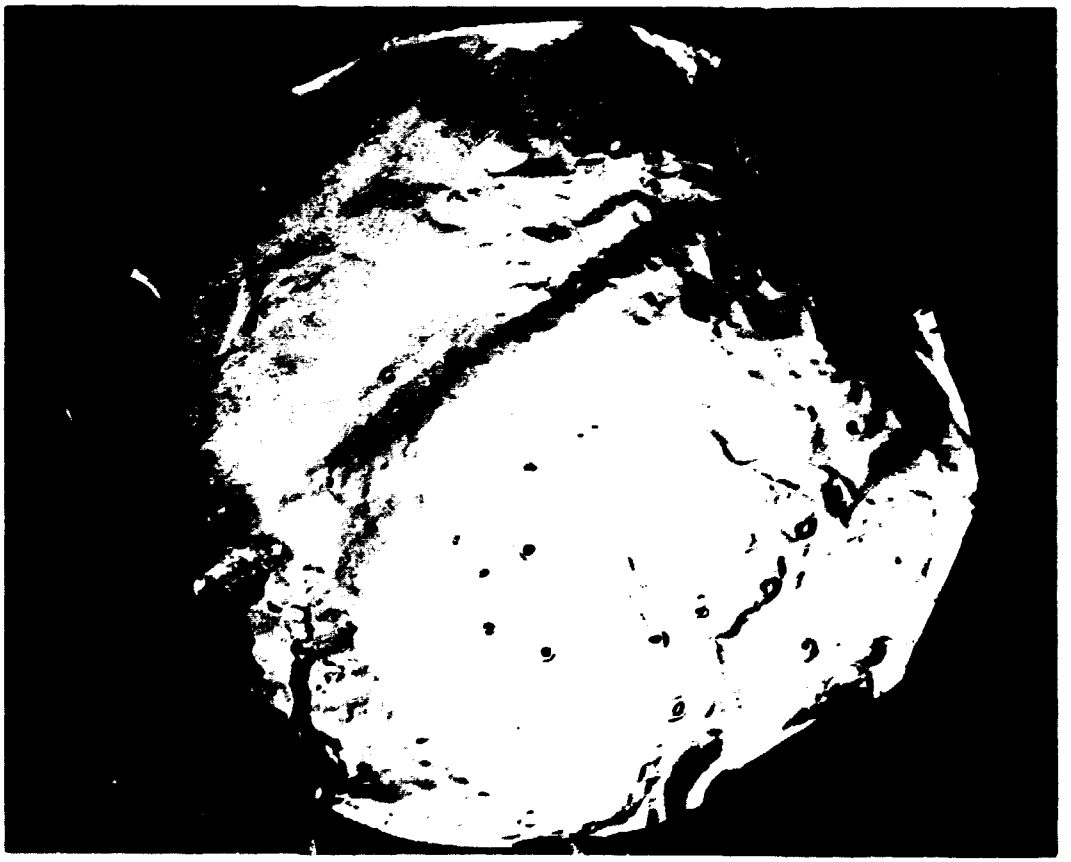

Fig. 40. Target foil showing the angular spread in pellet direction on leaving the bare guide tube. The distance between the end of the guide tube and the foil was 60 cm and the foil was circular with a diameter of 14 cm.

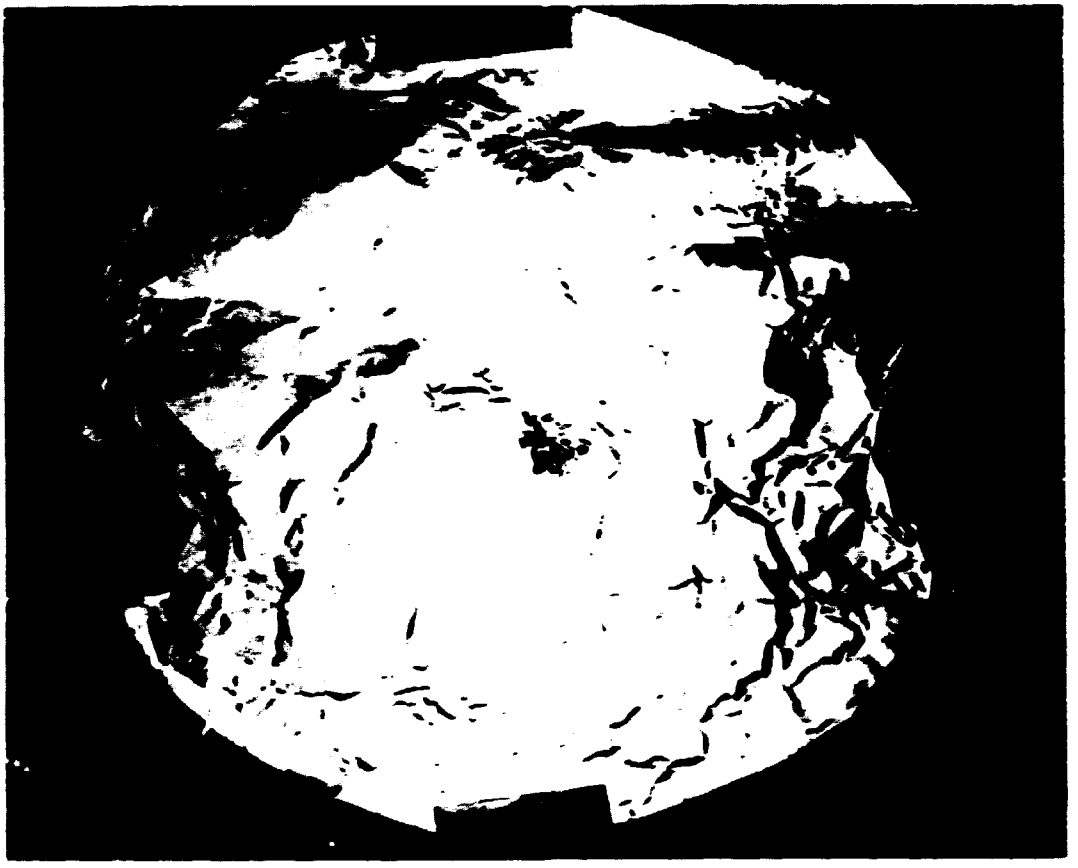

Fig. 41. Target foil showing the final angular spread in pellet direction on using the special launching unit.

With a pellet size not reproducible from shot to shot, it is desirable to measure the actual size of the pellet in each shot. This has been done by use of a microwave cavity passed by the pellet. The shift in resonance frequency is proportional to the mass of the pellet.

The ruby laser, Thomsen-scattering system, has been installed at the tokamak. Measurements of the local electron temperature are in agreement with the electron temperature measured by soft x-rays, within the measuring uncertainties. The Thomsen-scattering system has the capability of making two temperature measurements with a time difference of up to 0.8 ms. The idea of this capability is to measure the shift in electron temperature, when the pellet enters the plasma.

Measurements of plasma position by use of soft x-rays (detected by a single detector) have been used to check the plasma position given by magnetic loop measurements. Good agreement was obtained. A set-up of an array of detectors for soft x-rays is being built and mounted at the tokamak for measurements of plasma position, the profile of soft x-rays from the plasma, and to give indication of minor disruptions in the plasma.

A new pellet injector, giving smaller pellets than the first one, has been installed at the tokamak. The new pellet is cylindrical in shape, with a diameter and length of 0.4 mm. The dimensions are about a factor of ten lower than the dimensions of the first pellets. Such small pellets are very delicate to handle, and the pellet injector is still not working satisfactorily. Nevertheless, we have been able to inject small pellets into the plasma. This is seen in Fig. 42 where the emitted H_α light following the ablation process gives the trace of the pellet orbit. The drastic deflection of the orbit is more than expected from interaction with the thermal electrons, indicating, in agreement with earlier experiments, that we still have run away electrons in the plasma discharge.

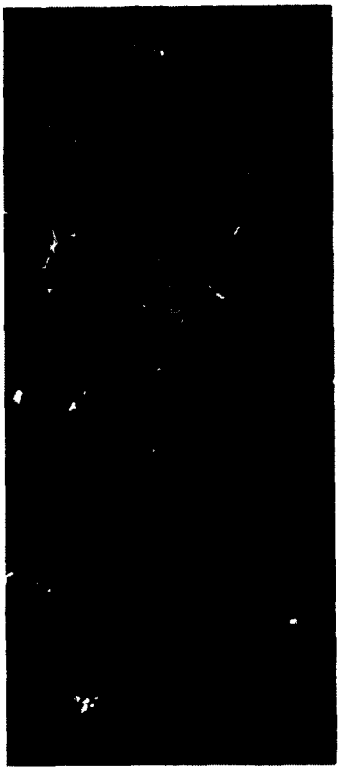

Fig. 42. Injection of a frozen deuterium pellet (0.4 mm× 0.4 mmϕ) into the hot plasma. The emitted H_α light following the ablation process gives the trace of the pellet orbit.

2.26. D_2-pellet handling and acceleration

(S.A. Andersen, K. Borman, J. Knudsen, A. Nordskov, J. Olsen, B. Sass, H. Sørensen and K.-V. Weisberg (Electronics Department, Risø))

The purpose of this work is to build D_2-pellet injectors for Dante, and also to develop pellet injection and acceleration methods that can be used in larger tokamaks. The latter part of the programme is financed by a three-year grant from the Danish Ministry of Energy.

Three different pellet injectors have been under construction this year. In all cases, the pellets are accelerated by the gas gun principle, i.e. a pellet is blown out from a gun barrel by means of a pressure burst of H_2 gas applied behind it.

A pellet injector to be used for injecting small pellets into Dante had previously been built and tested in manual operation (Andersen et al. 1980). It was thereafter tested through automatic operation at a test stand. Finally, a compact unit for automatic operation was designed and built, and the injector was then installed at Dante. The spread in direction was quite large for these small pellets, which must be led from the injector to Dante through a guide tube. Thus we had to use a slide between the injector and the guide tube in order to hit the guide tube. A slide is a circular metal rod with a groove on the inner side (Jensen and Andersen 1981). The pellet is forced to follow the bottom of the groove and the spread in direction is then reduced considerably. The slide deflects the direction of movement of the pellet and here we used a slide with a deflection of 90^{o}. The pellet size is approximately 0.01 mg = $1.6\ 10^{18}$ molecules. The velocity is ~ 100 m/s.

Two pellet injectors for larger pellets are under construction; one is for use at the tokamak at CEN Fontenay-aux-Roses, Paris, France (TFR), and one is for general studies of large pellets. In both cases the pellets are accelerated with pressurized H_2 gas taken from a H_2 bottle at room temperature. The burst of H_2

gas is let in by means of an electromagnetic valve which is opened by discharging a condenser bank.

The injector for the TFR is constructed according to a collaboration agreement between the Centre d'Etudes Nucléaire at Fontenay-aux-Roses and Risø National Laboratory, according to which Risø manufactures and delivers a pellet injector for use at the TFR. The injector will be a modified version of the first injector made for Dante (Nordskov et al. 1980 and Andersen et al. 1981). The injector has been thoroughly overhauled and a longer gun barrel (115 mm) has been mounted. The electromagnetic valve used for letting in the propellant gas is placed inside the vacuum system, close to the gun barrel. The tube length from the valve to the pellet position is ~ 150 mm. The injector is placed in a newly designed vacuum chamber pumped by a turbo pump. It has been tested several times by manual operation with propellant gas pressures of up to 16 bar, and velocities of upto 800 m/s have been registered. The main problem seems to be the extrusion of solid D_2, i.e. to get a pellet of good quality every time.

The fabrication and acceleration of a pellet is only the first of several problems which have to be solved. The second problem concerns the transport of the pellet into the tokamak. The injector has to be placed at some distance from the tokamak and the vacuum connection to the tokamak must be of fairly large dimensions. There will then be a very good connection between the vacuum system of the injector, where the pressure will correspond to the vapour pressure of H_2 at 4.2 K, i.e. approximately 5 10^{-6} mbar, and the tokamak, where the pressure should be orders of magnitude better. The problem of establishing an appropriate vacuum may be solved by means of a large differential pumping system. Another possibility is to transport the pellet into the tokamak through a guide tube, i.e. a smallbore tube where the pellet slides on the inner wall. This technique has been used successfully for low velocity pellets at Dante, with teflon tubes and brass tubes (Andersen et al. 1981), and for high velocity pellets at IPP Garching, with glass tubes.

For the TFR injector we choose the latter solution and will use a nylon tube with a 2-mm bore. The use of a nylon guide tube offers two advantages: Firstly, it is electrically insulating and secondly, it is translucent. A pellet can then be detected by a photodetector, and its velocity can be measured by two photodetectors. A pellet has a rather large spread in direction when leaving a guide tube; this spread can be reduced considerably by using a slide after the guide tube. Here, we use a slide with a deflection of 10°. At present, a 1.5 m long guide tube is in use, followed by a slide, and the pellets are shot onto household aluminium foil (16 μm) placed 0.35 m in front of the slide. Some pellets disintegrate when passing the system, while good pellets go right through the foil. We occasionally see the next good pellets pass through the same hole, i.e. the pellets may hit the foil within a circle of less than 2 mm diameter.

A third problem concerns the operation of the injector. It should run automatically after being started by an electrical pulse from the TFR control room. At the same time, the final firing of the injector should be timed together with the firing of the TFR. A set-up to accomplish this is under construction.

The other injector for accelerating large pellets is a new construction. The volume of solid D_2 used is twice that of the earlier-built injectors, and filaments of 2 mm in diameter are extruded. The filament is extruded through a 2-mm bore in a 4 mm cylinder, which is then rotated 90° so that the bore becomes a part of the gun barrel; the gun barrel is then loaded. The pellet size is 4 mm long and 2 mm in diameter. At this time, the injector is equipped with only a 65-mm gun barrel. Later, when a new vacuum chamber is ready, a longer barrel will be used. The injector has been fired by manual operation and velocities of up to 300 m/s have been obtained. This injector is now ready for automatic operation and will be tested in various ways; first with the short gun barrel and later with longer ones.

2.27. Single point Thomsen scattering system for JET (Joint European Torus)

(P. Nielsen)

The design of the system has proceeded to a detailed design stage. Drawings have been submitted for approval on top- and bottom-port benches, collecting tower, associated mirror assemblies and, on the west wall, alignment units. Final approval has not yet been obtained for any of these items, but most of the problems have been located, and approval of all of these components is expected in the beginning of 1982.

Tentative agreement has been reached for the radiation trap systems; a set of detailed drawings is being prepared.

The electronic system has been changed due to JET's implementation of the Line Surveillance Driver (LSD) system in place of input/output registers. In view of this, and with the knowledge of the laser system electronics, a new proposal has been submitted for approval. Approval of the principles has been given.

The ruby laser has been completed by the manufacturer. An acceptance test of the facilities of J.K. lasers took place in early December, 1981. The laser had a better performance in all modes than specified. A few simple changes to automate the mode switching were requested, and the modified system will be delivered to Risø in February 1982 for final acceptance tests.

2.28. References to Chapter 2

ANDERSEN, S., KNUDSEN, J., NORDSKOV, A., OLSEN, J., SASS, B., SKOVGÅRD, H., SØRENSEN, H. and WEISBERG, K.V. (1980). In: Risø-R-441, 107-108.

ANDERSEN, V., GADEBERG, M., JENSEN, P.B., NIELSEN, P. and SØRENSEN, H. (1981). In: Proceedings of the 11th Symposium on Fusion Technology, Oxford, September 1980, 1113-1118.

ARMSTRONG, R., PÉCSELI, H.L. and TRULSEN, J. (1980). In: Risø-R-441, 85-86.

ARMSTRONG, R.J., RASMUSSEN, J.J., STENZEL, R.L. and TRULSEN, J. (1981). Phys. Lett. 85A, 281-284.

BATES, D.R., KINGSTON, A.E. and McWHIRTER, R.W.P. (1962). Proceedings of Roy. Soc. (London) A267, 297-312.

BLOCK, L.P. (1981). In: Geophysical Monograph 25, AGU, Washington D.C., 218-225.

BØRGESEN, P., CHEN HAO-MING, SCHOU, J. and SØRENSEN, H. (1980). In: Risø-R-441, 91-92, 94-96.

BØRGESEN, P., SCHOU, J. and SØRENSEN, H. (1979). In: Physics Department, Annual Progress Report, Risø-R-414, 66-67.

BØRGESEN, P., SCHOU, J. and SØRENSEN, H. (1980). In: Proceedings of the Symposium on Sputtering, Vienna, April 1980, 822-831.

CHANG, C.T., JØRGENSEN, L.W., NIELSEN, P. and LENGYEL, L.L. (1980). Nucl. Fusion 20, 859-893.

COOK, C.J., JONES JR., E. and JØRGENSEN JR., T. (1953). Phys. Rev. 91, 1417-1422.

DOSE, V. and SELE, G. (1975). Z. Physik A272, 237-243.

DYSTHE, K.B., MJØLHUS, E., PÉCSELI, H.L. and STENFLO, L. (1978). Plasma Phys. 20, 1087-1099.

GILES, M.J. (1981). Phys. Rev. Lett. 47, 1606-1608.

GOLDMAN, M.V., WEATHERALL, J.C. and NICHOLSEN, D.R. (1981). Phys. Fluids 24, 668-672.

IIZUKA, S., MICHELSEN, P., RASMUSSEN, J. JUUL and SCHRITTWIESER, R. (1980). In: Physics Department, Annual Progress Report, Risø-R-441, 84-85.

IIZUKA, S., SAEKI, K., SATO, N. and HATTA, Y. (1979). Phys. Rev. Lett. 43, 1404-1407.

JENSEN, P.B. and ANDERSEN, V. (1981). Risø-M-2294.

KAN, J.R., LEE, L.C. and AKASOFU, S.-I. (1979). J. Geophys. Res. 84, 4305-4315.

KARPMAN, V.I. (1979). Phys. Scr. 20, 462-478.

LICHTENBERG, A.J., LIEBERMAN, M.A. and COHEN, R.H. (1980). Physica 1D, 291-305.

LYNOV, J.P. (1981). In: Solitary electron density waves in a magnetized, plasma loaded waveguide, Risø-R-432, 56-74.

LYNOV, J.P., MICHELSEN, P., PÉSCELI, H.L., RASMUSSEN, J. JUUL, SAEKI, K. and TURIKOV, V.A. (1979). Phys. Scr. 20, 328-335.

LYNOV, J.P., MICHELSEN, P., PÉCSELI, H.L. and RASMUSSEN, J. JUUL (1980b). In: Risø-R-441, 80-82.

LYNOV, J.P., MICHELSEN, P., PÉCSELI, H.L., RASMUSSEN, J. JUUL and THOMSEN, K. (1980a). In: Risø-R-441, 79-80.

MIKKELSEN, T. and PÉCSELI, H.L. (1978). Phys. Rev. Lett. 41, 951-954.

MORALES, G.J. and O'NEIL, T.M. (1972). Phys. Rev. Lett. 28, 417-420.

MULDREW, D.B. and GONFALONE, A. (1974). Radio Sience 9, 873-880.

NORDSKOV, A., SKOVGÅRD, H., SØRENSEN, H. and WEISBERG, K.V. (1980). Risø-M-2245.

PARKS, P.B. and TURNBULL, R.J. (1978). Phys. Fluids 21, 1735-1741.

PEREIRA, N.R. SUDAN, R.N. and DENAVIT, J. (1977). Phys. Fluids 20, 936-945.

PIERCE, J.R. (1944). J. Appl. Phys. 15, 721-726.

POCOBELLI, G. (1980). In: Proceedings of the International Conference on Plasma Physics, Nagoya, Japan, April 7-11. vol. 1, p. 20; and (1982), to be published.

RYPDAL, K. (1981). Non-linear Wave Phenomena in Plasma Media. Thesis. University of Tromsø Report.

SAEKI, K., MICHELSEN, P., PÉCSELI, H.L. and RASMUSSEN, J. JUUL (1979). Phys. Rev. Lett. 42, 501-504.

SCHAMEL, H. (1979). Phys. Scr. 20, 336-342.

SCHOU, J. (1979). Risø-R-391.

SCHOU, J. and HOFER, W.O. (1982). Sputtered Clusters from Niobium-Vanadium Alloys. To be published.

SCHOU, J. and SØRENSEN, H. (1978). J. Appl. Phys. 49, 816-821.

SMITH, F.B. (1959). Advances in Geophysics, Vol. 6, 193.

SØRENSEN, H. (1977). J. Appl. Phys. 48, 2244-2251.

SØRENSEN, H. and SCHOU, J. (1978). J. Appl. Phys. 49, 5311-5318.

SUGIHARA, R. and YAMANAKA, K. (1979). Nagoya University Research Report IPPJ-387.

TCHEN, C.M., PÉCSELI, H.L. and LARSEN, S.E. (1980). Plasma Phys. 22, 817-829.

TRIVELPIECE, A.W. and GOULD, R.W. (1959). J. Appl. Phys. 30, 1784-1793.

TRULSEN, J. (1980). PICBEAM, A Particle-in-Cell Plasma Simulation Code for Phenomena on the Ion plasma Period Time Scale. University of Tromsø Report.

TURIKOV, V. (1978). Risø-R-380.

YU, M.Y. and SHUKLA, P.K. (1977). Plasma Phys. 19, 889-893.

ZAKHAROV, V.E. (1972). Zh. Eksp. Teor. Fiz. 62, 1745-1759, [(1972) Sov. Phys. JETP 35, 908-914].

ZAKHAROV, V.E. and RUBENCHIK, A.M. (1973). Zh. Eksp. Teor. Fiz. 65, 997-1011, [(1974) Sov. Phys. JETP 38, 494-500].

3. PARTICIPATION IN THE UA2 COLLABORATION AT CERN

3.1. The UA2 collaboration at CERN

(O. Kofoed-Hansen, J. Dines Hansen*, P. Hansen*, B. Madsen* and R. Møllerud* (*Niels Bohr Institute, Copenhagen, Denmark))

This group of researchers participate together with similar or larger groups from Bern, Switzerland, CERN, Geneva, Switzerland, Orsay, France, Pavia, Italy, and Saclay, France, in the utilization of the UA2-detector to study $p\bar{p}$ interactions at the SPS-collider. The goal is a search for Z^0 and W^+ and W^- particles resulting from high-energy $p\bar{p}$-collisions. The work is described in a series of so-called $p\bar{p}$ notes. The construction and assembly of the detector was completed in the fall and the first test in actual $p\bar{p}$ beam conditions was carried out in November and December. The results are being analyzed.

4. METEOROLOGY

In 1957, when the meteorological investigations at Risø started, the main emphasis was on the subject of atmospheric dispersion of pollutants, because Risø is a nuclear research facility with a corresponding responsibility for the environment. From the very beginning instruments for recording of atmospheric parameters such as wind speed and wind direction were installed along the 123 m high tower. As a consequence, 25 years long time series, conveniently stored on computer tape, now exist and constitute an excellent source of information in climatological investigations.

The scientific environment at Risø and in particular in the Physics Department created over the years a general interest in starting both theoretical and experimental meteorological research. Consequently, by the late sixties the Meteorology Section was in a position to participate in joint international full scale field experiments concerned with the socalled atmospheric boundary layer (Kansas Windy Acres, JONSWAP, etc.). The turbulent flow in the atmospheric boundary layer in homogeneous as well as inhomogeneous situations has since then been the scientific backbone in the Section's work. In the following (4.1 - 4.15) a number of contributions elucidate the remarks above and illustrate applications to atmospheric dispersion theory.

In the second half of the seventies, when the scope of Risø's activities broadened within the field of energy research and financial support from different external sources became available for investigations in alternative ways of producing energy, the Meteorology Section made use of its basic expertise in both experimental and theoretical research and expanded its field of interest to include the study of wind energy. Recently, the section has studied different sides of chis subject including availability of wind energy (Danish Windatlas) and economy (see 4.16), wind turbine performance at the Test Plant for Small Wind

Mills and other installations, and the fatique lifetime of wind turbine rotors (see 4.17).

At present it seems reasonable to view the main efforts as a nucleus consisting of basic research within the field of micrometeorology in the entire atmospheric boundary layer, including climatology, and two major applications, namely air pollution modelling and wind energy research. Although this does not exhaust the list of activities completely, the bulk of the Section's production is probably well characterized in this way the next few years.

4.1. Particle Path Integration (PPI) theory for particle dispersion

(I. Troen, S.E. Larsen and T. Mikkelsen)

Starting with the assumption that a marked particle in a homogeneous turbulent fluid moves approximately following a first order auto-regressive process, viz.

$$v^{n+1} = v^n \cdot R(\Delta t) + \sqrt{1 - R^2(\Delta t)} \cdot \sigma_v^2 \cdot n(t) \ , \qquad (1)$$

an analytical theory for the probability density function as a function of travel time for single-particle dispersion has been developed. In Eq. (1) v^n is the particle velocity at time $n \cdot \Delta t$, Δt the timestep, R the exponential Lagrangian auto-correlation function, σ_v^2 the turbulent velocity variance, and n a Gaussian white noise process. The probability that a particle released at the source point with a certain initial velocity hits a target point after a specified travelling time can be thought of as the integral over all possible paths, or sequences of particle velocity, which conforms to these boundary conditions. From Eq. (1) a measure of probability for passage along a certain path Ω can be found as

$$Pr(\Omega) = \exp\left(-\frac{1}{4}\int_0^\tau (\ddot{n} + \dot{n})^2 \, d\tau\right) \ , \qquad (2)$$

where $\eta(\tau')$ is the path Ω described in terms of the scaled variables $\eta = y/(\sigma_v t_L)$, $\tau = t/t_L$ (t_L is the integral scale: $R = \exp(-t/t_L)$).

Formally it is not possible to perform an integration over the infinite dimension space of possible paths Ω. Particle Path Integration (PPI) theory consists in performing the integration indirectly following ideas originally due to Feynmann and Hibbs (1965). It is possible to show that the integration over all paths is equal to integration along one particular path obtained as the solution to the Euler differential equation except for a normalization factor. The Euler equation gives the solution to the variational problem of finding the extrema of the integral in Eq. (2). The equation can be written as:

$$\overset{4.}{\eta} + \overset{2.}{\eta} = 0 \qquad (3)$$

with the solution

$$\eta(\tau) = a\exp(\tau) + b\exp(-\tau) + c\tau + d \ , \qquad (4)$$

where the coefficients must be determined by the boundary conditions. From Eqs. (4) and (2) the following result is obtained:

$$Pr(\eta|\tau|0,\dot{\eta}_0) = F(\tau)\ \exp(-A^{-1}(\eta + \dot{\eta}_0(\exp(-\tau) - 1))^2) \qquad (5)$$

with

$$A = \frac{1}{2}\exp(-\tau)\cdot[\exp(\tau) + \exp(\tau) - 2 - (\exp(\tau) - 1 + \tau)\exp(\tau)].$$

Integration over the initial velocity $\dot{\eta}_0$, assuming this to be Gaussian distributed, leads to the result

$$Pr(\eta|\tau|0) = \frac{1}{\sqrt{2\pi}\sigma}\exp(-\frac{1}{2}\frac{\eta^2}{\sigma^2}) \qquad (6)$$

with $\sigma = 2(\tau + \exp(-\tau) - 1)$ which is the result obtained from the statistical theory of plume dispersion assuming as above an exponential Lagrangian autocorrelation function. The method can be generalised to give solutions for the dispersion of a plume traversing a step change in turbulent velocity variance and Lagrangian time scale asssuming each particle to have a continous velocity across the interface of the two homogeneous areas. In this case, the solution is obtained by matching solutions to Eq. (4) at the interface. More general inhomogeneous cases leads to a more complicated mathematical problem. The method, however, shows some promise as a development towards a plume dispersion theory including memory effects and inhomogeneity.

4.2. On the finite line-source problem in diffusion theory

(T. Mikkelsen, I. Troen and S.E. Larsen)

An alternative method to the virtual source concept (Slade 1968) for calculating dispersion from a finite line source has been formulated on the basis of statistical theory, involving practically no restrictions (Mikkelsen et al., (1982)). We found that the composite dispersion as a function of travel time t from a cross wind-oriented continuous line source could be expressed by

$$\langle D^2(t)\rangle = \Sigma^2 + \langle \tilde{y}^2(t)\rangle \ , \qquad (1)$$

where Σ^2 is the second moment of the source distribution function and $\langle \tilde{y}^2(t)\rangle$ is the dispersion from a single point source in homogeneous and stationary turbulence. The maximum relative error introduced by the use of the virtual source concept was typically found to be about 20%. Hence, the dispersion model in Eq. (1) is recommendable since its use does not require any additional information.

In Fig. 43 we compare the dimensionless dispersion

$$\alpha = \langle D^2\rangle^{1/2}/(t_1\langle v'^2\rangle^{1/2})$$

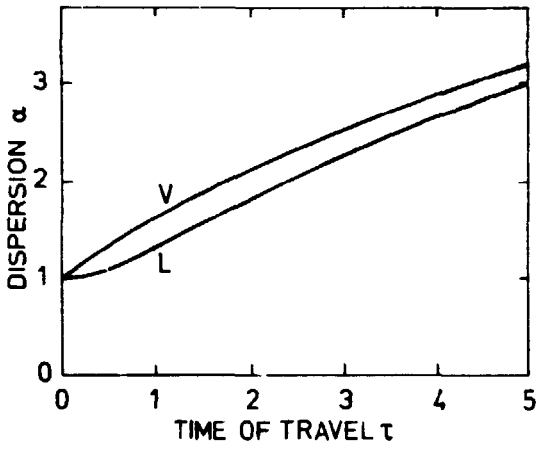

Fig. 43. Dimensionless dispersion $\alpha = \langle D^2\rangle^{1/2}/\langle v'^2\rangle^{1/2}t_1$ for the virtual source, V, and for the source, L, as a function of dimensionless time of travel $\tau = t/t_1$.

for the virtual source (V) and for the line source (L), as function of dimensional time of travel $\tau = t/t_1$. $\langle v'^2\rangle$ is the variance of the cross wind-turbulent fluctuations and t_1 is the time scale of the turbulence. The standard deviation of the source distribution Σ equals $t_1\langle v'^2\rangle^{1/2}$ in the case shown.

4.3. Turbulent diffusion of a Gaussian puff

(T. Mikkelsen, S.E. Larsen, I. Troen and H.L. Pécseli)

By assuming that the particle distribution function in a cloud of instantaneous released particles is Gaussian, we integrated the equation for growth of a cloud

$$\frac{1}{2}\frac{d\sigma^2}{dt} = \int_0^t \langle v_i(t)\cdot v_i(t-\tau)\rangle = \langle v_I^2(t)\rangle\, t_R(t) \qquad (1)$$

with respect to the time t after release for homogeneous and stationary turbulence. In Eq. (1) σ is the standard deviation of the cloud in the x-direction as defined in Fig. 44, and v_i denotes the velocity of the i'th particle of the cloud in its center of mass coordinate system, y. $\langle v_I^2(t)\rangle$ constitutes the variance participating in the instantaneous diffusion process and $t_R(t)$ is the corresponding time scale. An overbar in Eq. (1) denotes ensemble average over all realizations of the fluid whereas brackets implies an average over all particles in the cloud.

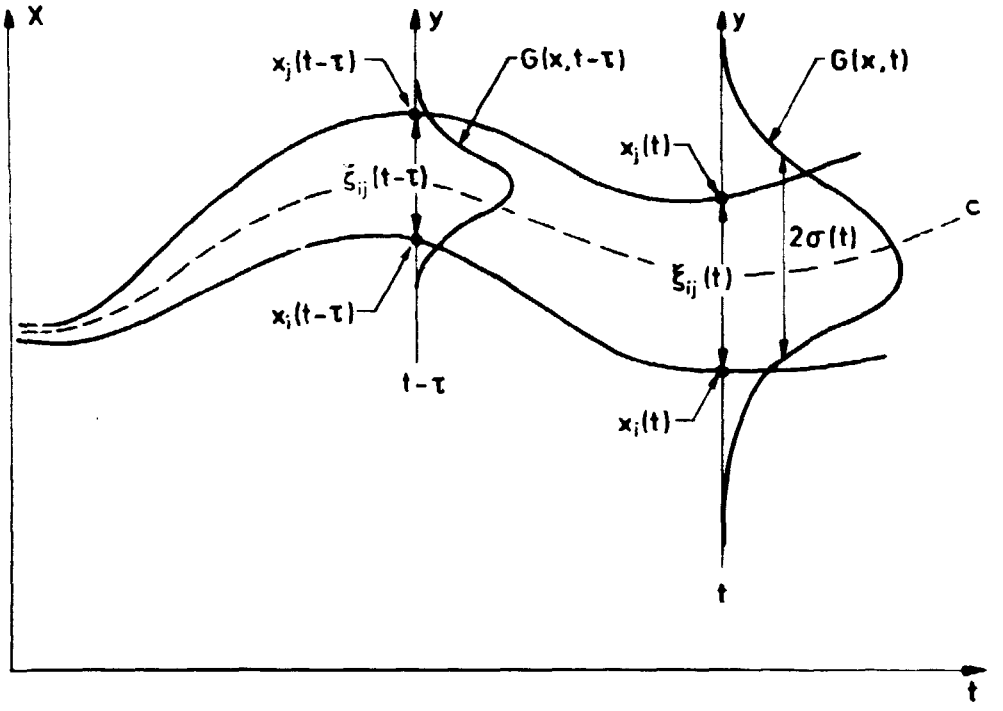

Fig. 44. A Gaussian cloud G with standard deviation σ at diffusion time t and at a previous time $t-\tau$ in homogeneous and stationary turbulence. The center of mass of the cloud c (dashed line) defines a relative coordinate system, y, in which the cloud dispersion is calculated. Also shown is the Lagrangian trajectory of two particles at x_i and x_j (full lines), belonging to the cloud.

The relative diffusion process is fundamentally based on "two-particle statistics". Therefore, we introduced the mixed Lagrangian-Eulerian correlation function

$$R(\xi,\tau) = \overline{u(x_i(t))u(x_j(t-\tau))} \qquad (2)$$

where $u(x_i(t))$ denotes the velocity of a particle (i) in the fixed coordinate system x at time t, and $u(x_j(t-\tau))$ denotes the velocity of another particle (j) at time $t-\tau$. The displacement between the two particles at time $t-\tau$ defines $\xi = x_i(t-\tau) - x_j(t-\tau)$ (c.f. Fig. 44). In the limit for $\xi \to 0$, $R(\xi,\tau)$ reduces to the Lagrangian auto-correlation function, whereas $R(\xi,\tau)$ becomes identical to the Eulerian space correlation when $\tau = 0$. The total variance of the turbulence $\bar{u}^2$ equals $R(0,0)$. In terms of the spectrum $S(\omega,k)$ corresponding to $R(\xi,\tau)$, where ω is fre-

quency and k is wavenumber, we derived the following solution to Eq. (1):

$$\overline{\langle v_i^2(t)\rangle} = \int_{-\infty}^{\infty} S(k)\ [1-e^{-k^2\sigma^2(t)}]\ dk \qquad (3a)$$

$$t_R(t) = \frac{1}{\overline{\langle v_i^2\rangle}} \int_0^t \iint_{-\infty}^{\infty} S(\omega,k)\ [1 - \exp(-\frac{1}{2} k^2 \Sigma_{eff}^2(t,\tau))] \qquad (3b)$$

$$\times \exp(i\omega\tau)d\omega dk d\tau$$

where

$$S(k) = \int_{-\infty}^{\infty} S(\omega,k)d\omega \text{ and } \Sigma_{eff}^2(t,\tau) = \sigma^2(t) + \sigma^2(t-\tau).$$

In the limit where σ is large compared with the length scale ℓ, defined as

$$\ell = (\overline{u^2})^{-1} \int_0^{\infty} R(\xi,0)d\xi\ ,$$

Eqs. (1) and (3) reduce to the usual Taylor formula (Pasquill, 1974) for single particle diffusion. For times larger than the Lagrangian time scale t_L, this is defined as

$$t_L = (\overline{u^2})^{-1} \int_0^{\infty} (R(0,\tau)d\tau\ ,$$

which asymptotically yields $\sigma^2 = 2\ \overline{u}^2\ t_L t$.

Generally, $S(\omega,k)$ must be evaluated in the turbulent field of interest, for instance by applying the β-transformation between the Lagrangian and Eulerian time scale (Pasquill, 1974). We investigated the result in Eq. (3) analytically by assuming a factorisation of $R(\xi,\tau)$ into $R(\xi)R(\tau)$, and, since $\sigma^2(t) \geq 1/2\ \Sigma_{eff}^2(t,\tau) \geq 1/2\ \sigma^2(t)$, we used the approximation $1/2\ \Sigma_{eff}^2(t,\tau) = \sigma^2(t)$. Equation (3b) then reduces to

$$t_R(t) = \int_0^t R(0,\tau)d\tau \ ,$$

which shows that the time scale for the relative diffusion process $t_R(t)$, with these approximations, equals the time scale appropriate for single particle diffusion.

By considering a wave number spectrum of the form $S(k) = \delta kP$, where $p < -1$, we found the following solutions to Eq. (1) applicable in the limit for $t << t_L$, where $t_R(t) \sim t$, and $\sigma(t) >> \sigma(0)$, where $\sigma(0)$ is the initial size of the cloud

$$\sigma(t) = \begin{cases} ct^{2/(p+3)} \text{ for } -3 < p < 1 \\ \sigma_o \exp(\frac{1}{4}\delta t^2) \text{ for } p = -3 \\ (ct^2 + \sigma(0)^{1/q})^{-q} \text{ for } p < -3 \end{cases}$$

where $c = -1/2\ \delta(p+3)/(p+1)$ and $q = 1/(p+3)$. The solution for $p < -3$ diverges for $t = (\sigma(0)^{1/q}/|c|)^{1/2}$, but this limit will not be reached because spectra of the form δkP, with $p < -3$, are not physical for $k \to 0$. Setting $p = -5/3$, Eq. (5) yields Richardson's well-known $t^{3/2}$power law describing relative diffusion in the inertial subrange.

4.4. Dispersion from a continuous ground-level source investigated by means of a K-model

(S.E. Gryning, S. Larsen and A. van Ulden (Royal Netherlands Meteorological Institute, The Netherlands))

The modelling approach is based on a numerical solution of the diffusion equation for a continuous point source

$$u(z)\ \frac{\partial \chi(x,z)}{\partial x} = \frac{\partial}{\partial z}\left\{K(z)\ \frac{\partial \chi(x,z)}{\partial z}\right\} \qquad (1)$$

where χ is the crosswind-integrated concentration, u the wind

speed, K the eddy diffusivity of matter in the vertical direction, x the downwind distance from the source, and z the height above ground. The wind-profile and eddy diffusivity are expressed in terms of Monin-Obukhov similarity relations. The wind-profile is taken as

$$u(z) = \frac{u_*}{\kappa} (\ln(z/z_o) - \psi(z/L))$$

where u_* is the friction velocity, κ the von Kármán constant, z_o the roughness length, and L the Monin-Obukhov length. The eddy diffusivity, K, are taken as

$$K(z) = \kappa u_* z/\phi_h(z/L) \ .$$

We used the expressions of $\psi(z/L)$ and $\phi_h(z/L)$ that was proposed by Businger (1973).

Equation (1) was solved numerically using a scheme proposed by Keller (1971). A number of characteristic parameters for the dispersion process were extracted from the numerical solutions, of which only a single one will be discussed here. We approximated the vertical concentration profile by

$$\chi(z) = \chi(0) \exp\{- B(z/\bar{z})^s\} \qquad (2)$$

where B depends on s alone, and $\bar{z}$ is the mean height of the plume for a given x. The shape parameter s was estimated by fitting Eq. (2) to the numerically calculated concentration profiles. It appears that the shape of the vertical concentration profile is a function of distance and stability; the variation of s is shown in Fig. 45.

An approximative analytical representation for s was worked out using Eq. (2) as an exact solution of the diffusion equation when the wind- and eddy diffusivity profiles are represented by power laws. Denoting the power of the wind profile m and that of the eddy diffusivity n, the shape parameter s is given as $s = 2 + m - n$. Thus, when we have approximations for m and n,

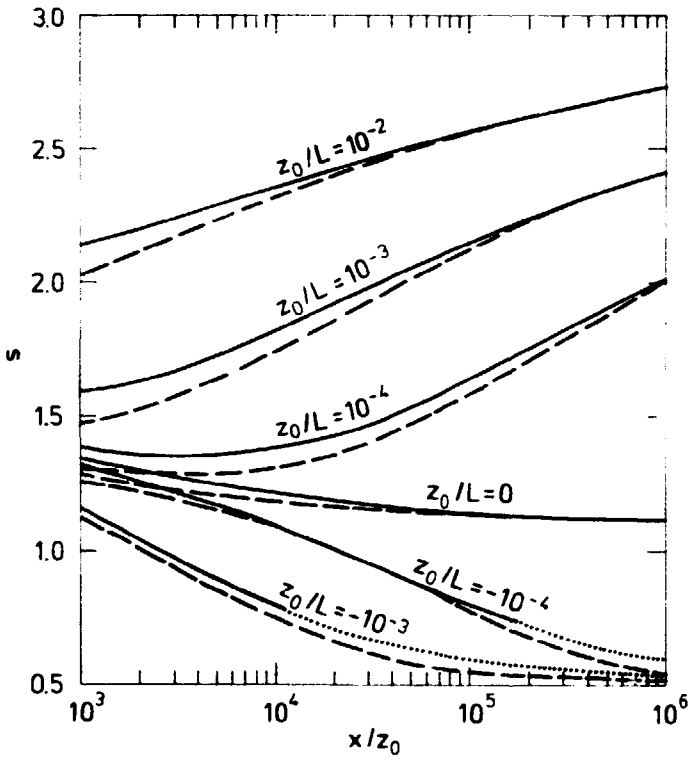

Fig. 45. The shape factor, s, as a function of downwind distance and stability. The dashed line shows the analytical approximations suggested in eq. (3). Portions of the curves for which $z/L < -1$ are dotted.

we also have an approximation for s. Several ways exists to fit a power law to a given profile. Here we forced the actual value and the first derivative of the power-law to coincide with the original profile at a given representative height $c\bar{z}$, where $c\bar{z}$ is the height at which the mean velocity of the particles in the plume equals the wind velocity. The expressions for the powers of the wind and eddy diffusivity profiles read

$$m(z_1) = \left\{\frac{d(\ell n\ u(z))}{d(\ell n z)}\right\}_{-cz} \quad , \quad n(z_1) = \left\{\frac{d(\ell n\ K(z))}{d(\ell n z)}\right\}_{-cz}$$

where one and the same height $c\bar{z}$ has been assumed to be representative for both profiles. This leads to the following formulas for the s-function

$$s = \frac{1-4.5c\bar{z}/L}{1-9c\bar{z}/L} + \frac{(1-15c\bar{z}/L)^{-0.25}}{\ell n(c\bar{z}/z_o)-\psi(c\bar{z}/L)} \qquad (3a)$$

for $L < 0$, and

$$s = \frac{0.74+9.4c\bar{z}/L}{0.75+4.7c\bar{z}/L} + \frac{1+4.7c\bar{z}/L}{\ell n(c\bar{z}/z_o)+4.7c\bar{z}/L} \qquad (3b)$$

for $L > 0$.

Under neutral conditions each expression reduces to

$$s = 1 + (\ell n(c\bar{z}/z_o))^{-1} \quad .$$

The analytical s-functions are illustrated in Fig. 45. For practical applications it is proposed to use $c = 0.8$ under stable conditions, $c = 0.6$ under near neutral conditions, and $c = 0.4$ under unstable conditions. In the limit of very stable conditions, the model has an analytical asymptote for s of 3, and in the convective limit s approaches 0.5.

An extensive analysis was undertaken to compare this numerical model with experiental results from the Prairie Grass dispersion experiments. The simulations were carried out with and without deposition. It is shown that the numerical solution of the diffusion equation yields a good approximation to both the vertical concentration profile and the crosswind-integrated ground-level concentrations when consideration is given to the effect of deposition of the tracer; the omission of the deposition resulted in the poorer comparisons.

4.5. The importance of the deposition rate for dose calculations in connection with releases from nuclear power plants

(S.E. Larsen and S. Thykier-Nielsen (Health Physics Department, Risø))

The deposition velocity and the wash-out coefficient are important parameters in connection with dose calculations for releases from nuclear power plants. They are difficult to estimate realistically for a multi-component release. Therefore, a parameter study was undertaken by Thykier-Nielsen and Larsen

(1982) on the variation with deposition rate of individual and collective doses as a result of modelled routine releases from suggested nuclear power plant sites in Denmark.

The deposition velocity was varied within the bounds given in the literature. However, because the amount of deposited material varies fairly strongly with the assumed deposition velocity a maximum realistic deposition velocity V_{gm} was estimated as function of roughness length z_o, Pasquill-stability class, and wind velocity. This was performed by evaluating the maximum possible flux of material, which the atmospheric turbulence can sustain down to a perfectly absorbing surface, as function of the above-mentioned parameters. The method used is described by Jensen (1981) and consist of setting

$$V_{gm} = u_*^2/u \qquad (1)$$

where u is the mean velocity at the height, where V_{gm} is estimated (5 m) and u_* is the friction velocity. It was found that V_{gm} varied from about 0.05 cm/s in Pasquill class F for wind velocities less than 1 m/s, up to about 2 cm in Pasquill class A with velocities larger than 10 m/s.

Also, the wash-out coefficient λ was varied within realistic bounds. A realistic estimate of the average wash-out coefficient as a function of Pasquill classes was obtained for gasses and sub micron particles, with a high and fast solubility rate in water by estimating the relative frequency of rain- and snowfall as well as the associated mean precipitation rates within the stability classes. This was done through analyses of climate data from Denmark, Studsvik (Sweden), and Carnsore Point (Ireland). It was found that the relative precipitation frequencies within stability classes A, B, C and F were was the same for the three areas in spite of their general climatic differences, showing up also in the total yearly precipitation.

The result of the parameter variational studies was that the total doses varied only insignificantly from the assumed deposition rates. The dose component from deposited material, how-

ever, was found to vary several hundred percent with deposition rate, as expected. The outcome of the study therefore will be the possibility of placing more realistic upper bounds on the amount of material, which deposits and thereby enters the radio-ecological circuit.

Another possible outcome is associated with consequence estimates of major accidential releases. The general modelling philosophy here is to try to specify the dispersion situations which are concidered to be the most serious, and perform the dose calculations for these. The consequences of accidental releases are found to be strongly dependent on the assumed deposition rates. With the estimates of V_{gm} described here, some of the situations considered so far will be less serious. This is especially so for situations with low wind-speed and high stability compared to situations with stronger wind, neutral stability, and rain. Since the latter can be better described with current modelling than the former, a result of the analysis described above is improved reliability of the consequence estimates for large accidental releases.

4.6. Evaluation of operational air quality models

(I. Troen, E.L. Petersen, T. Mikkelsen, S.E. Larsen, L. Kristensen, N.O. Jensen and S.E. Gryning)

An assesment of the quality of two operational air quality models was performed under a contract with the Danish Minestry of the Environment. Both models are based on Gaussian plume theory and standard curves for the horizontal and vertical plume spread as functions of distance from the source and estimated dispersion class (Turner, 1967). The theoretical basis of the models and the uncertainties in the model concentrations from a single stack were evaluated based on estimates of probable uncertainties in the input data and of the model parameters. Also, a test of the numerical schemes in the models was performed. From this exercise and by evaluating the choice of model parameters and comparing it with recommendations in the recent literature, a number of improvements were suggested for the models; it was found that with

these improvements incorporated into the models they could be relied upon as "state of the art" operational models for estimating average surface concentrations under reasonably homogeneous conditions. Moreover, it was found that their routine use for the estimating the maximum 99-percentile surface concentration - as required by Danish regulatory authorities - is highly questionable.

4.7. Measurements of effective stack heights by use of a LIDAR

(S.E. Gryning, S. Hanson (Electronics Department, Risø), E. Lyck (National Agency of Environmental Protection, Air Pollution Laboratory, Denmark)).

The height of a plume above the ground is a key parameter when estimating the impact on the environment of releases of pollution from stacks. Measurements of the height of the plume can be performed using LIDAR techniques. A study was undertaken in which the plume from a 120 m high stack at a coal-fired unit of Stigsnæsværket, a power plant in the south-western part of Sjælland, was mapped using a LIDAR available at the Electronics Department. The LIDAR works at a wavelength of 488 nm at a power of 0.5-1 W. A total number of six experiments has been carried out. The LIDAR allowed mapping of the plume out to a distance from the stack of 50-150 m, depending on the meteorological conditions. Thus this LIDAR turned out to be useable for mapping of the plume close to the stack, if mapping has to be carried out further downwind, modifications on the LIDAR have to be made.

4.8. Double tracer experiments to verify atmospheric dispersion models of fission products

(S.E. Gryning, S. Nielsen (Health Physics Department, Risø), E. Lyck (National Agency of Environmental Protection, Air Pollution Laboratory, Denmark), O. Karlberg (Studsvik, Sweden))

Four dispersion experiments were carried out in a two-week period of May at Ringhals, a Swedish nuclear power plant. The

aim of the project is to study the dispersion of simultaneous releases of a passive and a radioactive tracer. The experimental results constitutes a data set that can be used to validate dispersion and radiation models, e.g. the PLUCON-model developed at the Health Physics Department at Risø.

An experiment consisted of simultaneous releases of a radioactive tracer as well as an inactive tracer. The tracers were released through the 110 m heigh ventilation stack of unit 1, a boiling water reactor. The radioactive noble gases from the routine ventilation of the reactor were used as one of the tracers, the other was sulphur hexafluoride, which was injected into the ventilation stack during the experiments. During each experiment, the plumes were measured about 5 km downwind; the crosswind profile of the inactive SF_6-plume was measured with a one-hour tracer sampling time by use of 20 radio-controlled sampling-units, (developed at the Air Pollution Laboratory (Gryning, 1981)). These units were situated about 2^o apart near ground-level along roads running approximately circular about the ventilation stack, at a distance of about 5 km. Measurements of gamma radiation from the decay of the radioactive gases in the plume were carried out with three high-pressure ionization chambers which recorded the exposure-rate as a function of time, three mobile gamma-spectroscopic systems with Ge(Li) detectors placed near the ionization chambers during the experiments, and 11 GM-detectors.

An example of simultaneous measurements of the crosswind tracer concentration profile and a profile of the gamma radiation from the decay of the radioactive noble gases are shown in Fig. 46.

In order to characterise the meteorological situation during the experiments, a 13 m mast was erected on a flat area between the release point and the sampling series. In order to establish the Monin-Obukhov length and friction velocity during the experiments, the mast was instrumented for routine measurements of 10 minute averages of wind speed, direction, and temperature at the 2 and 8 m levels. Furthermore, the turbulent wind velocity components and the fluctuating temperature were continously measured

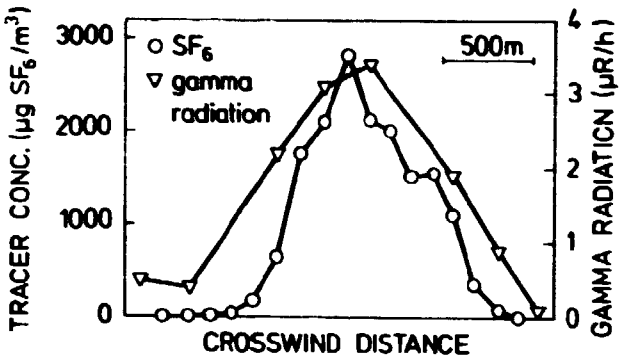

Fig. 46. Simultaneous measurements of concentrations of the tracer sulphur hexafluoride and of gamma radiation from the decay of radioactive noble gases; determined with a one hour sampling time. The measurements took place May 23, 1982, 4.2 km from the ventilation stack that served as release-point.

at the 13 m level during the experiments. These measurements were performed with a combination of a light-weight cup-anemometer, vane sensor, vertical propeller, and temperature sensor (Gryning and Thomson, 1979). The meteorological instrumentation included a mobile radiosonde system. A radiosonde was launched at each experiment, and from the measurements of temperature, wet bulb temperature and pressure, the height of the lowest inversion was extracted.

Presently, the data evaluation is only partly finished, but from the analysis already done it appears that the double tracer technique used here is fully applicable for these kind of investigations.

4.9. A tracer investigation of the dispersion of airborne releases from uranium mining at Kvanefjeld in Greenland

(S.E. Gryning and E. Lyck (National Agency of Environmental Protection, Air Pollution Laboratory, Denmark))

The ongoing experimental work of uranium extraction from the ore at Kvanefjeld, Greenland, has the purpose of investigating whether or not industrial extraction from the deposits of the uranium ore can be justified from a technical, economic and environmental point of view. Mining at Kvanefjeld will result in

releases of ore dust particles containing uranium, thorium, and their respective progenies, as well as releases of the noble gas radon. The purpose of this project, carried out in a four week period in July-August, is to investigate the dispersion of airborne releases in the potential mining area, with special emphasis on the impact, from an air pollution point of view, on a township in the neighbourhood. With the mining area situated on the Kvanefjeld and the township Narssaq situated at the outlet to the Fjord of a sloping valley, the dispersion process will be very complicated.

In order to gain insight into the dispersion process, the tracer sulphur hexafluoride was released at the mining area, and sampled with about twenty radio-controlled sampling units at the outlet of the valley. These measurements gave a direct measure of the dilution of the tracer releases. Meteorological parameters to characterise the dispersion process during the experiments were obtained from two existing 23 m high meteorological towers that have measured mean profiles (10 minute averages) of wind-direction and temperature since 1979.

One of the meteorological towers is situated in the valley, the other in the mining area. In addition to these routine measurements, the turbulent wind velocity components and the fluctuating temperature were continuously measured at the top of the valley mast during the experiments. These measurements were performed with a combination of a light-weight cup-anemometer, vane sensor, vertical propeller, and temperature sensor (Gryning and Thomson, 1979). The meteorological instrumentation at the valley mast included a mobile radiosonde system. A radiosonde was launched during each experiment, giving information about the vertical structure of air temperature and humidity near the valley mast.

All six experiments were carried out at night under conditions favourable for the development of drainage flow down the valley. Contrary to normal behaviour, the flow in these experiments was not continuously down the valley, but oscillated with periods of flow going up the valley, as shown in Fig. 47. These oscil-

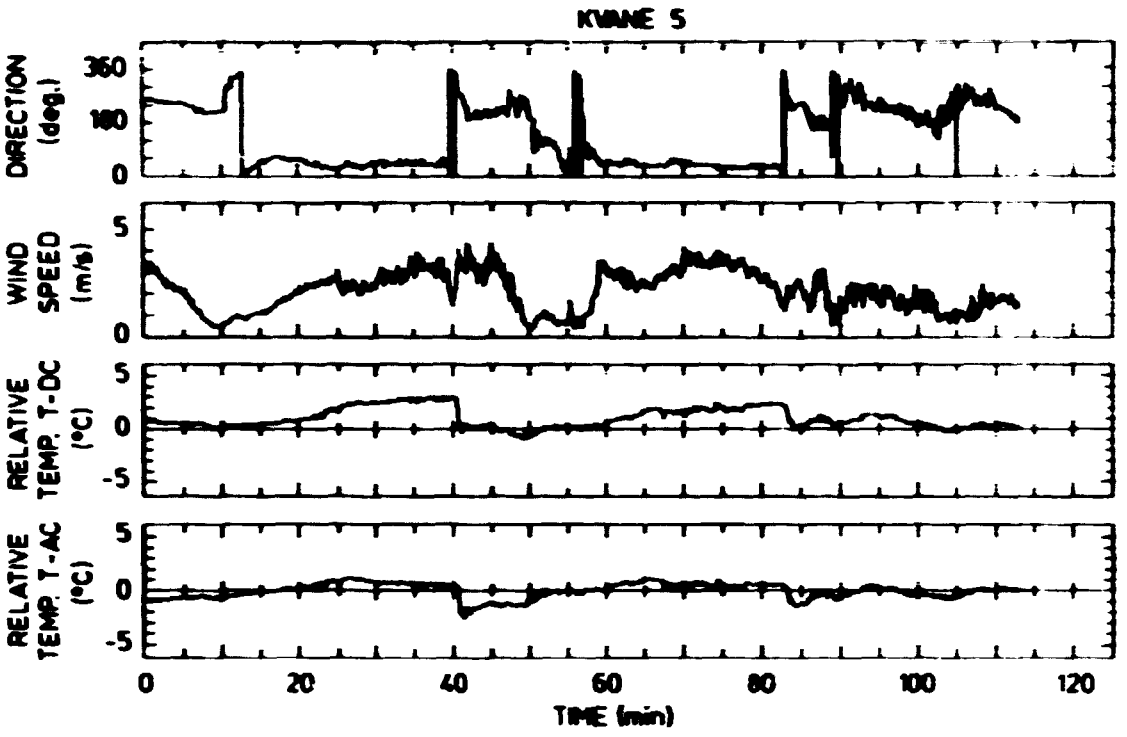

Fig. 47. Continuously measured record of wind direction, wind speed and relative temperature at a height of 43 m at the valley mast for the experiment of 7 August, 1981. The relative temperature denoted T-AC is high-pass filtered with a time constant of ~ 10 minutes; the corresponding time constant for the temperature denoted T-DC is ~ 75 minutes. Downwind flow corresponds to a wind direction of ~ 60°, upwind to ~ 240°. The record starts at 0252 local time.

lations in the flow resulted in a very low effective transport velocity of the tracer. The tracer was released about 4 km from the outlet of valley to the Fjord where the tracer sampling units were positioned. The tracer was released about two hours before the start of the one hour tracer sampling. This resulted in a very low tracer concentration measured by the samples. When the tracer release was started about six hours before sampling the tracer was found at all sampling positions.

A tentative explanation of the observed oscillations in the direction of the flow in the valley might be, the presence of a sea breeze flow of direction opposed to the drainage flow exists. The direction of the flow in the valley therefore depends on the strength of the breeze flow relative to the drainage flow; a front between the two air masses is then likely to be present in the valley.

4.10. Spatial structure of atmospheric turbulence

(L. Kristensen, P. Kirkegaard (Computer Installation, Risø) and D.H. Lenschow (NCAR, Boulder, Colorado, USA))

From an experimental point of view it is difficult and expensive to obtain direct information about the spatial structure of turbulence because in principle it requires a network of measuring stations. There are a number of well-established methods to derive some relevant information on the basis of data from a single measuring station. The most direct one is to install instruments along a mast and record synchronous time series of the turbulent quantities, i.e. velocity components, temperature, and other scalars. If these time series appear to be stationary from a practical point of view, then it is possible to calculate stable averages of the turbulent properties along the vertical direction. However, the lack of homogeneity of the turbulent field in this direction, at least in the surface layer, limits the usefulness of this method, because spatial cross correlations become functions of the height above the surface.

The same type of data can also be used to derive information about the turbulent spatial proporties in the horizontal direction, provided that the mast is situated in a terrain sufficiently flat for the turbulence to be considered horizontally homogenous up to a certain length scale. The time series of turbulent quantities from a fixed height can then be converted into "space series" by use of Taylor's hypothesis, which states that the temporal changes of a turbulent quantity as seen by a sensor indicates the passage of a rigid turbulent structure with the mean wind speed. The hypothesis can be illustrated in terms of the covariance function $R_{ij}(\vec{r},\tau)$ of the two fluctuating velocity components u_i and u_j, separated in space and time by the displacement vector $\vec{r}$ and the time lag τ. Let the mean wind velocity have the magnitude U and a direction along the horizontal unit vector $\vec{i}_1$.

Then

$$R_{ij}(\vec{r},\tau) = R_{ij}(\vec{r} - U\tau\vec{i}_1,0) \ . \qquad (1)$$

It is obvious that in order for this to be true the real temporal change of an "eddy", as observed in a frame of reference that follows the turbulence with the velocity $U\vec{i}_1$, must be small in the course of time it takes it to pass the instrument with the speed U. A straightforward semi-quantitative analysis, based on a rather lose eddy concept, shows the existence of the condition that the relative turbulent intensity, i.e. the root-mean-square turbulent velocity σ divided by U, is small compared to unity. This condition is usually fulfilled (except perhaps during calms), and although other conditions involving the mean wind shear must also be met (Lumley and Panofsky, 1964), Taylor's hypothesis seems to work very well in most situations. Making use of this, the spatial structure of the turbulence can be determined along the mean wind direction with a resolution that makes it possible to compute one-dimensional spectra with respect to wave numbers in the mean wind direction.

A very efficient way to determine spectra with respect to horizontal wave numbers is to use an airplane as a platform for making measurements, as an alternative to a fixed position. The true airspeed of the airplane must now replace U, and consequently the condition that the turbulent intensity must be small for Taylor's hypothesis to be valid is easily fulfilled. Furthermore, an airplane has freedom to move in any horizontal direction, so that the direction of the wave number in the one-dimensional spectra can be chosen freely.

The conventional methods discussed so far are of little use in obtaining spectra with respect to vertical wavenumbers. An exception is the situation in which the wavelengths under consideration are so small that the turbulence can be considered isotropic (local isotropy). Then there are only two different types of one-dimensional velocity spectra (Batchelor, 1953), namely the spectra with the wave number direction parallel and perpendicular to the turbulent wind component in question. For wavelengths equal to and larger than the scale of the turbulence, the isotropy assumption can in general, be unwarranted. In a situation where the height above the surface of the earth is so large that the wind shear can be neglected, but where the pres-

ence of the earth can still cause some vertical "squashing" of the velocity field, it is suggested that the turbulence can be considered axisymmetric with respect to the vertical (3 direction).

In the following a kinematical, axisymmetric model will be described and used to predict the vertical structure of the velocity turbulence. The spectral tensor

$$\phi_{ij}(\vec{k}) = \frac{1}{(2\pi)^3} \int R_{ij}(\vec{r},0)e^{-i\vec{k}\cdot\vec{r}}\, d^3r \qquad (2)$$

can then be written in standard tensor notation as

$$\phi_{ij}(\vec{k}) = A(k,k_3)(\delta_{ij} - \frac{k_i k_j}{k^2}) + B(k,k_3)(\delta_{3i} - \frac{k_3 k_i}{k^2})(\delta_{3j} - \frac{k_3 k_j}{k^2}) \qquad (3)$$

where

$$\vec{k} = k_1 \vec{i}_1 + k_2 \vec{i}_2 + k_3 \vec{i}_3 \qquad (4)$$

is the wave number with the components k_1, k_2 and k_3 along the three unit vectors $\vec{i}_1$, $\vec{i}_2$, and $\vec{i}_3$ defining a cartesian coordinate system. In Eq. (3), $A(k,k_3)$ and $B(k,k_3)$ are two scalar functions of k_3 and the magnitude k of $\vec{k}$. The reason that there are only these unspecified functions in Eq. (3) is that the atmospheric flow in accordance with the Boussinesq approximation for shallow convection (Dutton and Fichtl, 1969) is assumed incompressible. Under isotropic conditions Eq. (3) becomes

$$\phi_{ij}(\vec{k}) = \frac{E(k)}{4\pi k^2}(\delta_{ij} - \frac{k_i k_j}{k^2}) \quad , \qquad (5)$$

where $E(k) = 4\pi\, k^2 A(k,0)$ is the energy spectrum.

Upon expansion of $A(k,k_3)$ and $B(k,k_3)$ into Eq. (3) in even Legendre polynomials $P_{2\ell}(k_3/k)$ and truncation after the first term that contributes anisotropy terms to Eq. (3) reduces this expression to

$$\phi_{ij}(\vec{k}) = \frac{1}{4\pi k^2}\left[E(k) - \frac{P(k)+Q(k)}{3}\right] + \psi_{ij}(\vec{k}) , \tag{6}$$

where

$$\psi_{ij}(\vec{k}) = \frac{1}{4\pi k^2}\left\{P(k)\frac{k_3^2}{k^2}\left(\delta_{ij} - \frac{k_i k_j}{k^2}\right)\right.$$

$$\left. + Q(k)\left(\delta_{3i} - \frac{k_3 k_i}{k^2}\right)\left(\delta_{3j} - \frac{k_3 k_j}{k^2}\right)\right\} \tag{7}$$

is the anisotropic part of the tensor ϕ_{ij}. There are three unknown functions in Eq. (6): the energy spectrum $E(k)$ and $P(k)$ and $Q(k)$.

Assuming that Eqs. (6) and (7) can replace Eq. (5) in situations in which the turbulence is non-isotropic, it is possible to show that $E(k)$, $P(k)$, and $Q(k)$ can be determined from the three one-dimensional velocity spectra $F_{11}(k_1\vec{i}_1)$, $F_{22}(k_1\vec{i}_1)$, and $F_{33}(k_1\vec{i}_1)$ with the wavenumbers in the direction $\vec{i}_1$ of the mean wind or - in the case of airborne measurements - in the direction of the true airspeed. The subscripts 11, 22, and 33 denote the direction of the turbulent wind velocity components. The relations between these spectra and $\phi_{ij}(\vec{k})$ are

$$F_{pp}(k_1\vec{i}_1) = \int_{-\infty}^{\infty} dk_2 \int_{-\infty}^{\infty} dk_3 \; \phi_{pp}(\vec{k}) , \tag{8}$$

where pp can be 11, 22, or 33.

It can easily be shown (Batchelor, 1953) that for isotropic conditions there are the following relations between the one-dimensional spectra:

$$F_{22}(k_1\vec{i}_1) = F_{33}(k_1\vec{i}_1) = \frac{1}{2}\left(F_{11}(k_1\vec{i}_1) - k\frac{d}{dk}F(k_1\vec{i}_1)\right) . \tag{9}$$

Taking the rather general expression

$$F_{11}(k_1\vec{i}_1) = \frac{3A}{(B_1 + (|k|z_i)^{2\mu})^{5/6\mu}} , \tag{10}$$

where A, B_1, and μ are positive constants and z_i a scaling length, which in many cases can be set equal to the depth of the atmospheric boundary layer, we obtain an expression that is consistent with most experimental and theoretical findings. If Eq. (9) were true, then it is easily shown that

$$F_{22}(k_1\vec{i}_1) = \frac{A}{2}\frac{3B_1 + 8(|k|z_i)^{2\mu}}{(B_1 + (|k|z_i)^{2\mu})^{5/6\mu+1}} \tag{11}$$

In the general case we assume that Eqs. (10) and (11) can be fitted to experimental results. For axisymmetric turbulence $F_{33}(k_1\vec{i}_1)$ is assumed to be given by Eq. (11) with B_1 replaced by another constant B_3, which may or may not be equal to B_1. If B_1 and B_3 are equal, then we have isotropic turbulence, which in a convenient way then becomes a special case of axisymmetric turbulence. In other words,

$$F_{33}(k_1\vec{i}_1) = \frac{A}{2}\frac{3B_3 + 8(|k|z_i)^{2\mu}}{(B_3 + (|k|z_i)^{2\mu})^{5/6\mu+1}} \tag{12}$$

Using Eqs. (10), (11), and (12) we can find analytical, but rather complicated, expressions for E(k), P(k), and Q(k) in Eqs. (6) and (7).

With the spectral tensor $\phi_{ij}(\vec{k})$ determined it is possible to find expressions for one-dimensional spectra with wavenumbers in the vertical direction. These are particularly useful because the amount of vertical "squashing" of the turbulence can now be derived. If we define this as the ratio δ between the integral length scales of the longitudinal turbulent fluctuations in the

vertical and horizontal direction then it is possible to derive the following expression

$$\delta = \frac{1}{2}\left\{3\left(\frac{B_1}{B_3}\right)^{1/2\mu} - \left(\frac{B_1}{B_3}\right)^{1/3\mu}\right\} . \qquad (13)$$

Note that $\delta = 1$ for $B_1 = B_3$.

The experimental verification of this axisymmetric model has still not been done, but some data material suitable for this purpose is available. In the fall of 1979, NCAR's two Queen Airs performed a number of formation flights (Kristensen and Lenschow, 1980), during which wind velocities, temperatures, and humidities were measured. The two airplanes flew parallel to each other at several distances and heights. For each flight leg the cross spectra - or rather the so-called spectral coherences as defined by for example Lumley and Panofsky (1964) - between displaced velocity components were computed. Since the same quantities can be calculated from Eqs. (6) and (7) and the one-dimensional spectra based on the same flight data, there seems to be a good possibility for judging the model experimentally.

4.11. Spectra of velocity fluctuations in the unstable planetary boundary layer

(J. Højstrup)

Quantitative knowledge about the spectral distribution of velocity fluctuations is important for studies of the dispersion of pollutants and in predictions of the response of buildings and other structures to the fluctuating wind.

The unstable boundary layer is typical for daytime conditions, and this situation is also one of considerable practical importance because the largest turbulence intensities occur during unstable conditions. Velocity spectra in the surface layer are well understood, and simple models have previously been developed (Kaimal et al., 1972, Kaimal, 1978 and Højstrup, 1981). The

surface layer model of Højstrup (1981) has now been extended such that now it is possible to use the model to as high as the middle of the planetary boundary layer which is typically up to 500-1000 m.

There are two turbulence-generating mechanisms in the atmosphere: shear and buoyancy. The model is formulated as a sum of two non-interacting parts, one shear produced, and the other buoyancy produced, viz.:

$$n\,S_i(n) = A_i(f_i,\, z/z_i)w_*^2 + B_i(f_i,\, z/z_i)u_{*o}^2 \qquad (1)$$

where: i is u,v or w; n the frequency in Hz; z the height above ground; z_i the depth of the planetary boundary layer; $f = nz/u$, where u is the windspeed; $f_i = nz_i/u$; w_* the mixed layer scaling velocity, and u_{*o} is the surface friction velocity.

The mixed layer part $A_i w_*^2$ is stability dependent through w_*^2; B_i is independent of stability, and the only term left in the neutral limit. The shapes of the functions in Eq. (1) are illustrated in Fig. 48. For the horizontal components, A_u and A_v are

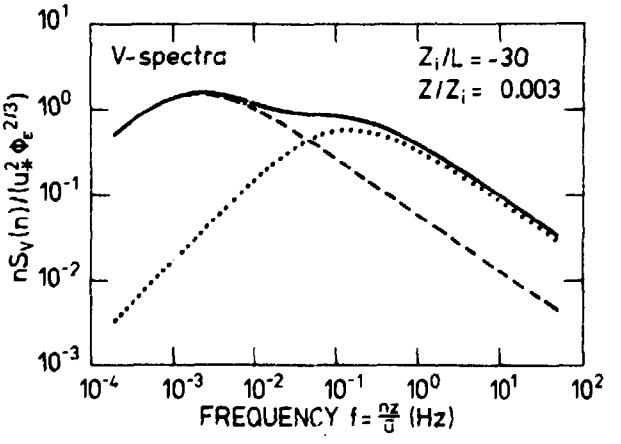

Fig. 48. Model V-spectrum. The dashed line is a plot of the function $A_v(f_i)$ in Eq. (2). The dotted line is $B_v(f)$ in Eq. (1). The full line is the resultant spectrum.

independent of height, but A_w is a high-pass filtered version of A_v since vertical fluctuations encounter a mechanical impedance that increases with decreasing z and decreasing frequency. In Fig. 49 the model spectra of the three components are shown for different heights and stabilities. The agreement between the model and data from homogeneous terrain is excellent with respect to variances, dissipations, peak frequencies, and spectral shapes. One example from the Minnesota experiment is shown in Fig. 50.

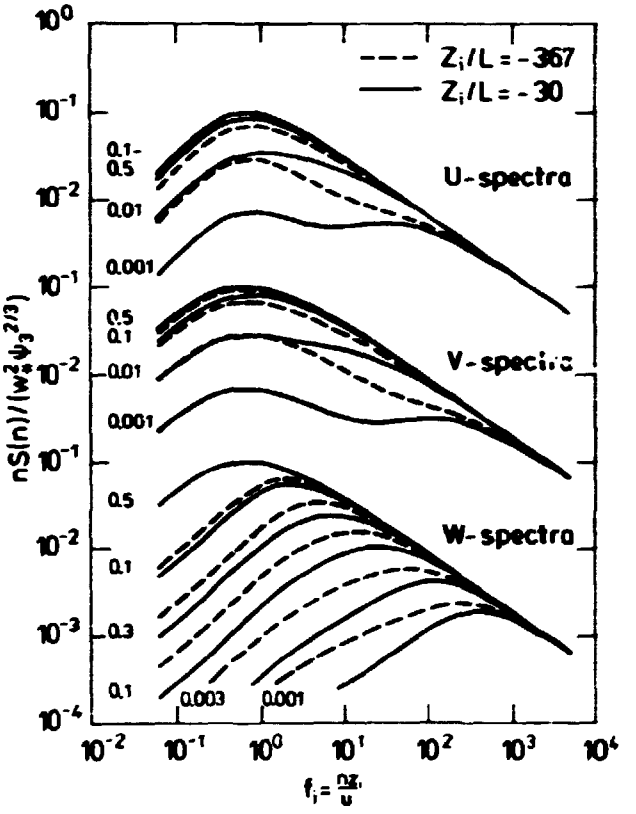

Fig. 49. Model spectra. Two curves are plotted for each height, one for conditions as the most unstable found in the Minnesota data (dashed lines) and one for the most neutral conditions (full lines).

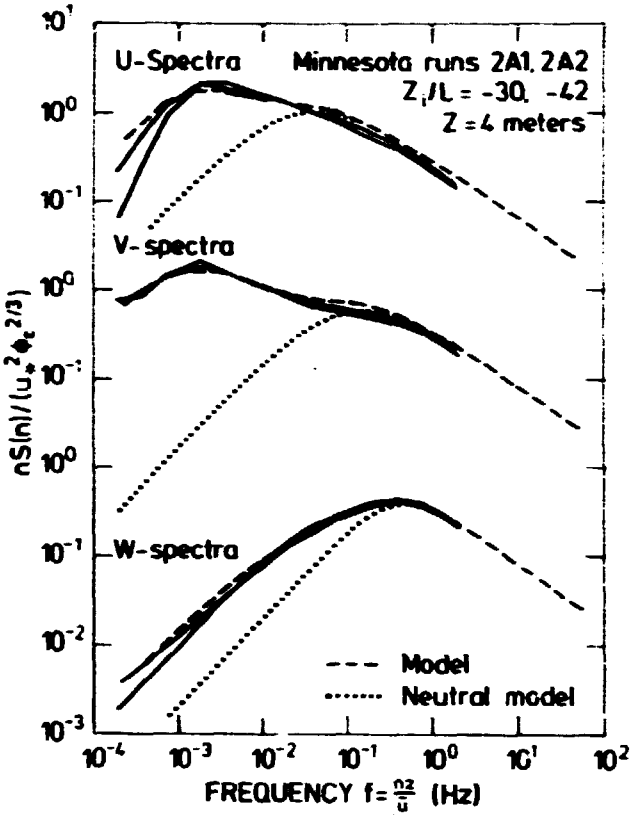

Fig. 50. Minnesota data, near neutral runs 2A1, 2A2, z = 4 m, z_i = 1250, 1615 m. Dashed line: Model. Dotted line: Neutral model, but normalized to coincide with dashed line at high frequencies.

4.12. A simple method of estimating the Monin-Obukhov length under convective conditions

(N.O. Jensen)

In the description of atmospheric diffusion from low-level sources it is useful to know the Monin-Obukhov length L (for a definition, see e.g. Lumley and Panofsky (1964)). This is so because the spread is proportional to the standard deviation of the velocity fluctuations according to the diffusion theorem of G.I. Taylor. Furthermore, the latter has been shown to obey similarity relations based on L (see e.g. Busch, 1973, Businger, 1973, Wyngaard, 1973 and Panofsky et al., 1977). Strictly speaking, Taylors diffusion formula is valid for homogeneous turbulence only, but in practice it seems to work also in sheared turbulence (Grysing and Lyck, 1980).

A simple way to estimate L in the stable boundary layer was given by Venkatram (1980). Here we propose a method which should be valid during very unstable conditions. We take a starting point in the proportionality between the standard deviations of the lateral wind fluctuations, σ_v and the convective velocity scale $w_* \equiv (g/T\ \overline{\theta' w'} z_i)^{1/3}$ (Panofsky et al., 1977) which also can be written as

$$\frac{\sigma_v}{u_*} = \alpha\left(-\frac{z_i}{L}\right)^{1/3} \quad . \tag{1}$$

Here $\overline{\theta' w'}$ is the vertical turbulent kinematic heat flux, α a constant of order 1, z_i the height of the atmospheric mixed layer and u_* the friction velocity. Next, we consider the equation for the wind profile in the surface layer

$$u(z) = \frac{u_*}{k}\left(\ln\frac{z}{z_o} - \phi_m\left(\frac{z}{L}\right)\right) \quad , \tag{2}$$

where u is the mean wind spead at height z, k von Kármán's constant (= 0.4), and z_o the surface roughness length. The function ϕ_m is defined as

$$\phi_m = \int_0^{z/L} (1 - \phi_m(\xi))\ \frac{d\xi}{\xi} \quad , \tag{3}$$

where ϕ_m is the dimensionless wind gradient

$$\phi_m\left(\frac{z}{L}\right) = \frac{du}{dz}\left(\frac{u_*}{kz}\right)^{-1} \quad . \tag{4}$$

Various empirical expressions for ϕ_m exist. First of all, data show that wind gradients scaled as in Eq. (4) really collapse onto a dependence on z/L olone. Secondly, it shows also that ϕ_m may be approximated by a simple power law of the form

$$\phi_m = \left(1 - a\ \frac{z}{L}\right)^{-b} \tag{5}$$

For strong convective conditions, dimensional arguments show that b = 1/3, whereas experimental results seem to favour

b = 1/4. However, irrespective of which power we choose ψ_m has the limiting value

$$\psi_m = \ell n(-\frac{z}{L}) + A \quad , \tag{6}$$

under very unstable conditions. In Eq. (6) A is a constant of order 1 which is only weakly dependent on the choice of a and b. Combining Eq. (1), (2) and (6) and neglecting A, we obtain

$$(-\frac{L}{z_o})^{1/3} \ell n(-\frac{L}{z_o})^{1/3} = \frac{ku}{3a\sigma_v} (\frac{z_i}{z_o})^{1/3} \quad . \tag{7}$$

This result may be recognized as the "inner-layer equation" $x\ell nx = y$ which is encountered in a variety of problems, for example, the determination of the height of internal boundary layers or the depth of the stress-perturbed region in flow over hills. As a more curious example, the determination of the deposition velocity which for given source and dispersion conditions gives the largest "contaminated" area. For a very wide range of x this equation is well approximated by $x = y^{4/5}$; hence

$$-L = C\ (z_o^{1/5}\ z_i^{4/5})/(\sigma_\theta^{12/5}) \tag{8}$$

where the variance of the wind direction fluctuations σ_θ has been introduced to replace σ_v/μ. The constant of proportionality, C, is of order 10^{-2}. However, C depends on the height at which u is defined.

Thus, a rough estimate of z_o, a fair guess on z_i (just a bit better than a factor of two is sufficient if we compare with the usual uncertainty in calculating L from directly measured turbulent fluxes), and measurements of σ_θ, which are now being made routinely on a climatological basis (Bush et al., 1976), should be enough to give a qualified guess on the Monin-Obukhov length under convective conditions.

Figure 51 shows a comparison of Eq. (8) with (a) data from the Prairie Grass (Nieuwstadt, 1980) and Minnesota experiments

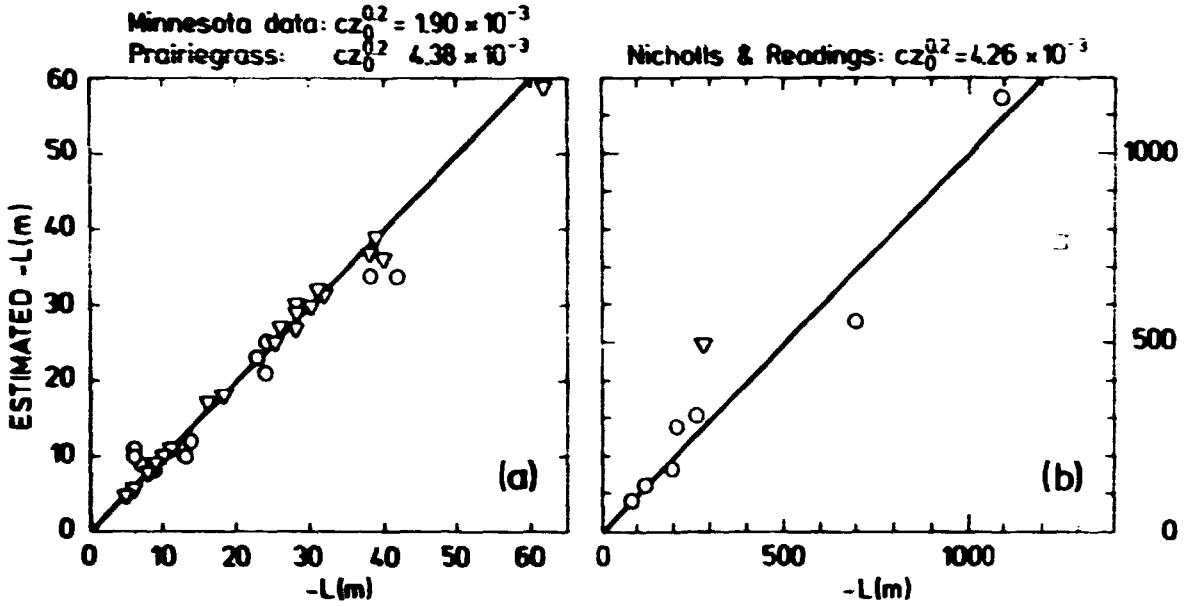

Fig. 51. Measured values of the Monin-Obukhov length, L, versus values estimated from Eq. (8) (see 4.12) in which the value of σ_θ was taken as w_*/u. Note the different scales in (a) and (b). The outlier point (□) in (b) pertains to a wind velocity of 21 m/s, conditions under which the above theory is not expected to be valid. Also the point (▽) corresponds to rather extreme mixed layer conditions (11 m/s and z_i = 350 m). In spite of that, the predictions come out with an error of less than a factor of two.

(Izumi and Caughey, 1976), and (b) some over-water data by Nicholls and Readings (1979). It should be mentioned that the Prairie Grass data provide only a check on the consistency of the above derivations, as no independent flux measurements were made in this case. Regarding the over-water data it is interesting to note that in some of the cases the total heat flux was made up from a latent heat flux which was almost half as large as the sensible, and that the value of L in many cases was of the order of z_i (including cases were it actually was larger) indicating that Eq. (8) is applicable very close to neutral conditions.

Also the implied linear dependence of L on $u^{2.4}$ compares favourably with GATE (GARP (Global Atmospheric Research Programme) Tropical Experiment) data exemplified by the regression line given in Figure 4 of Fitzjarrald (1978). However, for practical use the constant C needs calibration by standardizing height of observation and averaging time.

4.13. The atmospheric boundary layer over complex terrain

(E.P. Bradley and N.O. Jensen)

An adequate knowledge of the behaviour of the atmospheric surface layer, based on Monin-Obukhov similarity concepts and resulting from two decades of research over homogenous terrain is now finding practical application in all types of environmental problems. Such specific matters as the aerodynamics of buildings and dispersal of pollutants immediately transpose the problem from the idealised one-dimensional prototype to the real world of hills, valleys, and surface-mounted obstacles. Hence, a need for a better understanding of such situations is accumulating.

Another need for an improved knowledge of surface layer mechanics is connected with our ability to study large-scale and meso scale phenomena to a greater extend than before. A sophistication and variety of observational techniques and the co-ordination of large-scale experiments have enabled detailed measurements to be made through the depth of the mixed layer. This implies an extensive and necessarily inhomogeneous lower boundary to the atmospheric volume under study and hence a further unknown source of influence on the dynamics involved.

In practice, surface layer studies tend to consider the influence on the lower atmosphere of simple surface features such as low hills, roughness changes and shelter belts. The concern in large-scale studies, on the other hand, is in the integrated effects of complicated topography and spatially varying terrain on momentum and heat transfer. Although the two scales seem to be rather separate, an understanding of the interaction between surface layer and mixed layer mechanisms is central to the description of meso scale transport processes.

In general, the necessity for a correct specification of the important scales involved in complex terrain studies must be emphasized. The importance of buoyancy, for example, may be related to a length scale L of the topography in the definition of a Froude number. From climatological knowledge of atmospheric stratification it then follows that buoyancy effects are almost

always important on scales greater than a few kilometres. They can also be important on shorter scales, but only under nocturnal conditions.

Another length scale of importance is provided by current analytical models for airflow over isolated features (hills, escarpments), generally based on the well known theory of Jackson and Hunt (1975), who divide the flow into an "inner" region of depth ℓ in which a balance between stress and pressure gradients are dominant, and an "outer" region, which is essentially inviscid. While this theory predicts a mean flow field which compares well with observations, a higher order theory is required to predict the behaviour of the Reynolds stresses. For scales greater than ℓ, diffusion is unimportant and the upstream turbulence subject to "rapid distortion", while for scales much less than ℓ, there is local equilibrium. However, on the important scale ℓ, the full Reynolds stress equations are involved. Also, from an conceptual point of view, turbulence measurements are as yet poorly defined. When flow separation takes place, the situation is even more complicated.

Considerable gaps in our basic knowledge exist in this field and reliable data from experimental work is badly needed. Despite the work of Mason and Sykes (1979), Bradley (1980), Sacré (1979), and Peterson et al. (1980), it is still not clear how turbulence is affected by terrain features. Very little is known as yet about the effects of stability over even the simplest terrain inhomogeneities. The distinction between the stable and unstable regime over complex terrain is likely to be more striking than over flat terrain because of the possibility of katabatic flows and terrain-influenced gravity waves. The extent to which the presence of hills influences the net drag on the surface is still a matter for controversy, and, given the range of vertical and lateral scales involved over extensive complex terrain the question of which scales are needed and how many to parameterize the lower atmosphere properly is a central issue in modelling techniques.

With the objective of meeting the above identified needs, it has been decided to carry out a major cooperative field experiment to measure the spatial characteristics of mean wind and turbulence over a solitary hill in detail. The results will be compared with mathematical and physical (i.e. wind tunnel) models in order to assess the faithfulness with which such models can predict the actual flow. The models to be verified are eventually to be applied to more complex terrain, where they could be used both to assess the wind power potential of particular sites and to identify areas of high wind shear which may be important for wind energy generator structural loading and performance considerations.

The experiment is planned through the International Energy Agency's Executive Committee on Research and Development on Wind Energy Conversion Systems (R & D on WECS). Participants in the task will be: The National Research Council of Canada in collaboration with the Department of the Environment (Canada); The Danish Ministry of Energy in collaboration with Risø National Laboratory (Denmark); Kernforschungsanlage Jülich (F.R.G.) in collaboration with University of Hannover (F.R.G.); The New Zealand Department of Transport in collaboration with University of Canterbury, Christchurch (New Zealand); ERA Technology Ltd. (Electricity Research Association, U.K.). The result of the cooperative field experiment will include observations of the distribution of near surface wind speed and direction on and around a selected hill site and, in addition tower-based mean wind and turbulence profiles to about 50 m at selected locations. Wind and temperature profiles to higher levels will be obtained from kite - or balloon supported instruments. The project is expected to be completed in a period of three years (1982-1984). The experimental work will take place on and around the hill Askervein on the Island of South Uist in the Outer Hebridies, which was selected on basis of a number of suitable hillsites in each of the participating countries.

4.14. Results from an experimental investigation of a spatial step change in surface heat flux

(J. Højstrup, S.E. Larsen and N.O. Jensen)

The influence of simple terrain inhomogeneities on the flow field has attracted much interest, and a large number of numerical models have been developed to describe the simplest of these situations, i.e. simple two-dimensional roughness changes, smooth hills, and escarpments. Most of these consider only neutral conditions, although diabatic cases are more common. Furthermore, a roughness change is often associated with a stability change because of differences in heat capacity and albedo for the two surfaces. This becomes especially obvious when we consider the large roughness change between water and land. To study the influence of stability changes, an experiment was designed to provide data useful for testing the stability change aspects of existing models and provide a basis for development of better models. The experiment was planned at a site that exhibited small changes in surface roughness and the possibility of very large changes in surface heat flux. The site was a flat sandy beach. Earlier measurements have shown (Vugts and Cannemeijer, 1981) that the roughness change for onshore flow would amount to no more than a factor of five in roughness length z_o. Because of the small absolute value of z_o (at 5 m/sec, z_o is of the order of 50 μm) this change is of little importance for the flow dynamics.

The experiment was set up on the northward-facing beach of the small Dutch island of Schiermonnikoog. The bulk of the instrumentation was positioned along a line perpendicular to the coastline on a flat sandy beach. The masts were from 2 to 20 m high. The instrumentation was very comprehensive, including sonic anemometers, hotwires, coldwires, wet and dry thermocouples for turbulence measurements, cups and, vanes, and thermocouples for profile measurements, (see Vugts, 1980, Larsen et al., 1979 for details).

The data reported here stem from the sonic anemometers at the coastline (No. 1) and at distances 39 m (No. 2), 82 m (No. 3),

and 120 m (No. 4) from the coastline, all at 2 m height. The two runs selected for preliminary analyses have the same wind directions, approximately perpendicular to the coastline, but were otherwise very different. Run 16 (June 16, 1979, 1230-1353) had the highest windspeed (5.2 m/sec at the two-meter level). The sky was slightly clouded, and this run was selected because it showed a small stability change such that it could be used to verify the assumption of a negligible roughness change of the site. Run 23, on the other hand (June 18, 1979, 1500-1623) had a lower windspeed (3.7 m/sec at the two meter level), clear skies, and a large change in surface heat flux.

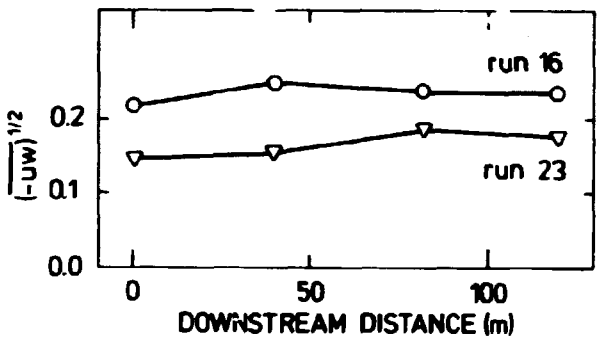

Fig. 52. Downstream development of shear stress two meters above the surface for Runs 16 and 23.

The downstream development of shear stress is plotted in Fig. 52, and indeed the downstream change in shear stress is small. In both runs we see a slight increase followed by a slow decrease. This would result from a change towards more unstable situations if one simply imagines the velocity profile as consisting of two usual logarithmic profiles with stability corrections, one profile inside the internal boundary layer, and the other outside the internal boundary layer identical to the upstream profile. The two profiles are matched at the top of the internal boundary layer forcing the lower profile to an increased stress for more unstable conditions downstream.

Figure 53 shows the downstream development of heat flux as measured by the sonics. The temperatures used here are those

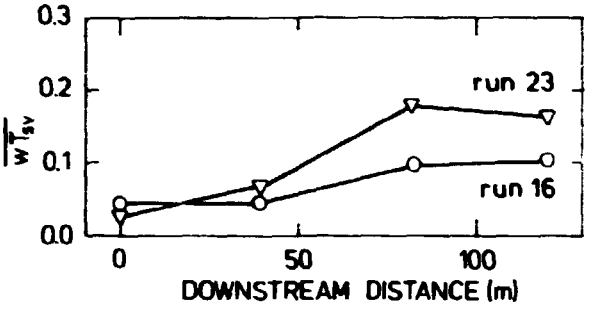

Fig. 53. Downstream development of heatflux for Runs 16 and 23.

measured by the sonics, the so-called sound virtual temperature which to a good approximation equals the virtual temperature. We see that Run 16 exhibits a change in surface heat flux of a factor of two, whereas Run 23 shows almost an order of magnitude change. The downstream development of velocity and temperature spectra is shown in Figs. 54 and 55. The upper set of spectra in

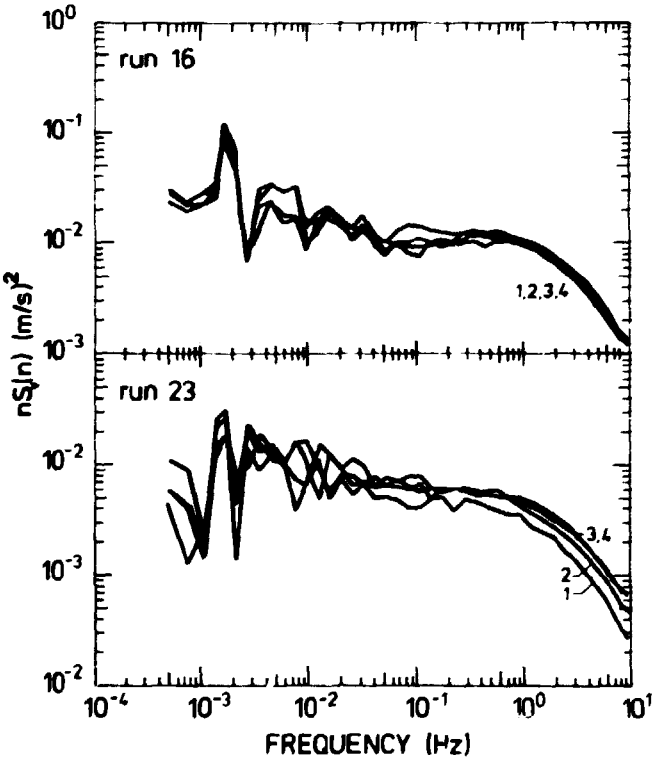

Fig. 54. X-spectra at the coastline (No. 1) at distances from the coastline: 39 m, (No. 2), 82 m (No. 3), and 120 m (No. 4) (all at two meters height). The uppermost set at spectra is from Run 16 (small heatflux change), the lowermost set from Run 23 (large heatflux change).

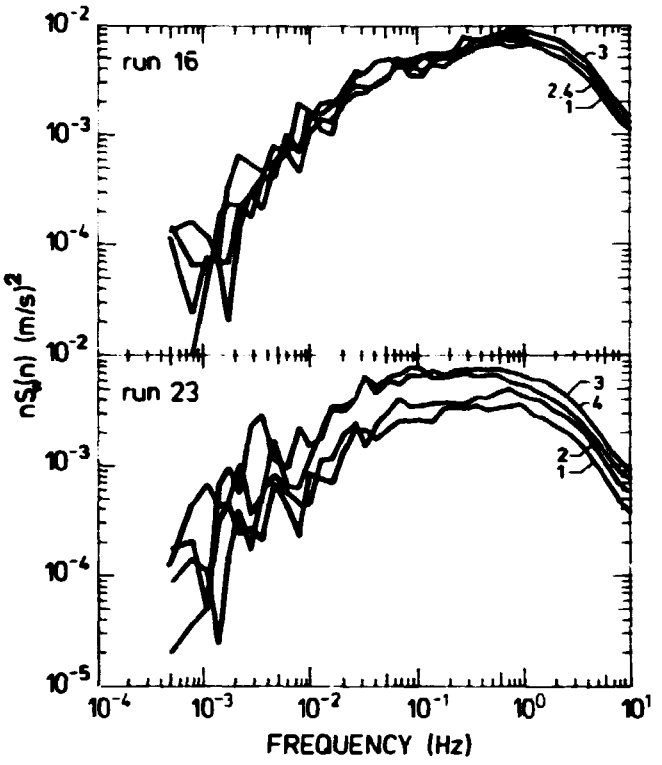

Fig. 55. W-spectra. Numbering as in Fig. 54.

each figure is always Run 16 (small stability change). None of the velocity spectra from this run show any significant development downstream, as expected, indicating a negligible change of conditions downstream.

In Run 23 the velocity spectra are adjusting gradually, first at high frequencies, and much more slowly at lower frequencies except for the w-component that seems to have adjusted in almost the entire frequency range. This is inconsistent with the model of Højstrup (1981) for the adjustment of spectra. According to this model the rate of adjustment of a spectrum at a given wavenumber is proportional to the square root of the logarithmic spectrum at this wavenumber. In contrast to this, we have here a w-spectrum with less energy than the horizontal spectra, and still it adjusts more rapidly. A likely explanation for this discrepancy is that the model, in fact, assumes that only the velocity spectra are adjusted by horizontal gradients, the vertical exchange of energy is neglected. This is reasonable for situations which are not too unstable and holds always for the

horizontal spectra since their most energetic parts are unchanged with height. For the w-component, it seems that the vertical exchange of energy must be taken into account in very unstable situations since those are the ones with the largest vertical gradients of σ_w.

From the simple model of Højstrup (1981) the ratio of the up-to-down stream spectra at high frequencies can be calculated as

$$(\phi_{\varepsilon 1}^{2/3} u_{*1}^{2})/(\phi_{\varepsilon 2}^{2/3} u_{*2}^{2}) \ .$$

For Run 23 this comes to 0.5 (upstream L = -9.1 m, downstream L = -2.5 m) in very good agreement with the results shown in Figs. 54 and 55. For Run 16 the ratio comes to 0.80 which is within the experimental scatter of the data shown in Figs. 52 and 53. So we conclude that for the situation of a dominant heat flux change, the high-frequency portions of the velocity spectra adjust according to theory as does the low-frequency part of the horizontal component. For the w-spectra in very unstable conditions the data indicate that in order to model the downstream development of the spectra, it is necessary to take into account both the horizontal and vertical exchanges of variance.

4.15. Hot- and cold-wire studies

(S.E. Larsen and J. Højstrup)

For a wire sensor placed along the x-axis the fluctuations of the wire temperature T_w' can be approximately described by the following equation (Larsen, 1982),

$$\tau \frac{\partial}{\partial t} T_w' = \Delta^2 \frac{\partial^2}{\partial x^2} T_w' - T_w' + \gamma T_a' - \frac{\gamma}{4} \frac{R_e^{0.45}}{Nu} (\bar{T}_w - \bar{T}_a)(u'/\bar{u}) + \frac{2\gamma R(T_{ws}) I_g^2}{\pi \ell k_a Nu} (I'/\bar{u}) \qquad (1)$$

which relates T_w' to fluctuations in velocity u', ambient temperature T_a', and heating current, I'. τ, Δ, and γ are parametes describing the wire time constant, heat conduction along the wire, and overheat, respectively. Average variable values are indicated by an overbar. Re, Nu, and R(T) are the Reynolds- and Nusselt-numbers and wire resistance, while k_a is the heat conductivity of air and ℓ the wire length. Equation (1) is solved by Fourier expansion. T_a' and u' are assumed to be spatially homogeneous, and as boundary conditions it is assumed that the prong tips act as first-order filters with a time constant τ_p (Højstrup et al., 1976).

With $I' = 0$, Eq. (1) describes a cold-wire, while it describes a hot-wire in constant temperature mode if $\langle T_w' \rangle_\ell = 0$, where $\langle\ \rangle_\ell$ indicate averaging along the wire.

The solution leads to four different frequency transfer functions, for cold wires:

$$dZ_{T_m}(\omega) = Hc_T(\omega)dZ_T(\omega) - cHc_U(\omega)dZ_U(\omega) \qquad (2)$$

and for hot wires

$$dZ_{u_m}(\omega) = Hh_U(\omega)dZ_U(\omega) - \alpha_T\bar{u}Hh_T(\omega)dZ_T(\omega)\ , \qquad (3)$$

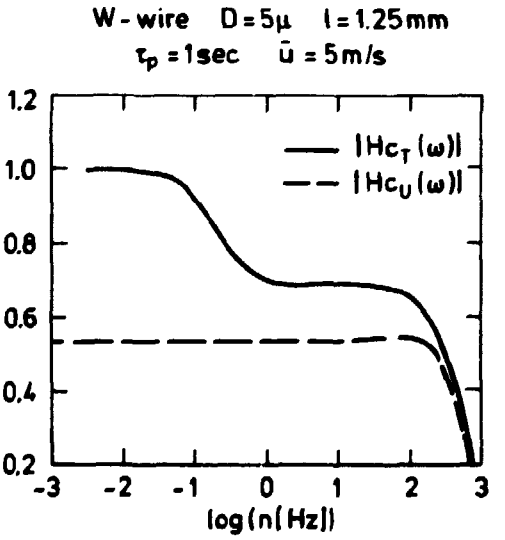

Fig. 56. The transfer-functions $|Hc_T(\omega)|$ and $|Hc_U(\omega)|$, describing the temperature and velocity sensitivity of a typical cold wire.

where c (Wyngaard, 1971) and α_T (Larsen and Busch, 1976) describe the static sensitivities of cold wires to velocity and hot wires to temperature, respectively. The subscript m means measured. The four transfer functions given by Eqs. (2) and (3) are shown for typical probes in Figs. 56 and 57.

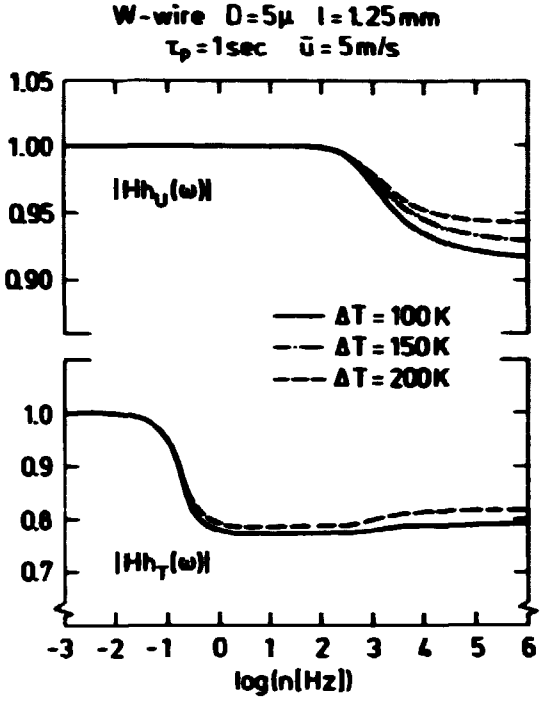

Fig. 57. The transfer-function $|Hh_u(\omega)|$ and $|Hh_t(\omega)|$ describing the velocity and the temperature sensitivity of a typical hot-wire.

The second-order statistical parameter, which is most sensitive to the above-described mixed response is the co-spectrum between u_m and T_m. Combining Eqs. (2) and (3 yields

$$Co_{u_m T_m}(\omega) = Hc_T(\omega)Co_{uT}(\omega) - cHc_U(\omega)S_u(\omega) \qquad (4)$$

$$- \alpha_T \bar{u} Hh_T(\omega)Hc_T(\omega)S_T(\omega) \ ,$$

which shows that the measured co-spectrum relative to the true one is contaminated by the power-spectra of velocity and temperature.

At higher frequencies the co-spectrum goes to zero with increasing frequence so much faster than the power spectra, that the

contribution to $Co_{u\,T}(\omega)$ from the power-spectra will be very large even for small values of c and α_T. In this frequency region, knowledge about the form of the transfer functions therefore is important. This is illustrated in Fig. 58. Here $Co_{u\,T}(\omega)$ has been corrected by use of Eq. (4) to recover $Co_{uT}(\omega)$. In Fig. 58a Hh_T and Hc_T have been neglected (i.e. $H = 1$), while they have been accounted for in Fig. 58b. $Hc_U(\omega)$ is included in both cases. From Fig. 57 is seen that, to a good approximation this function, can be considered constant in the frequency region of interest. In both cases the total co-variance, $\overline{u'T'}$, is recovered with an approximately 30% reduction in $\overline{u_m T_m}$. A correction of $Co_{u\,T}(\omega)$ in the high-frequency region by use of (u) is bound to be very noise sensitive. In spite of this, Fig. 58 shows that neglect of Hh_T and Hc_T in the correction leads to a systematic overcorrection in the high-frequency region.

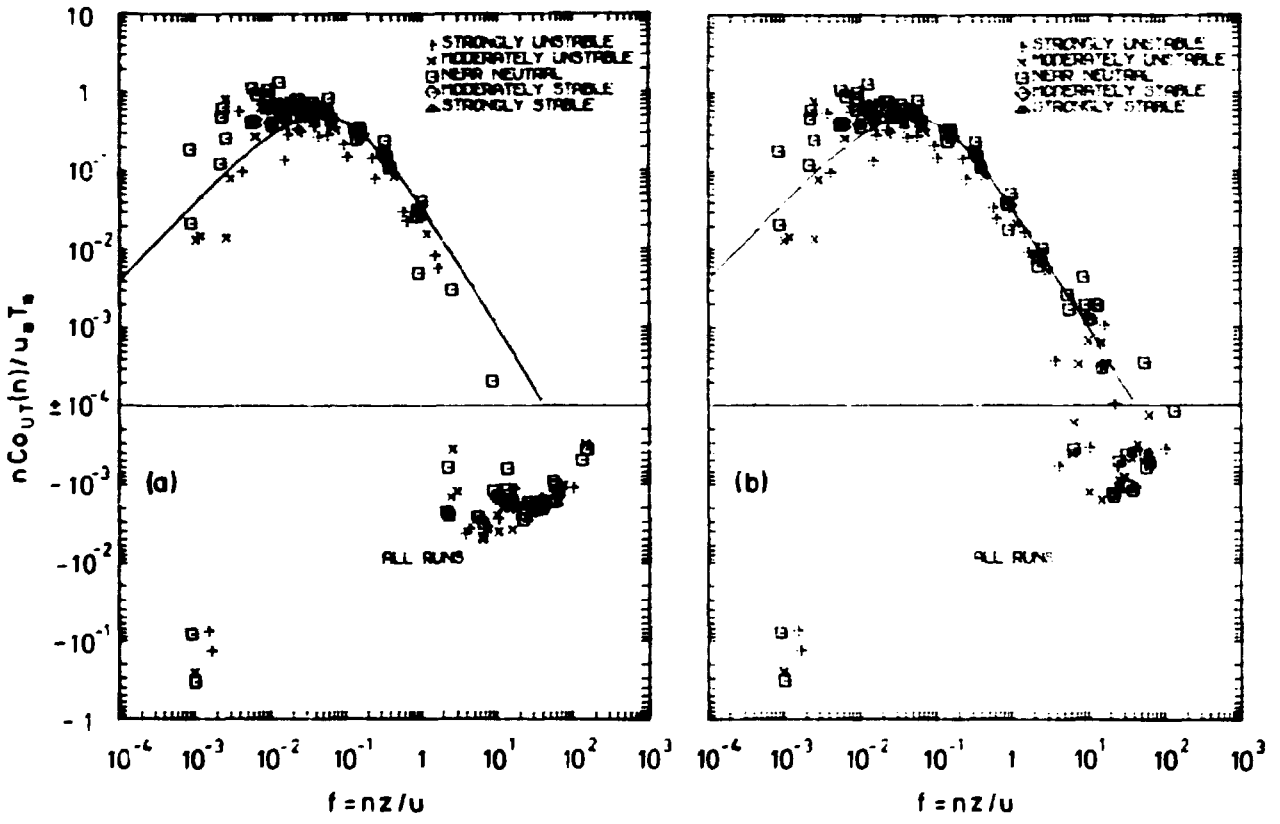

Fig. 58. Nine runs of measured $nCo_{uT}(n)$ versus $f = nz/\bar{u}$, n being frequency in Hz, z measuring height in m and $\bar{u}$ the mean velocity. In (a) the directly measured co-spectra have been corrected by use of Eq. (4) but with $Hh_T(\omega) = Hc_T(\omega) = 1$, while in (b) these function have been given values in accordance with Figs. 56 and 57. The solid curves are from Kaimal et al. (1972).

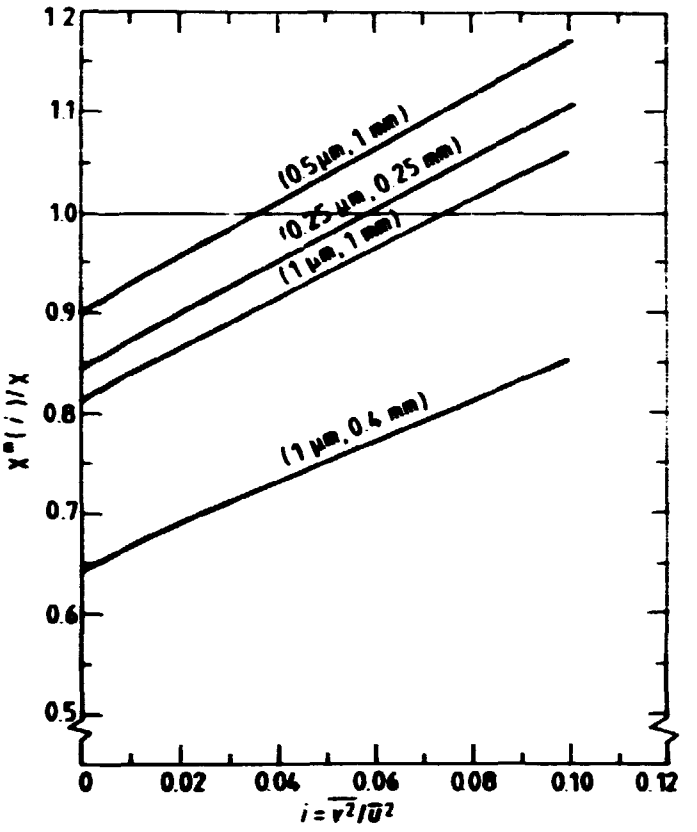

Fig. 59. The ratio between temperature dissipation estimates of different noise less probes and the true dissipation as a function of the turbulence intensity squared (Larsen and Højstrup, 1982).

The transfer functions in Eqs. (2) and (3) was derived for spatially homogeneous conditions. In (Larsen and Højstrup, 1979) it was shown that the spatial averaging of the sensor in an inhomogeneous turbulence field could be included for $Hc_T(\omega)$ to obtain a transfer function of the form $Hc_T(k_s,\omega)$, where k_s is the wavenumber along the direction of the wire. By use of a model for the wavenumber frequency spectrum for temperature, we were able to estimate the accuracy by which different typical sensors could be used for direct determination of the temperature dissipation (Larsen and Højstrup, 1982). The results are shown in Fig. 59, which displays the ratio between the measured and the "true" dissipation as a function of the turbulence intensity.

4.16. Energy technology characterization

(C.J. Christensen and L.H. Nielsen (Energy System Analysis, Risø))

As a service to the Danish Ministry of Energy a number of energy production technologies have been examined and characterized. The work is a sub-task for the International Energy Agency's Energy Technology Systems Analysis project. A detailed list of the technologies characterized can be found in Section 6.2 under C.J. Christensen. The characterizations shall serve as input data for various energy systems analysis purposes. The only common denominator for this sub-task concerns the definition of descriptors. We have experienced the importance and difficulties in establishing very precise and understandable descriptors and subsequently in imposing the discipline on the assessors when using the descriptors as intended. If one fails to come to grips with this, the work is wasted. As an example of the subsequent use of the characterizations, Table 4 shows a price comparison between

Table 4. Example of the use of energy characterizations

	Improved future MIDE-A	55 kW commercial windturbine	Coal and electricity	
Lifetime: 35 years(coal), 20 years(wind), Real rent: 6%				
Design capacity, DC	630	55	$610 \cdot 10^3$	kW
Capacity factor, CF	22	21	67	%
Capital cost, CC	1350	910	495	$/kW
Fixed annual costs, FAC	125	92	40	$/kW·yr
FAC/CF·8760, FAC/kWh	0.065	0.050	0.007	$/kWh
Variable/kWh	0.000	0.000	0.018	$/kWh
Total kWh-cost	0.065	0.050	0.025	$/kWh
Lifetime: 35 years(all), Real rent 2%				
FAC	74	49	27	$/kW·yr
FAC/kWh	0.038	0.027	0.005	$/kWh
Variable/kWh	-	-	0.018	$/kWh
Total kWh-cost	0.038	0.027	0.023	$/kWh

electricity produced by one of two Danish wind turbines or by a conventional coal-fired power station. Such numbers in tables look very convincing, but several problems do warrant great care. The capacity factor, for instance, strongly influences the comparison and requires careful measurements of wind speed distributions. To a high degree capital cost is guesswork when discussing such prototype machines as these two wind-turbines are. The price comparison is extremely sensitive to the assumed interest rate (real rent) and the technical lifetime.

4.17. Estimate of the fatigue lifetime of wind-turbine rotors

(S. Frandsen, P. Hauge Madsen and L. Kristensen)

During the last few years it has become clear that one major obstacle in the development of optimized wind-energy conversion systems has been the limited possibilities of estimating the fatigue life of the rotors. Several incidents of failure have been recorded in Denmark as well as in other countries, which retrospectively can be explained only by component fatigue.

Another problem relates to the very complex pattern of operational modes and thereby load cases, such as different wind speeds, degree of stall on the blades, skew wind, brakings, etc. Actually, a number of computer programs are available that calculate the structural response of wind turbines exposed to well-defined loads, while the problem of combining the various load cases into a consistent and realistic load history is only poorly solved.

A study specificaly aiming at solving these two problems has been initiated. The structural model itself and the modelling of each load case are kept as simple as possible without limiting the accuracy significantly. In order to be able to perform the analysis in the frequency domain both the structural model and the load are assumed linear, and the response is split into (i) a stochastic - and (ii) deterministic response. Three sub-tasks of the study are discussed in some detail below. Figure 60 gives an overview of the elements of the computer program, under development.

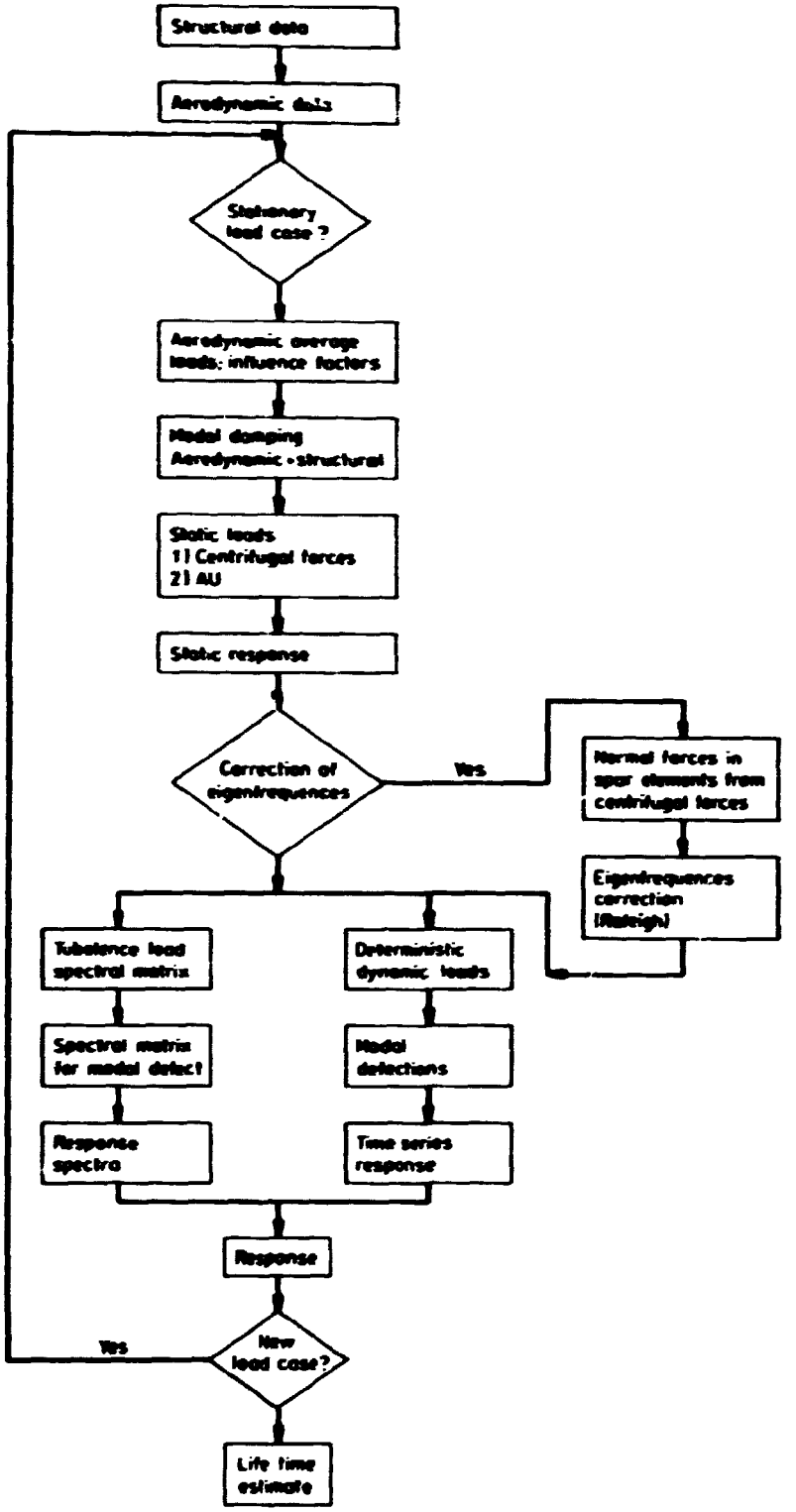

Fig. 60. Flow chart for computer program (ROTORDYNE).

a) The structural model

The structural behaviour of the wind-turbine rotor has been modelled by a linear lumped-mass system. This choice makes it possible to use a general-purpose linear finite-element program to discretize the rotor system and perform the initial vibration analysis. At Risø the linear finite-element program SAP IV, originally from Berkeley, California, U.S.A. is available in an updated version from ASEA-ATOM, Sweden. This program contains among other types of elements, beam and truss elements, which are suitable for dynamic rotor analysis. It furthermore has excellent facilities for model analysis, i.e. solving the eigenvalue problem to obtain the natural frequencies and mode shape vectors of the undamped structure.

The turbine is modelled in standard cartesian coordinates which rotates with the rotor. This implies that all loads caused by the rotation, such as centrifugal and gyro forces, must be accounted for explicitly. An example of the idealized rotor and the chosen coordinate system is shown in Fig. 61.

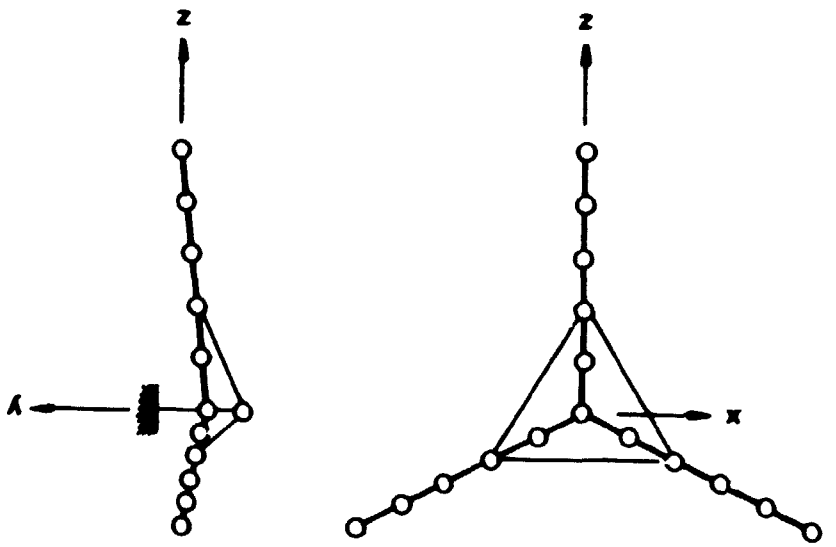

Fig. 61. The idealized rotor model.

The governing equation of motion is the well known matrix equation

$$\overline{\overline{M}}\,\ddot{\vec{x}} + \overline{\overline{C}}\,\dot{\vec{x}} + \overline{\overline{K}}\,\vec{x} = \vec{P}(\vec{x},\dot{\vec{x}},t) \qquad (1)$$

where $\overline{\overline{M}}$, $\overline{\overline{C}}$ and $\overline{\overline{K}}$ are the mass, damping, and stiffness matrices, respectively, and dots denote differentiation with respect to time. The coupling between the response $\vec{x}$ and the wind load contained in the load vector $\vec{P}$ must be linearized to

$$\vec{P}(\vec{x},\dot{\vec{x}},t) \approx \vec{P}_o + \vec{P}(t) + \overline{\overline{A}}\,\vec{x} + \overline{\overline{B}}\,\dot{\vec{x}} \qquad (2)$$

in order to preserve linearity and thereby computational efficiency. In Eq. (2), A and B constitute (with reverse signs) both concepts: aerodynamic stiffness and damping.

For the static mean loads the structural response is determined using the full global stiffness matrix K, while the dynamic response is expressed in terms of a few fundamental modes

$$\vec{x}(t) \approx \sum_{i=1}^{M} \vec{v}_i T_i(t)$$

where v_i is the mode shape vector of mode i, and T_i is the modal displacement which is found by solving the vector problem of reduced order

$$\left[1\right]\ddot{\vec{T}}(t) + \left\{\left[2\omega_i\delta_i\right] + B^*\right\}\dot{\vec{T}}(t) + \left[\omega_i^2\right]\vec{T}(t) = \vec{q}(0)$$

where the aerodynamic stiffness due to its minor effect is neglected. B^* is the aerodynamic damping (transformed into modal generalized coordinated) and forms the coupling between the equations. $2\omega_i\delta_i$ is the structural damping term and ω_i the natural modal frequency. $\vec{q}(t)$ is the generalized load vector defined by $q_i(t) = (\vec{v}_i^T\,P(t))/(\vec{v}_i^T\,\overline{\overline{M}}\,\vec{v}_i)$.

The frequency response matrix is of importance when the spectrum of the response to turbulence is desired. It is in the context defined as

$$\bar{\bar{H}}(\omega) = \left\{\left[\omega_i^2\right] - \omega^2 \left[1\right] + i\omega \left\{\left[2\omega_i \delta_i\right] + B^*\right\}\right\}^{-1}$$

where $\{\quad\}^{-1}$ denotes inversion of the matrix inside the bracket.

For a turbulent wind component with spectral matrix $\bar{\bar{S}}_{uu}(\omega)$, the spectrum of the response can be written as:

$$S_{xx}(\omega) = \bar{\bar{A}}^T \overline{\bar{\bar{H}}(\omega)}\ S_{uu}(\omega)\ \bar{\bar{H}}(\omega)\bar{\bar{A}}$$

where the linear relationship between the modal displacements and the response is expressed by $\bar{\bar{A}}$.

Apart from the discretization and the calculation of ω_i and V_i, which can be determined by any linear finite element program, all calculations are performed by the program for dynamic rotor analysis and a fatigue lifetime estimate, which is under development.

b) Model for power spectra measured on the blade of a wind turbine

During the last few years the problem of how the turbulent wind structure looks when observed from a wind turbine blade moving in a vertical plane perpendicular to the wind direction has attracted some attention. In particular, the spectra redistribution is of great interest as discussed by Connell (1980).

Verholek (1978) did an experiment with 8 Gill uvw-anemometers equally spaced on the circumference of a vertical circle with a radius of 24.4 m and the center positioned 24.4 m off the ground. The signals were scanned in cyclic order and in this way it was possible to simulate the wind field in the direction of the mean wind as felt by a moving tip of a blade in the ideal situation, when the disturbance from the blades can be neglected. A similar experiment was performed by Hardesty et al (1981). In this case a CO_2-laser anemometer was moved in such a way that the center of the measuring volume described a circle

in a vertical plane perpendicular to the wind direction. The conclusion from both experiments was that the power spectrum of the turbulent velocity spectrum of the component in the wind direction - the so-called u_1-spectrum - was distorted in comparison with a u_1-spectrum measured from a non-moving coordinate system. Apart from showing resonance at the frequencies n/T, n being a positive integer and T the time of revolution, the variance seemed to have been moved from lower to higher frequencies. A very simple model, originally proposed by Rosenbrock (1955), seems to explain this behaviour, at least qualitatively, this behaviour.

A wind turbine typically revolves once per few seconds. The tip of the turbine blade will consequently experience a wind field that varies significantly in time, not only because the mean wind advects the turbulence, but also because the tip of the blade sweeps through a region of turbulence of a typical size of 50 m in a rather short time. Under the assumptions that the turbulence is stationary, homogeneous, isotropic, and incompressible and that Taylor's hypothesis is valid, it is possible (Rosenbrock, 1955) to derive a formula for the autocovariance function for the turbulent wind component of the mean wind direction in a frame moving with the tip of the blade of a wind turbine. Using Rosenbrock's approach and assuming that the energy spectrum has the analytical form suggested by von Karman (1948)

$$E(k) = \frac{2^{5/3}\,\Gamma(17/6)}{\sqrt{2\pi}\;\Gamma(1/3)}\;\sigma_o^2\;L\;\frac{L^4k^4}{(1+L^2k^2)^{17/6}} \qquad (1)$$

an analytical expression for this auto-covariance function is obtained, and the application of a digital Fourier transform thus yields the corresponding power spectrum. In Eq. (1) Γ is the gamma-function, k the wavenumber, σ_o^2 the variance of one velocity component, and L some length scale characterizing the turbulence.

The auto-covariance function becomes

$$R(\tau) = \frac{2\sigma_o^2}{\Gamma(1/3)}\;\theta^{1/3}\;\left\{K_{1/3}\,(2\theta) - \frac{\alpha^2\sin^2(\omega_o i/2)}{\theta}\;K_{2/3}\,(2\theta)\right\} \qquad (2)$$

Here α is the ratio between the radius of the revolution and L, ω_o the angular velocity, and τ the lag. The quantity θ is given by

$$\theta = \alpha(\sin^2(\omega_o\tau/2) + 1/2(\omega_o\tau)^2/\lambda_T^2)^{1/2} \qquad (3)$$

where λ_T is the so-called tip speed ratio, i.e. the ratio between $a\omega_o$ and the mean wind speed U, which is assumed perpendicular to the plane of rotation. The functions $K_{1/3}$ and $K_{2/3}$ are modified Bessel functions of the second kind of order 1/3 and 2/3, respectively (Olver, 1972).

Figure 62 shows an example of a power spectrum, found by means of a digital Fourier transform. The parameters L and λ_T are chosen such that they correspond to Verholek's (1978) findings.

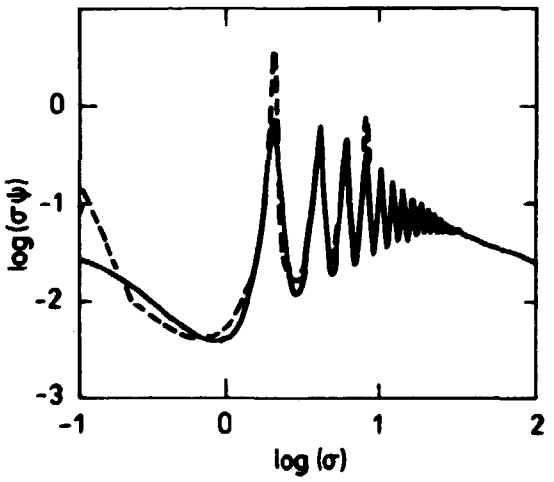

Fig. 62. The logarithm of the power spectrum, multiplied by frequency, versus the logarithm of frequency. The dashed line is the result of Verholek's data analysis and the full line shows the result of the present model. The variable σ is twice the frequency normalized by the angular velocity of the rotation.

Assuming now that this model accounts quantatively for most of the features of the power spectrum, it seems natural to utilize the simple ideas behind it to compute cross-spectra between perpendicular velocity components at two different places in the plane of the rotating wind turbine blades. The results from such an analysis could help explain the dynamical loads from the turbulent wind on the rotating parts.

Letting the two distances from the hub be a_1 and a_2 and the angle between the radii between the two points be γ, one can generalize the approach 2 given in (a) in the following way:

Let

$$\alpha = \sqrt{a_1 a_2}/L \ , \tag{4}$$

$$\delta = (a_2 - a_1)/2L) \ , \tag{5}$$

and

$$\theta_1 = \alpha\{\sin^2((\omega_o\tau)/2 + \gamma/2) + ((\omega_o\tau)/2)^2 + \delta^2)/\lambda_T^2\}^{1/2} \tag{6}$$

Then the cross covariance function becomes

$$R_{12}(\tau) = \frac{2\sigma_o^2}{\Gamma(1/3)}\ \theta_1^{1/3}\ \{K_{1/3}\ (2\theta_1) - \frac{\alpha^2\sin^2((\omega_o\tau)/2 + \gamma/2)}{\theta_1}\ K_{2/3}\ (2\theta_1)\} \tag{7}$$

c) Loads on the rotor structure

As mentioned above, the loads on the rotor divide into a deterministic and stochastic part. The source of the stochastic load is - at least at the present state of the development of the program - assumed solely to be the turbulent wind. Having derived the spectrum of the v-component of the wind velocity as observed from a rotating blade and employing the assumption of linearity of air loads, the load spectrum on a cross-section element is easily determined:

$$S_{ff}(n) = C_{fv}^2 \cdot S_{vv}(n)$$

where C_{fn}^2 is the influence factor and $S_{vv}(n)$ the spectrum determined proviously in (a). The diagonal terms in the load spectral matrix are determined in a straightforward way, while the off-diagonal spectra - the cross-spectra for different blade elements - in principle are easily computed but in practice might cause some problems.

The deterministic loads include static and dynamic components. The static load is due to centrifugal forces and the average aerodynamic loads, calculated by means of the blade element theory. The dynamic loads are the gravity loads, the load from an average wind shear and the loads due to interference between the tower of the turbine and skew winds relative to the rotor disc. All deterministic dynamic loads are assumed to be represented well enough by harmonic functions, though the effect of interference with the tower has to be modelled by an expansion in a Fourier series. The resulting loads have the form

$$F_{DD}(t) = \sum_{k=0}^{n} C_k \exp(i\omega_o kt)$$

where C_k is a complex constant and ω_o the rotational frequency.

At least one type of non-stationary plenomenon of significance has to be represented in the integrated load history, namely a stopping or braking of the machine. No explicit solution to this problem has been found yet, and the outcome might be that time series analysis must be used.

When the response spectrum in the different load cases is determined, each spectrum is properly weighted in accordance with the wind speed statistics for the site and the available information on the operational mode of the wind turbine, the result being the data needed for the final estimate of fatigue life for the considered blade spar cross section.

4.18. References to Chapter 4

BATCHELOR, G.K. (1953). In: Cambridge Monographs on Mechanics and Applied Mathematics, Cambridge University Press.

BRADLEY, E.F. (1980). Quart. J. Roy. Meteorol. Soc. 106, 101-123.

BUSCH, N.E. (1973). In: Workshop on Micrometeorology. Edited by D.A. Haugen (American Meteorol. Soc.), 1-65.

BUSCH, N.E., DORPH-PETERSEN, P., CHRISTENSEN, C.J. and KRISTENSEN, L. (1976). In: Risø-R-352, 67-71.

BUSINGER, J.A. (1973). In: Workshop on Micrometeorology. Edited by D.A. Haugen (American Meteorol. Soc.), 67-100.

CONNELL, J.R. (1980). Report PNL-3426, Battelle Pacific Northwest Laboratory, Richland, Washington 99352.

DUTTON, J.A. and FICHTL, G.H. (1969). J. Atmos. Sci. 26, 241-254.

FEYNMANN, R.P. and HIBBS, A.R. (1965). Quantum Mechanics and Path Integrals (McGraw-Hill, New York).

FITZJARRALD, D.E. (1978). J. Appl. Meteorol. 17, 213-221.

GRYNING, S.E. (1981). Risø-R-446.

GRYNING, S.E. and LYCK, E. (1980). Atmosph. Env. 14, 923-931.

GRYNING, S.E., and THOMSON, D.W. (1979). J. Appl. Meteorol. 18, 1674-1678.

HARDESTY, R.M., KORREL, J.A. and HALL, Jr., F.F. (1981). Lidar Measurement of Wind Velocity Spectra Envountered by a Rotating Turbine Blade, NOAA Technical Memo, to be published.

HØJSTRUP, J. (1981). Boundary-Layer Meteorol. 21, 341-359.

HØJSTRUP, J., RASMUSSEN, K., and LARSEN, S.E. (1976). DISA-Information No. 20, 22-30.

IZUMI, Y. and CAUGHEY, J.S. (1976) Minesota 1973 Atmospheric Boundary Layer Experiment Data Report. AFCRL-TR-76-0038, Environmental research papers, No. 547.

JACKSON, P.S. and HUNT, J.C.R. (1975). Quart. J. Roy. Met. Soc. 101, 929-955.

JENSEN, N.O. (1981). Health Physics 40, 887-891.

KAIMAL, J.C. (1978). J. Atmos. Sci. 35, 18-23.

KAIMAL, J.C., WYNGAARD, J.C., IZUMI, Y., COTE, O.R. (1972). Quart. J. Roy. Meteorol. Soc. 98, 653-689.

KELLER, H.B. (1971). In: Numerical Solutions of Partial Differential Equations 2, Academic Press, New York, 327-350.

KRISTENSEN, L. and LENSCHOW, D.H. (1980). In: Risø-R-441, 135-136.

LARSEN, S.E. (1982). Risø Report 232. In press.

LARSEN, S.E. and BUSCH, N.E. (1976). DISA-Information No. 20, 5-211.

LARSEN, S.E., CANNEMEIJER, F., HØJSTRUP, J., JENSEN, N.O. and VUGTS, H.F. (1979). In: Risø-R-414, 45-47.

LARSEN, S.E. and HØJSTRUP, J. (1979). In: Risø-R-414, 115-118.

LARSEN, S.E. and HØJSTRUP, J. (1982). J. Phys. E. 15, 471-477.

LUMLEY, J.L. and PANOFSKY, H.A. (1964). In: The Structure of Atmospheric Turbulence, (Interscience Monographs and Texts in Physcis and Astronomy, John Wiley & Sons, New York-London-Sydney) 239 pp.

MASON, P.J. and SYKES, R.I. (1979). Quart. J. Roy. Meteorol. Soc. 105, 383-395.

MIKKELSEN, T., TROEN, I. and LARSEN, S.E. (1982). On the Finite Line Source Problem in Diffusion Theory. Accepted for publication in Atm. Environment.

NICHOLLS, S. and READINGS, C.J. (1979). Quart. J.Roy. Meteorol. Soc. 105, 785-802.

NIEUWSTADT, F.T.M. (1980). J. Appl. Meteorol. 19, 157-162.

OLVER, F.W.J. (1972). In: Handbook of Mathematical Functions. Edited by M. Abramowitz and I. Stegun (Dover Publications, Inc., New York), 355-433.

PANOFSKY, H.A., TENNEKES, H., LENSCHOW, D.H., and WYNGAARD, J.C. (1977). Boundary-Layer Meteorol. 11, 355-361.

PASQUILL, F. (1974). In: Atmospheric Diffusion (2nd Edition, John Wiley & Sons, New York).

PETERSON, E.W., TAYLOR, P.A., HØJSTRUP, J., JENSEN, N.O., KRISTENSEN, L. and PETERSEN, E.L. (1980). Boundary-Layer Meteorol. 19, 303-313.

ROSENBROCK, H.H. (1955). Report C/T 113, ERA Technology Ltd., Cleeve Road, Leatherhead, Surrey KT22 7SA, England, 53 pp.

SACRÉ, E. (1979). Boundary-Layer Meteorol. 17, 381-401.

SLADE, D.H. (1968). Meteorology and Atomic Energy, N.S. Atomic Energy Commision, TID 24190, 445 pp.

THYKIER-NIELSEN, S. and LARSEN, S.E. (1982). Risø-M-2205. In press.

TURNER, B. (1967). Workbook on Dispersion Estimates. U.S. Environmental Protection Agency. Office of air Programs AP-26. Research Triangle Park North Carolina.

VENKATRAM, A. (1980). Boundary-Layer Meteorol. 19, 481-485.

VERHOLEK, M.G. (1978). Report PNL-2518, Battelle Pasific Northwest Laboratory, Richland, Washington 99352, 37 pp.

VON KARMAN, T. (1948). Proc. National Acad. Sci. 34, 530-539.

VUGTS, H.F. (1980). Bull. of the American Meteorol. Soc. 61, 568-569.

VUGTS, H.F. and CANNEMEIJER (1981). J. Appl. Meteorol. 20, 335-340.

WYNGAARD, J.C. (1971). J. Fluid. Mech. 48, 763-769.

WYNGAARD, J.C. (1973). In: Workshop on Micrometeorology. Edited by D.A. Haugen, (American Meteorol. Soc.), 101-149.

5. LIQUID N_2 AND He PLANT

The production of liquid N_2 and He amounted to 200 000 and 17 000 litres, respectively. Out of these amounts, 7 000 litres of liquid He were delivered to laboratories in Copenhagen, Odense, and Aarhus.

6. PUBLICATIONS AND EDUCATIONAL ACTIVITIES

6.1. Publications

ALMEIDA, M., CARNEIRO, K. and ALCACER, L. (1981). Neutron scattering studies of photons and vibrons in TEA(TVNQ)$_2$. Chem. Scr. 17, 102-103.

ALPORT, M., D'ANGELO, N. and PÉCSELI, H.L. (1981). A laboratory experiment on EM-backscatter from Farley-Buneman and gradient drift waves. J. Geophys. Res. A86, 7694-7702.

ALS-NIELSEN, J. (1981). Liquid crystals studied by perfect crystals. In: Symmetries and Broken Symmetries in Condensed Matter Physics. Proceedings of the Colloque Pierre Curie, Paris, France, September 1-5, 1980. Edited by N. Boccara. Idset-Paris, 107-122.

ALS-NIELSEN, J. and BURAS, B. (1981). ESRF at Risø, Denmark. Study prepared for the Danish Science Research Council, (Risø National Laboratory, Roskilde, Denmark), 19 pp.

ANDERSEN, V., GADEBERG, M., JENSEN, P.B., NIELSEN, P. and SØRENSEN, H. (1981). Acceleration and injection of D_2-pellets. In: Fusion Technology 1980. Proceedings of the 11th Symposium on Fusion Technology. Oxford, U.K., September 15-19, 1980, (Pergamon Press, Oxford) (EUR-7035) Vol. 2, 1113-1118.

ARMSTRONG, R.J., RASMUSSEN, J. JUUL, STENZEL, R.L. and TRULSEN, J. (1981). Observations of obliquely propagating electron Bernstein waves. Phys. Lett. 85A, 281-284.

BALMASHNOV, A.A., LYNOV, J.P., MICHELSEN, P. and RASMUSSEN, J. JUUL (1981). Excitation of whistler waves by a helical wave structure. J. Phys. D14, 1803-1809.

BALMASHNOV, A.A. and RASMUSSEN, J. JUUL (1981). Enhanced plasma confinement in a magnetic well by whistler waves. Phys. Lett. 84A, 65-67.

BECHGAARD, K., CARNEIRO, K., JACOBSEN, C.S., OLSEN, M., RASMUSSEN, F.B. and RINDORF, G. (1981). Superconductivity in an organic solid at zero pressure: (TMTSF)$_2$ClO$_4$. Physica 108B+C, 1193-1194.

BESENBACHER, F., BØTTIGER, J., GRAVERSEN, O., HANSEN, J.L. and SØRENSEN, H. (1981). Stopping power of solid argon for helium ions. Nucl. Instrum. Methods 188, 657-667.

BESENBACHER, F., BØTTIGER, J., GRAVERSEN, O., HANSEN, J.L. and SØRENSEN, H. (1981). The erosion of frozen argon by swift helium ions. Nucl. Instrum. Methods 191, 221-234.

BURAS, B., POURME, R. and KOCH, M.H.J. (1981). X-ray diffraction, principles and applications. DESY and HASYLAB, Internal Report 81/11, 192 pp.

BURAS, B., GERHARD, L., OLSEN, J. STAUN and STEENSTRUP, S. (1981). A spectrometer for x-ray energy-dispersive diffraction using synchrotron radiation. (Deutsches Elektronen-Synchrotron, Hamburg, 1981) DESY SR-81/10, 12 pp.

BURAS, B. and LEBECH, B. (1981). Nyt, fantastisk "lys" - Synkrotron-stråling og dens anvendelse indenfor krystallografi (New, fantastic light - Synchrotron radiation and applications in crystallography). Naturens Verden, special issue, May 1981, 59-64.

BURAS, B. and MØLLER, H. BJERRUM (1981). Det europæiske synkrotron-strålingscenter og mulighederne for at opføre det ved Risø. (The European center of synchrotron radiation research and the possibilities for its location at Risø) Risø Nyt, September.

CARNEIRO, K., PASSELL, L., THOMLINSON, W. and TAUB, H. (1981). Neutron diffraction from the second layer of ^{4}He on graphite. Physica 107B+C, 237-238.

CARNEIRO, K., PASSELL, L., THOMLINSON, W. and TAUB, H. (1981). A neutron diffraction study of the solid layers at the liquid-solid boundary in ^{4}He-films adsorbed on graphite. Phys. Rev. B24, 1170-1176.

CHANG, C.T. (1981). PELREP - A numerical code for computing the ablated state of a refuelling pellet. Risø-M-2219, 27 pp.

CHANG, C.T. and MICHELSEN, P. (1981). On the drag effect of a refuelling pellet. J. Fusion Energy 1, 253-257.

CHRISTENSEN, A. NØRLUND and LEBECH, B. (1981). Magnetic transition temperature of terbium hydroxide oxide. Structure of ytterbium hydroxide oxide. Acta Crystallogr. B37, 425-427.

CLAUSEN, B.S., TOPSØE, H., CANDIA, R., VILLADSEN, J., LENGELER, B., ALS-NIELSEN, J. and CHRISTENSEN, F. (1981). Extended x-ray absorption fine structure study of Co-Mo hydrodesulfurization catalysts. J. Phys. Chem. 85, 3868-3872.

CLAUSEN, K., HAYES, W., HUTCHINGS, M.T., KJEMS, J.K., SCHNABEL, P. and SMITH, C. (1981). Quasi-elastic diffuse neutron scattering from fluorites in the fast ion phase. Solid State Ionics 5, 589-592.

CLAUSEN, K. and NIELSEN, O.V. (1981). Magnetic anisotropy in single crystals of Ho_2Co_{17} and Ho_2Fe_{17}. J. Magn. Mater. 23, 237-240.

CLAUSEN, K.N. (1981). Magnetic excitations in Ho_2Co_{17} and Ho_2Fe_{17}. An inelastic neutron scattering study, Risø-R-426, 85 pp.

FEILE, R., KJEMS, J.K., LOEWENHAUPT, M. and HOENIG, H.E. (1981). Influence of superconductivity on crystal field transitions in $La_{1-x}Tb_xAl_2$. Phys. Rev. Lett. 47, 610-613.

FRANDSEN, S. (1981). Der kræves resevoirer af anselig størrelse (On the impact of water reservoir storage on the steadiness of energy output from wind turbines). Ingeniøren 7, no. 26, 6-7.

FRANDSEN, S., CHRISTENSEN, C.J., JENSEN, E. and NIELSEN, P. (1981). Measurements on the Nibe wind turbines. January 1980 - March 1981. (DEFU, Copenhagen, Denmark (EEV-81-04) 120 pp.

GIEBULTOWICZ, T., KEPA, H. BURAS, B., CLAUSEN, K. and GALAZKA, R.R. (1981). Neutron diffraction study of magnetic ordering in $Cd_{1-x}Mn_xTe$. Solid State Commun. 40, 499-501.

GIEBULTOWICZ, T., MINOR, W., BURAS, B., LEBECH, B. and GALAZKA, R.R. (1981). Neutron scattering studies of the antiferromagnetic phase of $Cd_{1-x}Mn_xTe$. (H.C. Ørsted Institute, Copenhagen, Denmark), KU-HCOE-F12-R-81-32, 15 pp.

GJØRUP, H. L., JENSEN, P. HEDEMANN, PETERSEN, E. LUNDTANG, PETERSEN, T., ROED, J., THYKIER-NIELSEN, S., VINTHER, F, HEIKEL, WARMING, L. and AARKROG, A. (1981). Konsekvensen af en landforurening med radioaktive stoffer på Sjælland efter et hypotetisk kernenedsmeltningsuheld på Barsebäck (Some consequences of land containation on Danish territory

from radioactivity following a hypothetical core-melt accident at the Barsebäck Nuclear Power Plant). Risø-M-2212, 195 pp.

GRYNING, S.E. and LARSEN, S.E. (1981). Relation between dispersion characteristics over surfaces with dissimilar roughness and atmospheric stability under conditions of equal geostrophic winds. Atmos. Environ. 15, 983-987.

HANSEN, N., LEFFERS, T. and KJEMS, J.K. (1981). Recrystallization kinetics in copper investigated by in situ texture measurements by neutron diffraction. Acta Metall. 29, 1523-1533.

HEILMANN, I.U., KJEMS, J.K., ENDOH, Y., REITER, G.F., SHIRANE, G. and BIRGENEAU, R.J. (1981). One- and two-magnon excitations in a one-dimensional antiferromagnet in a magnetic field. Phys. Rev. B24, 3939-3953.

HUTCHINGS, M.T., ALS-NIELSEN, J., LINDGÅRD, P.-A. and WALKER, P.J. (1981). Neutron scattering investigation of the temperature dependence of long wavelength spin waves in ferromagnetic Rb_2CrCl_4. J. Phys. C14, 5327-5345.

HØJSTRUP, J. (1981). A simple model for the adjustment of velocity spectra in unstable conditions downstream of an abrupt change in roughness and heat flux. Boundary Layer Meteorol. 21, 341-356.

IIZUKA, S., MICHELSEN, P., RASMUSSEN, J. JUUL, SCHRITTWIESER, R., HATAKEYAMA, R., SAEKI, K. and SATO, N. (1981). Experimental investigations of the ionization effect on strong double-layers. In: Proceedings of the XV International Conference on Phenomena in Ionized Gases, Minsk, U.S.S.R., July 14-18. Contributed papers Part I, International Scientific Committee, Moscow) 501-502.

IIZUKA, S., MICHELSEN, P., RASMUSSEN, J. JUUL, SCHRITTWIESER, R., HATAKEYAMA, R., SAEKI, K. and SATO, N. (1981). Measurements of fast temporal evolutions of the plasma potential by a simple emissive probe. THUP-2, Tohoku University, Sendai, Japan. 23 pp.

IIZUKA, S., MICHELSEN, P., RASMUSSEN, J. JUUL, SCHRITTWIESER, R., HATAKEYAMA, R., SAEKI, K. and SATO, N. (1981). A method for measuring fast time evolutions of the plasma potential by means of a simple emissive probe. J. Phys. E14, 1291-1295.

JAN, J.-P. and SKRIVER, H.L. (1981). The electronic structure of calcium. J. Phys. F11, 805-820.

JANSSEN, P.A.E.M. and RASMUSSEN, J. JUUL (1981). Limit cycle behaviour of the bump-on-tail and ion-acoustic instability. Risø-M-2235, 37 pp.

JANSSEN, P.A.E.M. and RASMUSSEN, J. JUUL (1981). Limit cycle behaviour of the bump-on-tail instability. Phys. Fluids 24, 268-273.

JENSEN, N.O. (1981). Entrainment through the top of a heavy gas cloud. In: Air Pollution Modeling and its Application I. Proceedings of the 11th NMO-CCMS International Technical Meeting Amsterdam, The Netherlands, November 24-27, 1980. Edited by C. De Wispelaere. (Plenum Press, New York), 477-487.

JENSEN, N.O. (1981). Studies of the atmospheric surface layer during change in surface conditons. In: Colloque Construire avec le vent, CSTB, Nantes, France, June 15-19, 1981, Tome I No. I-4, (Centre Scientifique et Technique du Bâtiment, Nantes), 20 pp.

JENSEN, N.O. (1981). A micrometeorological perspective on deposition. Health Phys. 40, 887-891.

JENSEN, N.O. (1981). Scales of atmospheric turbulence. Risø-M-2263, 40 pp.

JENSEN, N.O. (1981). On the calculus of heavy gas dispersion. Risø-R-439, 45 pp.

JENSEN, P.B. and ANDERSEN, V. (1981). Handling of deuterium pellets for plasma refuelling. Risø-M-2294, 20 pp.

JENSEN, V.O. (1981). Fusionsforskningen står ved en milepæl (Fusion research at a milestone). Ingeniøren 7, no. 32, 8-9.

JOHANSSON, B., SKRIVER, H.L. and ANDERSEN, O.Krogh (1981). Electronic structure of the actinide metals. In: Physics of Solids under High Pressure. Proceedings of an International Symposium. Bad Honnef, F.R.G., August 10-14, 1981. Edited by J.S. Schilling and R.N. Shelton. (North-Holland, Amsterdam), 245-262.

KEPA, H., GIEBULTOWICZ, T., BURAS, B., LEBECH, B. and CLAUSEN, K. (1981). A neutron scattering study of lattice dynamics of HgTe and HgSe. (H.C. Ørsted Institute, Copenhagen, Denmark) KU-HCOE-F12-R-81-18, 11 pp.

KNORR, K., LOIDL, A. and KJEMS, J.K. (1981). Singlet ground-state magnetism: III magnetic excitons in antiferromagnetic TbP. Z. Phys. B40, 287-292.

KRISTENSEN, L., JENSEN, N.O. and PETERSEN, E.L. (1981). Lateral dispersion of pollutants in a very stable atmosphere; the effect of meandering. Atmos. Environ. 15, 837-844.

KRISTENSEN, L., PANOFSKY, H.A. and SMITH, S.D. (1981). Lateral coherence of longitudinal wind components in strong winds. Boundary Layer Meteorol. 21, 199-205.

LARSEN, S.E. (1981). Summary of ongoing research on air-sea interaction at Risø. In: HEXOS - Humidity Exchange Over the Sea. Proceedings of NATO a Workshop, Dartmouth, Nova Scotia, Canada, April 28 - May 1, 1981. Edited by S.D. Smith and K.B. Katsaros. (Bedford Institute of Oceanography, Dartmouth, N.S. Canada) BI-R-81-17, 77.

LARSEN, S.E. and CHRISTENSEN, O. (1981). A three-dimensional propeller anemometer design for climatological measurements. In: HEXOS Humidity Exchange Over the Sea. Proceedings of NATO a Workshop, Dartmouth, Nova Scotia, Canada, April 28 - May 1, 1981. Edited by S.D. Smith and K.B. Katsaros. (Bedford Institute of Oceanography, Dartmouth, N.S. Canada) BI-R-81-17, 75-77.

LEBECH, B. (1981). Neutron diffraction studies of the modulated magnetic structures of CeSb and Nd metal. J. Appl. Phys. 52, 2019-2024.

LOEWENHAUPT, M. and MØLLER, H. BJERRUM (1981). Magnetic field dependence of the excitation energies in the mixed valent compound TmSe. Physica 108B+C, 1349-1350.

LYNOV, J.P., MICHELSEN, P., PÉCSELI, H.L., RASMUSSEN, J. JUUL and THOMSEN, K. (1981). Numerical simulation of the initial damping and frequency shift of nonlinear electron plasma waves. In: Proceedings of the XV International Conference on Phenomena in Ionized Gases, Minsk, U.S.S.R., July 14-18, 1981. Contributed papers, Part I, (International Scientific Committee, Moscow) 161-162.

McMAHAN, A.K., SKRIVER, H.L. and JOHANSSON, B. (1981). The s-d transition in compressed lanthanum. Phys. Rev. B23, 5016-5029.

McMAHAN, A.K., SKRIVER, H.L. and JOHANSSON, B. (1981). Shock anomaly and s-d transition in high pressure lanthanum. In: Physics of Solids under High Pressure. Proceedings of an International Symposium, Bad Honnef, F.R.G., August 10-14, 1981. Edited by J.S. Schilling and R.N. Shelton. (North-Holland, Amsterdam), 169-174.

MICHELSEN, P. (1981). Investigations of electrostatic ion waves in a collisionless plasma. Risø-R-417, 130 pp.

MIKKELSEN, T., PÉCSELI, H.L., ALPORT, M. and D'ANGELO, N. (1981). Experimental investigations of turbulence in magnetized, partially ionized plasmas. In: Physics of Auroral Arc Formation. Edited by S.-I. Akasofu and J.R. Kan. Geophysical Monograph 25 (American Geophysical Union, Washington D.C.) 393-397.

MIKKELSEN, T. and TROEN, I. (1981). Comments on "On lateral dispersion coefficients as function of averaging time". J. Appl. Meteorol. 20, 731-732.

MIKKELSEN, T., TROEN, I. and LARSEN, S.E. (1981). On the finite line source problem in diffusion theory. Risø-M-2309, 17 pp.

NIELSEN, M., ALS-NIELSEN, J., BOHR, J. and McTAGUE, J.P. (1981). Pressure driven commensurate-incommensurate transition in low temperature submonolayer krypton on graphite. Phys. Rev. Lett. 47, 582-585.

OLSEN, J. STAUN, BURAS, B., GERWARD, L., JOHANSSON, B., LEBECH, B., SKRIVER, H.L. and STEENSTRUP, S. (1981). High pressure diffraction studies of YbH_2 up to 28 GPa. DESY SR-81/13, 10 pp. and in: Physics of Solids under High Pressure. Proceedings of an International Symposium, Bad Honnef, F.R.G., August 10-19, 1981. Edited by J.S. Schilling and R.N. Shelton. (North-Holland, Amsterdam) 305-309.

OLSEN, J. STAUN, BURAS, B., GERWARD, L. and STEENSTRUP, S. (1981). A spectrometer for x-ray energy-dispersive diffraction using synchrotron radiation. J. Phys. E11, 1154-1158.

PÉCSELI, H.L., ARMSTRONG, R.J. and TRULSEN, J. (1981). Experimental observation of ion phase-space vortices. Phys. Lett. 81A, 386-390.

PETERSEN, E.L., TROEN, I. and FRANDSEN, S. (1981). Vindatlas i folkeudgave (Windatlas made popular). Ingeniøren 7, no. 11, 37.

PETERSEN, E.L., TROEN, I., FRANDSEN, S. and HEDEGAARD, K. (1981). Danish Windatlas. A rational method of wind energy siting. Risø-R-429, 229.

PEDERSEN, T. FRIIS (1981). Rotor, gear og generator tilpasning for stall-reguleret vindmølle (Rotor, gear, and generator alignment for a stall-regulated windmill). Risø-M-2282, 21 pp.

PEDERSEN, T. FRIIS (1981). Status for smedemestermøllen (Status of the "Master Smith" mill). Risø-M-2272, 20 pp.

PEDERSEN, T. FRIIS and RASMUSSEN, F. (1981). Eksperimentel bestemmelse af en Darrieus rotors opførsel i fri vind (Experimental determination of a Darrieus rotors' performance in free wind). Risø-M-2280, 133 pp.

PEDERSEN, T. FRIIS (1981). Prøvebelastning af rotorblade med trekantlast (Load test of a rotor blade with triangular loading). Risø-M-2282, 92 pp.

RASMUSSEN, K. RØMER, LARSEN, S.E. and JØRGENSEN, F.E. (1981). Study of flow deformation around wind-vane mounted three-dimensional hot-wire probes. DISA-Inf. No. 26, 27-34.

RASMUSSEN, P. (1981). Afprøvning af 15 kW gyro-mølle fra Dansk Vindkraft Industri ApS (Test report for a 15 kW gyromill from Danish wind power industry ApS). Risø-M-2310, 43 pp.

RASMUSSEN, P. (1981). Afprøvning af styringsenhed til vindmølle fra Freke, type AGC 130 (Test of a controller unit for windmills: FREKE AGC 130). Risø-M-2323, 17 pp.

SATO, N., HATAKEYAMA, R., IIZUKA, S., MIENO, T., SAEKI, K., RASMUSSEN, J. JUUL and MICHELSEN, P. (1981). Ultra-strong stationary double layers in a nondischarge magnetoplasma. Phys. Rev. Lett. 46, 1330-1333.

SATO, N., HATAKEYAMA, R., IIZUKA, S., MIENO, T., SAEKI, K., RASMUSSEN, J. JUUL and MICHELSEN, P. (1981). Stationary double-layers in a non-discharge magnetoplasma. THUP-1, (Tohoku University, Sendai, Japan) 28 p.

SKRIVER, H.L. (1981). The electronic structure of antiferromagnetic chromium. J. Phys. F11, 97-111.

SKRIVER, H.L. (1981). Electronic transitions in praseodymium under pressure. In: Physics of Solids under High Pressure. Proceedings of an International Symposium, Bad Honnef, F.R.G., August 10-14, 1981. Edited by J.S. Schilling and R.N. Shelton. North-Holland, Amsterdam) 279-282.

SKRIVER, H.L. and MACKINTOSH, A.R. (1981). Energy bands and mass enhancement in yttrium. In: Physics of Transition Metals 1980. International Conference - University of Leads, U.K., August 18-22, 1980. Edited by P. Rhodes. Conference series No. 55. (Institute of Physics, London) 29-30.

SVENDSEN, L.G. and BØRGESEN, P. (1981). Corrosion inhibition by ion implantation of Al or Mg in Cu investigated by RBS. Nucl. Instrum. Methods 191, 141-145.

TROEN, I. and PETERSEN, E.L. (1981). Vindatlas (Windatlas). Vejret 3, 28-38.

WATKINS, D.M., JACOBSEN, C.S. and CARNEIRO, K. (1981). Neutron scattering measurements, thermopower studies and the influence of cation polarization effects on some 1-D bis(oxalato) platinats salts. Chem. Scr. 17, 193-194.

6.2. Contract reports

CHRISTENSEN, C.J. (1981). A series of energy technology characterizations. IEA Workshop on Energy Technology Systems Analysis Project, Jülich, F.R.G., November 18-19, 1981. Eleven articles entitled:

Nibe-A wind turbine (630 kW) coupled to the utility grid
3-bladed wind turbine (55 kW, grid + heating).
Multi-vaned Mill (heating only).
Biogas reactor using manure from large feedstock.
610 MW coal fired electric power plant.
87 MW coal fired power plant with 174 MW backpressure district heating.
11 MW heatpump (diesel driven) for district heating.
Earth/water electric heatpump for older house.
Earth/water electric heatpump for newer house.
Air/water electric heat pump for older house.
Air/water electric heat pump for newer house.

FRANDSEN, S. (1981). Recommended practices for wind turbine performance testing. Summary report from the 3rd IEA Expert Meeting, Geilo, Norway, February 19-20. (Risø National Laboratory, Roskilde) 82 pp.

FRANDSEN, S. (1981). Danida Mission to the Cape Verde Islands. Concerning wind turbines for electricity production. August 12-23, (Risø National Laboratory, Roskilde, Denmark) 50 pp.

HØJSTRUP, J. (1981). Meteorological measurements at the Nibe site March 5, 1980 - March 23, 1981, Work done under contract to DEFU/RISØ.

JENSEN, N.O. (1981). Frigørelses- og spredningsbetragtninger vedrørende klor. (Considerations regarding the release and spreading conditions of Chlorine. In: Risikoanalyse af den planlagte ændring af klortappestationen på Grinsted Products A/S anlæg i Grenå. Edited by J.R. Taylor. Work done under contract to Grindstedværket A/S.

JENSEN, N.O. and DALSGAARD, G. (1981). Anemometer til måling af lave vindhastigheder (Anemometer for measurements of low wind speeds). Work done under contract to ELSAM, 15 pp.

LARSEN, S.E. (1981). Preliminær analyse of meteorologiske data fra Katholm (Preliminary analysis of meteorological data from Katholm). Contract Report for ELSAM, 23 pp.

PETERSEN, E.L., KRISTENSEN, L. and JENSEN, N.O. (1981) Meteorology. In: The Carnsore accident study. Edited by O. Walmod Contract work done for the Energy Supply Board, Ireland.

PETERSEN, E.L., KRISTENSEN, L. and JENSEN, N.O. (1981). The meteorological part of: Some consequences of land contamination on Danish territory from radioactivity following a hypothetical coremelt accident at the Barsebäck nuclear power plant (in Danish, edited by H.L. Gjørup). Work done for the Ministry of the Environment. Risø-M-2212, p 31-64.

TROEN, I. (Editor) (1981). Vurdering af udvalgte danske beregningsmodeller til beregning af immissionskoncentrationsbidrag fra høje kilder. (An evaluation of Danish models for calculating concentrations resulting from releases from tall stacks). Contract work made to the Ministry of the Environment. 201 pp.

6.3. Conference contributions

ALEKSEEV, P.A., SADIKOV, I.P., SCHITIKOV, Y.L., MARKOVA, I.A., CHRISTYAKOV, O.D., SAVITSKIL, E.M. and KJEMS, J.K.. Crystalline electric field effects in Pr(La,Y)Al_3. 4th International Conference on Crystal Field and Structural Effects in f-Electron Systems, Wroclaw, Poland, September 22-25.

ALS-NIELSEN, J., NIELSEN, M., BOHR, J. and McTAGUE, J.P.. Synchrotron x-ray study of phase transitions in monolayers of Ar, Kr and Xe on graphite. Nordic Solid State Physics Conference 1981, Copenhagen, Denmark, August 10-12.

ANDERSEN, N. HESSEL, KJEMS, J.K. and POULSEN, F.W.. Neutron scattering studies of the ionic conductor LiI·$D_2O(H_2O)$. Nordic Solid State Physics Conference 1981, Copenhagen. Denmark, August 10-12.

ANDERSEN, V., BEJDER, H., GADEBERG, M., JENSEN, P.B. and NIELSEN, P.. Pellet ablation studies in Dante. 8th Annual Conference on Plasma Physics, Swansea, U.K., July 8-10.

BAUER, R.. Multimetal EXAFS studies applied to the Zn, Cu enzyme superoxide dismutase. Symposium on the Impact of Crystallography on Natural Sciences in the 20th Century, Copenhagen, Denmark, May 18-19.

BESENBACHER, F., BØTTIGER, J. and SØRENSEN, H.. Stopping power of solid argon for He ions and the applicability of the Bethe theory in describing S_e for He with energies $0.5 < E_{He} < 3$ keV. 9th International Conference on Atomic Collisions in Solids, Lyon, France, July 6-10.

BESENBACHER, F., BØTTIGER, J., GRAVERSEN, O., HANSEN, J.L. and SØRENSEN, H. (1981). The erosion of frozen argon by swift ions. 5th International Conference on Ion Beam Analysis, Sydney, Australia, February 16-20.

BOHR, J., ALS-NIELSEN, J., NIELSEN, M. and McTAGUE, J.P.. Synchrotron x-ray study of phase transitions in Kr-monolayers on graphite. Nordic Solid State Physics Conference 1981, Copenhagen, Denmark, August 10-12.

BØRGESEN, P., CHEN HAO-MING and SØRENSEN, H.. Stopping of 1-2 keV/amu hydrogen ions in solid N_2. 9th International Conference on Atomic Collisions in Solids, Lyon, France, July 6-10.

BRADLEY, E.F. and JENSEN, N.O.. Summary of proceedings of the atmospheric boundary layer over complex terrain. IAMAP 3rd Scientific Assembly, Hamburg, F.R.G., August 17-28.

BURAS, B.. Neutron scattering (General Survey). 10th Nordic Meeting on Structural Chemistry, Special Session on Neutron Scattering, Helsingfors, Finland, January 5-7.

CHANG, C.T.. Theoretical consideration of H_α-line emission from a refuelling pellet. 23rd Annual Meeting, Division of Plasma Physics, American Physical Society, New York, U.S.A., October 12-16.

CHRISTENSEN, C.J.. A series of energy technology characterizations. IEA workshop Energy technology systems analysis project, Jülich F.R.G., November 1-8.

CHRISTENSEN, C.J.. On the economy of wind-vs. coal-produced electricity. IEA Expert Meeting on Wind Turbine Costings, Copenhagen, Denmark, November 18-19.

CHRISTENSEN, C.J.: The characterization of WECS as energy production technology. IEA-Implementing agreement LS WECS. Expert Meeting: Costings for Wind Turbines. Copenhagen, November 18-19.

CLAUSEN, B.S., TOPSØE, H., CANDIA, R., VILLADSEN, J., LENGELER, B., ALS-NIELSEN, J. and CHRISTENSEN, P.. EXAPS study of catalysts. Symposium on the Impact of Crystallography on Natural Sciences in the 20th Century, Copenhagen, Denmark, May 18-19.

CLAUSEN, K. and LEBECH, B.. Magnetic excitations in Ho_2Co_{17} and Ho_2Fe_{17}. Institute of Physics 18th Annual Conference on Solid State Physics, York, U.K., January 7-8.

CLAUSEN, K. and LEBECH, B.. Magnetic excitations in Ho_2Co_{17} and Ho_2Fe_{17}. Institute of Physics, Magnetism Group Meeting on Current Research in Magnetism, London, U.K., March 25.

FRANDSEN, S.. Recommended Practises for Wind Turbine Performance Testing. Results from IEA Expert Committee. British Wind Energy Association Conference, Brighton, U.K., August 27-29.

GIEBULTOWICZ, T., MINOR, M., BURAS, B., LEBECH, B. and GALAZKA, R.R.. Neutron scattering studies of the antiferromagnetic phase of $Cd_{1-x}Mn_xTe$. Nordic Solid State Physics Conference 1981, Copenhagen, Denmark, August 10-12.

GRYNING, S.E. and LYCK, E.. Results from elevated source urban area dispersion experiments compared to model calculations. 12th NATO/CCMS International Technical Meeting on Air Pollution Modelling and its Application, Palo Alto, California, U.S.A., August 25-28.

HAZELL, R.G., LARSEN, F.K., KRÆMMER, S. and LEBECH, B.. Effect of scan type on integrated intensity. 12th Congress and General Assembly. International Union of Crystallography, Ottawa, Canada, August 16-25.

HØJSTRUP, J.. Velocity spectra in unstable conditions downstream of an abrupt change in roughness and heatflux. IAMAP Third Scientific Assembly, Hamburg, F.R.G., August 17-28.

IIZUKA, S., MICHELSEN, P., RASMUSSEN, J. JUUL, SCHRITTWIESER, R., HATAKEYAMA, R., SAEKI, K. and SATO, N.. Experimental investigations of the ionization effect on strong double-layers. XV International Conference on Phenomena in Ionized Gases, Minsk, U.S.S.R., July 14-18.

JENSEN, D. JUUL, HANSEN, N., KJEMS, J.K. and LEFFERS, T.. Neutron diffraction texture measurements as a tool for the investigation of recrystallization kinetics. 6th International Conference on Textures of Materials, Tokyo, Japan, September 28 - October 3.

JENSEN, N.O.. Studies of the atmospheric surface layer during change in surface conditions. Colloque: Construire avec le vent, Centre Scientifique et Technique du Bâtiment, Nantes, France, June 15-19.

JENSEN, N.O.. Land-sea wind adjustment. Joint Conference with the Royal Meteorology Society and the Institute of Mathematics and its Applications on Local Wind Environments, Cambridge, U.K., March 16-17.

JENSEN, P.B., ANDERSEN, V., BEJDER, H., GADEBERG, M. and NIELSEN, P.. Ablation studies in Dante. 23rd Annual Meeting, Division of Plasma Physics, American Physical Society, New York, U.S.A., October 12-16.

JOHANSSON, B., SKRIVER, H.L. and ANDERSEN, O.K.. Electronic structure of the actinide metals. International Symposium on the Physics of Solids under High Pressure, Bad Honnef, F.R.G., August 10-14.

KEPA, H., GIEBULTOWICZ, T., BURAS, B., LEBECH, B. and CLAUSEN, K.. A neutron scattering study of lattice dynamics of HgTe and HgSe. Nordic Solid State Physics Conference 1981, Copenhagen, Denmark, August 10-12.

KEPA, H., GIEBULTOWICZ, T., BURAS, B., LEBECH, B. and CLAUSEN, K.. A neutron scattering study of lattice dynamics of HgTe and HgSe. 4th International Conference on the Physics of Narrow Gap Semiconductors Linz, Austria, September 1-2.

KEPA, H., GIEBULTOWICZ, T., BURAS, B., CLAUSEN, K. and LEBECH, B.. Neutron scattering studies of phonon dispersion relations in HgTe and HgSe. 12th Congress and General Assembly. International Union of Crystallography, Ottawa, Canada, August 16-25.

KJEMS, J.K., CLAUSEN, K., HAYES, W., HUTCHINGS, M.T., SCHNABEL, P. and SMITH, C.. Quasi-elastic diffuse neutron scattering from fluorites in the fast ion phase. Conference on Fast Ion Transport in Solids, Gathinburg, Tennessee, U.S.A., May 18-22.

KJEMS, J.K., KAKURAI, K. and STEINER, M.. Neutron inelastic scattering study of the spin dynamics of $CsNiF_3$. Nordic Solid State Physics Conference 1981, Copenhagen, Denmark, August 10-12.

LARSEN, S.E.. Summary of ongoing research on air-sea interaction at Risø. JONSWAP and Lake Washington analyses. NATO-Workshop on HEXOS - Humidity Exchange over the Sea. Bedford Institute of Oceanography, Dartmouth, Nova Scotia Canada, April 28 - May 2.

LARSEN, S.E. and O. CHRISTENSEN. A three-dimensional propeller anemometer designed for climatological measurements. NATO-Workshop on HEXOS - Humidity Exchange over the Sea. Bedford Institute of Oceanography, Dartmouth, Nova Scotia Canada. April 28 - May 2.

LINDGÅRD, P.-A.. Correlation theory applied to the paramagnetic scattering in EuO. Nordic Solid State Physics Conference 1981, Copenhagen, Denmark, August 10-12.

LINDGÅRD, P.-A.. Correlation theory applied to the static and dynamic properties of EuO and EuS. 27th Annual Conference on Magnetism and Magnetic Materials, Atlanta, Georgia, U.S.A., November 10-13.

LOEWENHAUPT, M. and H. BJERRUM-MØLLER. Magnetic-field-dependence of the excitation energies in the mixed-valent compound TmSe. 16th International Conference on Low Temperature Physics, UCLA, Los Angeles, U.S.A., August 19-26.

LUNDSAGER, P.. Status and needs for research and development for small wind turbines, based on experience with small Danish wind turbines. International Colloquium on Wind Energy, Brighton, U.K., August 27-28.

LUNDSAGER, P.. Danish experience of small wind powered generators. Conference on Energy for Rural and Island Communities, Inverness, Scotland, September 5-7.

LUNDSAGER, P.. On the power regulation of small wind turbines, based on experience with small Danish wind turbines. 5th Biennial Conference and Workshop on Conversion Systems, Washington D.C., U.S.A., October 5-7.

LYNOV, J.P., MICHELSEN, P., PÉCSELI, H.L., RASMUSSEN, J. JUUL and THOMSEN, K.. Numerical simulation of the initial damping and frequency shift of nonlinear electron plasma waves. 15th International Conference on Phenomena in Ionized Gases, Minsk, U.S.S.R., July 14-18.

McMAHAN, A.K., SKRIVER, H.L. and JOHANSSON, B.. Shock anomaly and s-d transitions in high pressure lanthanum. International Symposium on the Physics of Solids under High Pressure, Bad Honnef, F.R.G., August 10-14.

MICHELSEN, P., RASMUSSEN, J. JUUL, HATAKEYAMA, R., IIZUKA, S., SAEKI, K., SATO, N. and SCHRITTWIESER, R.. Ultra-strong stationary double-layers in a collisionless magnetized plasma. Danish Physical Society, Spring Meeting, Risø, Roskilde, Denmark, May 21-22.

MØLLER, H. BJERRUM. Small angle scattering. International perspective. Situation in Denmark. 10th Nordic Meeting on Structural Chemistry, Helsingfors, Finland, January 4-8.

MØLLER, H. BJERRUM. Inelastic neutron scattering. Situation in Denmark. 10th Nordic Meeting on Structural Chemistry, Helsingfors, Finland, January 4-8.

NIELSEN, M., BOHR, J. and ALS-NIELSEN, J.. Synchrotron radiation studies of physisorbed monolayers of Kr and Ar atoms. Symposium on the Impact of Crystallography on Natural Sciences in the 20th Century, Copenhagen, Denmark, May 18-19.

NIELSEN, P. and GADEBERG, M.. Single point Thomsen scattering system for JET. 23rd Annual Meeting, Division of Plasma Physics, American Physical Society, New York, U.S.A., October 12-16.

OLSEN, J. STAUN, BURAS, B., GERWARD, L., JOHANSSON, B., LEBECH, B., SKRIVER, H.L. and STEENSTRUP, S.. High pressure diffraction studies of YbH_2 up to 28 GPa. Nordic Solid State Physics Conference 1981, Copenhagen, Denmark, August 10-12.

OLSEN, J. STAUN, BURAS, B., GERWARD, L., JOHANSSON, B., LEBECH, B., SKRIVER, H.L. and STEENSTRUP, S.. High pressure diffraction studies of YbH_2 up to 28 GPa. International Symposium on the Physics of Solids under High Pressure, Bad Honnef, F.R.G., August 10-14.

OLSEN, J. STAUN, BURAS, B., GERWARD, L. and STEENSTRUP, G.. An x-ray energy-dispersive diffractometer for synchrotron radiation. 12th Congress and General Assembly, International Union of Crystallography, Ottawa, Canada, August 16-25.

PÉCSELI, H.L., ALPORT, M. and D'ANGELO, N.. Microwave scattering from cross field instabilities. 16th Nordic Symposium on Plasma and Gas Discharge Physics, Gausdal, Norway, February 11-13.

PÉCSELI, H.L.. Nonlinear electron plasma waves. Danish Physical Society, Spring Meeting, Risø, Roskilde, Denmark, May 21-22.

RASMUSSEN, J. JUUL. Laboratory double-layers. 16th Nordic Symposium on Plasma and Gas Discharge Physics, Gausdal, Norway, February 11-13.

SCHOU, J., FLENTJE, G., HOFER, W.O. and LINKE, U. Secondary ion emission from NbV-alloys. 3rd International SIMS Conference, Budapest, Hungary, August 30 - September 5.

SCHOU, J.. Determination of impurities at the plasma edge of the stellarator W VIIA. Danish Physical Society, Spring Meeting, Risø, Roskilde, Denmark, May 21-22.

SKRIVER, H.L., McMAHAN, A.K. and JOHANSSON, B.. The s-d transition in compressed lanthanum. Nordic Solid State Physics Conference 1981, Copenhagen, Denmark, August 10-12.

SKRIVER, H.L.. Electronic transitions in praseodymium under pressure. International Symposium on the Physics of Solids under High Pressure, Bad Honnef, F.R.G., August 10-14.

SKRIVER, H.L., JOHANSSON, B. and ANDERSEN, O.K.. Cohesion and electronic structure of the actinide metals. International Conference on Actinides, Pacific Grove, U.S.A., September 10-15.

SKRIVER, H.L.. Pressure calculations for the actinides including spin-polarization. Actinide Workshop, Los Alamos, U.S.A., September 16-18.

THOMSEN, K., JOVANOVIĆ, D. and PÉCSELI, H.L.. Nonlinear transient signal propagation in plasmas. Danish Physical Society, Spring Meeting, Risø, Roskilde, Denmark, May 21-22.

THOMSEN, K.. A "hybrid" plasma simulation model. 16th Nordic Symposium on Plasma and Gas Discharge Physics, Gausdal, Norway, February 11-13.

6.4. Lectures

ALS-NIELSEN, J.. Phase transitiens in liquid crystals. HASYLAB, DESY, Hamburg, F.R.G. (January).

ALS-NIELSEN, J., Liquid crystals studied by perfect crystals, Oxford University, Oxford, U.K. (January).

ALS-NIELSEN, J.. Kernefysik (Lecture series in nuclear physics) Technical University of Denmark, Lyngby, Denmark, (spring semester).

BØRGESEN, P.. Deposition of energy in solid hydrogens by keV electrons and ions. Max-Planck-Institute for Plasma Physics, Garching, F.R.G. (December).

BØRGESEN, P.. On the erosion of condensed gases by 1-3 keV electrons. Max-Planck-Institute for Plasma Physics, Garching, F.R.G. (December).

CHANG, C.T.. Computational studies of the neutral shielding model of an ablating pellet.

1) Department of Aerospace, Princeton University, Princeton, New Jersey, U.S.A. (October).
2) Plasma Physics Laboratory, Columbia University, New York, U.S.A. (October).

GRYNING, S.E.. Air pollution. Seminar on Environmental Systems and Analysis. Royal College of Surgeons, Dublin, Ireland (April).

GRYNING, S.E.. Elevated source SF_6-tracer dispersion experiments in the Copenhagen area.
1) Battelle, Pacific Northwest Laboratories, Richland, Washington, U.S.A. (September).
2) University of New York at Buffalo, Buffalo, New York, U.S.A. (September).

GRYNING, S.E.. On the dispersion from ground-level sources investigated by a K-model. Pennsylvania State University, Pennsylvania, U.S.A. (September).

JENSEN, N.O.. Air pollution. Seminar on Environmental Systems and Analysis. Royal College of Surgeons, Dublin, Ireland (April).

JENSEN, N.O.. Atmosfærisk spredning af luftforurening (Atmospheric dispersion of pollution). Meeting of the Danish Meteorological Society, Risø, Denmark (May).

JENSEN, N.O.. Studies of the atmospheric surface layer during change in surface conditions. Etablissement d'Etudes et de Recherches Météorologiques, Paris, France (June).

JENSEN, N.O.. Spredning af tunge gasser (Dispersion of heavy gases). SNODAS Meeting, Risø, Denmark (September).

JENSEN, V.O.. The European fusion programme. University of Innsbruck, Austria (March).

JENSEN, V.O.. On α-particle heating and diffusion in toroidal devices. University of Innsbruck, Austria (March).

JENSEN, V.O.. Udsigterne for fusionsenergien (Prospects for fusion energy). Naturvidenskabeligt Samfund and REO, Odense, Denmark (April).

JENSEN, V.O.. Plasma Physics I and II. Two lecture series on plasma physics and fusion research. Technical University of Denmark, Lyngby, Denmark (spring and fal semester).

JENSEN, V.O.. Hvor langt er man med fusionsforskningen (The status of fusion research). Lecture given to physics teachers, Voksenpædagogisk Center, Copenhagen, Denmark (May).

JENSEN, V.O.. Fusion. Ingeniørforeningen, Copenhagen, Denmark (October).

JENSEN, V.O.. JET's placering i fusionsforskningen (JET's role in fusion research). Fysisk Forening, Copenhagen, Denmark (December).

KJEMS, J.K.. Ionic motion in the fluorites studied by neutron scattering.
1) Oak Ridge National Laboratory, Tennessee, U.S.A. (May).
2) Brookhaven National Laboratory, New York, U.S.A. (June).
3) Bell Laboratories, Murray Hill, New York, U.S.A. (June).

KRISTENSEN, L.. Plume meandering in a stable atmosphere.
1) Oregon State University, Corvallis, U.S.A. (May).
2) National Center of Atmospheric Research, Boulder, Colorado, U.S.A. (May).
3) Pennsylvania State University, State College, Philadelphia, Penasylvania, U.S.A. (May).

LARSEN, S.E.. Hot wire and cold wire measurements in an atmospheric environment. Symposium on Danish Technology on Energy and Pollution Control. Keidanren, Kaikan, Tokyo, Japan (April).

LARSEN, S.E.. The change of terrain roughness problem extended to mesoscale fetches.
1) Atmospheric Sciences Colloguium, Department of Atmospheric Sciences, University of Washington, Seattle, Washington, U.S.A. (May).
2) Department of Meteorology, Naval Postgraduate School, Monterey, California, U.S.A. (May).
3) Department of Atmospheric Sciences, Oregon State University, Corvallis, Oregon, U.S.A. (May).

LARSEN, S.E.. Interpretation of high frequency temperature spectra taking into account the interplay between a fluctuating advection velocity and sensor response.
1) Energy Transfer Seminars, Department of Atmospheric Sciences, University of Washington, Seattle, Washington, U.S.A. (May).
2) Physical Oceanography Seminars, School of Oceanography, Oregon State University, Corvallis, Oregon, U.S.A. (May).

LARSEN, S.E.. Udvikling af instrumentering på Risø (Instrumental development at Risø). Danish Meteorology Society Meeting, Risø, Denmark (May).

LARSEN, S.E.. Indflydelse af ruhedsændring på strømninger på mesoscala (The change of terrain roughness problem extended to mesoscale fetches). SNODAS Meeting, Risø, Denmark (September).

LARSEN, S.E.. Mesoscale theory and measurements for the change of terrain roughness problem. Meereskundliches Kolloquium, University of Kiel, F.R.G. (December).

LINDGÅRD, P.-A.. Correlation theory of static and dynamic properties of multi-level systems: A generalization of the RPA theory.

1) Oak Ridge National Laboratory, Tennessee, U.S.A. (January).
2) Argonne National Laboratory, Illinois, U.S.A. (March).
3) National Bureau of Standards, Washington D.C., U.S.A. (April).
4) Ames National Laboratory, Iowa, U.S.A. (May).

LINDGÅRD, P.-A.. Theory of paramagnetic properties of EuO and EuS.

1) Brookhaven National Laboratory, New York, U.S.A. (November).
2) Oak Ridge National Laboratory, Tennessee, U.S.A. (November).

LUNDSAGER, P.. The Test Plant for Small Windmills. Status of small Danish windmills.

1) Windmill Seminar, Dublin, Ireland (April).
2) Rocky Flats Test Centre, Golden, Colorado, U.S.A. (July).

LUNDSAGER, P.. Prøvestationen for mindre vindmøller. Status for mindre danske vindmøller (The test plant for small windmills. Status of small Danish windmills).

1) Herning Messen, Herning, Denmark (September).
2) Risø information meeting for programme secretaries at the Danish Radio, Risø, Denmark (November).

LUNDSAGER, P.. On the lifetime of windmills. AIAA 50th Anniversary Celebration, State University of New York at Buffalo, New York, U.S.A. (October).

LUNDSAGER, P.. An inside look at the Danish windpower programme. AIAA 50th Anniversary Celebration, State University of New York at Buffalo, New York, U.S.A. (October).

MICHELSEN, P.. Investigations of electrostatic ion waves in a collisionless plasma. Aarhus University, Aarhus, Denmark (October).

MIKKELSEN, T.. Formulation and experimental evaluation of an operational puff model.
1) U.S. Naval Postgraduate School, Monterey, California, U.S.A. (October).
2) U.S. Naval Environmental Prediction and Research Establishment, Monterey, California, U.S.A. (October).
3) Oregon State University, Corvallis, Oregon, U.S.A. (October).
4) National Center of Atmospheric Research (NCAR), Boulder, Colorado, U.S.A. (November).
5) University of Buffalc, New York, U.S.A. (November).
6) Pennsylvania State University, State College, Philadelphis, Pennsylvania, U.S.A. (November).

MØLLER, H. BJERRUM. Some recent neutron scattering studies at Risø. Oak Ridge National Laboratory, Tennessee, U.S.A. (August).

NIELSEN, M.. Physisorbed monolayers studied by x-ray and neutron diffraction. University of Hamburg, Hamburg, F.R.G. (December).

PÉCSELI, H.L.. Field aligned striations in ionospheric heating experiments. Danish Space Research Institute, Lyngby, Denmark (April).

PÉCSELI, H.L.. Series of lectures given at the University of Tromsø, Tromsø, Norway (fall semester).
1) Non-linear transients in homogeneous plasmas.
2) Microwave scattering of plasma irregularities.
3) The present status of ion phase space vortexes.
4) Turbulent diffusion made easy.
5) Laboratory observations of three-dimensional double-layers.

PÉCSELI, H.L.. Nonlinear evolution of ion-ion beam instabilities. University or Bergen, Bergen, Norway (October).

PÉCSELI, H.L.. University of Oslo, Oslo, Norway (October).
1) A thermal oscillating two-stream instability.
2) Ion phase space vortexes and their relation to ion beam instabilities.

PETERSEN, E.L.. Meteorology, air pollution and wind energy. Symposium on Danish Technology on Energy and Pollution Central. Keidanren, Kaikan, Tokyo, Japan (April).

PETERSEN, E.L.. Meteorologi og vind energi (Meteorology and wind energy). Herning Messen, Herning, Denmark (September).

PETERSEN, E.L. and LARSEN, S.E.. Research programmes of the meteorology section at Risø. Joint Seminars of Tsukuba Science City, Tsukuba, Japan (April).

PETERSEN, E.L. and LUNDSAGER, P. and FRANDSEN, S.. Wind turbine technology and siting. Wind Power Technology Seminar arranged by IFRS and Risø and held in Dublin, Ireland (April).

SCHOU, J.. Transport theory for kinetic emission of secondary electrons from solids by ion and electron bombardment. Gesamthochschule Kassel, F.R.G. (June).

SKRIVER, H.L.. Band structures. University of Copenhagen, Copenhagen, Denmark (January).

SKRIVER, H.L.. Electronic structure and cohesion of actinide metals.

1) Lawrence Livermore Laboratory, Livermore, California, U.S.A. (September).
2) Iowa State University, Iowa, U.S.A. (October).
3) National Research Council, Ottawa, Canada (October).

6.5. Degrees, students, etc.

Poul Michelsen defended a dissertation entitled "Investigations of electrostatic ion waves in a collisionless plasma". (Risø-R-417) on October 30th, 1981, at the University of Aarhus.

The following acquired the degree of lic. techn. or lic. scient. (Ph.D) for work carried out in the department:

Kurt Clausen (Solid-State Physics)

The following postgraduates carried out research which will lead to the degree of lic. techn. or lic. scient. at the department:

Henrik Bejder	(Plasma Physics)
Jakob Bohr	(Solid-State Physics)
Peter Børgesen	(Plasma Physics)
Finn E. Christensen	(Solid-State Physics)
Mogens Gadeberg	(Plasma Physics)
Sven-Erik Gryning	(Meteorology)
Dorte Juul Jensen**	(Solid-State Physics)
Kristian Kjær	(Solid-State Physics)
Torben Mikkelsen	(Meteorology)
Knud Thomsen	(Plasma Physics)
Ib Troen	(Meteorology)

The following students from the Technical University of Denmark and the University of Copenhagen worked on Masters' thesis projects:

John Jørgensen	(Plasma Physics)
Stig Holten Sørensen	(Plasma Physics)
Michael Wulff	(Solid-State Physics)

During January, February, August, and September, students from the Universities of Aarhus and Copenhagen participated in the following laboratory courses:

1) Neutron Scattering, organized by B. Buras, N. Hessel Andersen and K. Carneiro.
2) P. Michelsen, H.L. Pécseli, J. Juul Rasmussen and Knud Thomsen.

Two foreign students sponsored by the IASTE carried out practical work at the Department as part of their general training.

** Also at the Metallurgy Department, Risø

7. STAFF OF THE PHYSICS DEPARTMENT

Head	Hans Bjerrum Møller
Office staff:	Lone Astradsson, Anne Carlsen, Kæth Kjøller, Inge Pedersen**, Gerda Stauning, Alice Thomsen+, and temporary assistants.
The sections:	7.1. Solid-State Physics
	7.1.1. Liquid N_2 and He plant
	7.2. Plasma Physics
	7.3. Meteorology
	7.3.1. Test Plant for Small Wind Turbines.

7.1. Solid-State Physics

Scientific staff	Technical staff
Jens Als-Nielsen	Bjarne Breiting
Niels Hessel Andersen++	Kaj Christensen
Rogert Bauer*	Bent Heiden
Jørgen Kjems	John Z. Jensen
Bente Lebech	Louis G. Jensen
Per-Anker Lindgård	Steen Jørgensen
Hans Bjerrum Møller	Werner Kofoed
Mourits Nielsen	Jens Linderholm
	Morits Lund
	Jørgen Munck
	Allan Thuesen

---

* From February 1

** From September 15

\+ Until August 31

++ Also at the Metallurgy Department, Risø

Collaborators	Postgraduates
Bronislav Buras[+]	Jakob Bohr
Kim Carneiro[+]	Finn Christensen
Allan R. Mackintosh[+]	Dorte Juul Jensen[$]
Hans L. Skriver[++]	Kristian Kjær

Short-term visitors (two to twelve weeks)

P. Alekseev	Kurchatov Institute, Moscow, U.S.S.R.
M. Almeida	Instituto Superior Technico, Lisbon, Portugal
A. Bakka	Rigshospitalet, Oslo, Norway
R. Begum	University of Southhampton, U.K.
B. Bowermann	Birmingham University, U.K.
D. Eriksen	Oslo University, Oslo, Norway
R. Feile	Joh. Gutenberg University, Mainz, F.R.G.
H. Fjellvåg	Oslo University, Oslo, Norway
T. Giebultowicz	University of Warsaw, Poland
M.T. Hutchings	AERE, Harwell, U.K.
H. Ikeda	Ochanomizu University, Japan
K. Kakurai	Hahn-Meitner Institute, Berlin
H. Kepa	University of Warsaw, Poland
G.P. Knudsen	Technical University of Copenhagen, Denmark
G. Krexner	Österreichissches Forschungszentrum, Seibersdorf, Austria
M. Lehmann	ILL, Grenoble, France
A. Lehmann-Szweykowska	Poznan University, Poland
A. Loidl	Johs. Gutenberg University, Mainz, F.R.G.
K.A. McEwen	University of Salford, U.K.
J.P. McTague	University of California, Los Angeles, California, USA
W. Minor	University of Warsaw, Poland

[$] Also at the Metallurgy Department, Risø

[+] From the University of Copenhagen

[++] Also at NORDITA, Copenhagen

R. Nevald	Technical University of Denmark
L. Nielsen	Technical University of Denmark
L. Nilsson	Chalmers Institute of Technology, Göteborg, Sweden
P. Pershan	Harvard University, Massachusetts, USA
P. Pincus	École Superieure de Physique et de Chimie, Paris, France
G. Quittner	Österreisches Forschungszentrum, Seibersdorf, Austria
I. Sadikov	Kurchatov Institute, Moscow, U.S.S.R.
A. Stebler	University of Bern, Switzerland
M. Steiner	Hahn-Meitner Institute, Berlin
K. Tilli	Technical Research Centre of Finland, Otakaari, Finland
M. Wassak	University of Zürich, Switzerland
D. Witchel	Birmingham University, U.K.

7.1.1. Liquid N_2 and He Plant

Technical staff

Bent Heiden

John Z. Jensen

7.2. Plasma Physics

Scientific staff	Technical staff
Stig A. Andersen	Paul Andersen
Verner Andersen	Claus Bormann*
Che-Tyan Chang	Bengt Hurup Hansen
Palle B. Jensen	Jens A. Knudsen+
Vagn O. Jensen	Mogens Nielsen

* From September 1

+ Until August 31

Otto Kofoed-Hansen[$]
Jens-Peter Lynov
Poul Michelsen
Per Nielsen
Hans L. Pécseli
Jens Juul Rasmussen
Jørgen Schou[*]
Hans Sørensen
Stig Holten Sørensen[**]
Knud W. Weisberg[$$]

Arne Nordskov
Jørgen Olsen
John Petersen
Børge Reher
Bjarne Sass

Postgraduates

Henrik Bejder
Peter Børgesen
Mogens Gadeberg
Knud Thomsen

Consultant

Chan Mou Chen[+++]

Short-term visitors (two to twelve weeks)

E. Mjølhus	University of Tromsø, Norway
G. Popa	Al I Cuza University Iasi, Romania
K. Rypdal	University of Tromsø, Norway
M. Sanderloviciv	Al I Cuza University Iasi, Romania
R. Schrittwieser	Insbruck University, Austria

Long-term visitors

D. Jovanović[++]	Institute of Physics, Beograd, Yugoslavia
Chen Hao Ming	Tsing Hua University, Peking, China

---

[*] From April 1
[**] From September 15
[++] Until September 30
[$] Also at the Niels Bohr Institute, Copenhagen
[$$] Also at the Electronics Department, Risø
[+++] From City University, New York, USA

7.3. Meteorology

Scientific Staff	Technical staff
Carl Jørgen Christensen	Jørgen Christensen
Ole Christensen+	Gunner Dalsgaard
Sten Frandsen	Morten Frederiksen
Sven-Erik Gryning	Arent Hansen
Jørgen Højstrup	Jan H. Hansen°
Niels Otto Jensen	Finn Hansen
Leif Kristensen	Gunnar Jensen
Søren E. Larsen	Arni Nicolajsen°
Per Lundsager	Knud Sørensen
Niels Hauge Madsen*	
Torben Mikkelsen	
Erik Lundtang Petersen	
Ib Troen	

Collaborators	
Søren A. Jensen	Danish Ship Research Laboratory, Technical Univ. of Denmark
Eigil Jensen	DEFU, Technical University of Denmark
Poul Nielsen	DEFU, Technical University of Denmark
Peter Dorph-Petersen	Danish Meteorological Institute, Copenhagen

Consultant	
Chan Mou Tchen++	Postgraduates

---

* From October 1

\+ Until October 31

++ From City University, New York, USA

° Temporary assistant

Long-term visitors

W.K. George	State University of New York at Buffalo, New York, USA
E.F. Bradley	C.S.I.R.O., Canberry City, Australia

Short-time visitors (two to twelve weeks)

D.H. Lenschow	National Center for Atmospheric Research, Boulder, Colorado, U.S.A.
J.E. Tillman	University of Washington, Seattle, USA
A.P. van Ulden	KNMI, The Netherlands

7.3.1. Test Plant for Small Wind Turbines

Scientific staff	Technical staff
Peter Hjuler Jensen	Joel Ethelfeld+
Jørgen Krogsgaard	Flemming Hagensen
Per Lundsager	Ib Nørregaard*
Troels Friis Pedersen	Verner Sørensen**
Flemming Rasmussen	
Peter Rasmussen	

Consultants

Chris Mora-Jensen

Helge Petersen

---

* From June 1

** From July 1

\+ Until May 31

Sales distributors:
Jul. Gjellerup, Sølvgade 87,
DK-1307 Copenhagen K, Denmark

Available on exchange from:
Risø Library, Risø National Laboratory,
P. O. Box 49, DK-4000 Roskilde, Denmark

ISBN 87-550-0858-
ISSN 0106-2840